WADD TECHNICAL REPORT 60-699
VOLUME III

ENERGY CONVERSION SYSTEMS REFERENCE HANDBOOK

VOLUME III — DYNAMIC THERMAL CONVERTERS

C. W. Stephens
R. Spies
W. R. Menetrey

Electro-Optical Systems, Inc.

SEPTEMBER 1960

Flight Accessories Laboratory
Contract Nr. AF 33(616)-6791
Project Nr. 4769
Task Nr. 61048

WRIGHT AIR DEVELOPMENT DIVISION
AIR RESEARCH AND DEVELOPMENT COMMAND
UNITED STATES AIR FORCE
WRIGHT-PATTERSON AIR FORCE BASE, OHIO

700 — May 1961 — 30-1127

ABSTRACT

Volume III incorporates a detailed discussion of the two dynamic thermal converters which appear most useful in future power systems in the next decade, the Stirling engine and the Rankine cycle turbine. Empirical and theoretical equations are presented describing engine performance, and estimates are made of future performance possibilities with new working fluids, higher operating temperatures, etc.

Also discussed are electrostatic and electromagnetic generators which are coupled with the dynamic thermoconverters. Anticipated weights, efficiencies and other performance characteristics are described.

ENERGY CONVERSION SYSTEMS REFERENCE HANDBOOK

LIST OF VOLUME AND SECTION TITLES WITH AUTHORS

LIST OF VOLUME AND SECTION TITLES WITH AUTHORS (CONT'D)

A complete detailed Table of Contents for all volumes of Energy Conversion Systems Reference Handbook is included in Volume I.

ENERGY CONVERSION SYSTEMS REFERENCE HANDBOOK

Volume III - Dynamic Thermal Converters

Section A

STIRLING ENGINE

C. W. Stephens
Energy Research Division
ELECTRO-OPTICAL SYSTEMS, INC.

Manuscript released by the author
September 1960 for publication in this
Energy Conversion Systems Reference Handbook

WADD Technical Report 60-699

C O N T E N T S

I L L U S T R A T I O N S

T A B L E S

III DYNAMIC THERMAL CONVERTERS

A. STIRLING ENGINE

The first Stirling engine was built in 1816 by Robert Stirling, a Scottish clergyman who also conceived the Stirling cycle -- one of the first heat engine cycles to be reduced to an actual working device. The engine model produced only a few horsepower, weighed several hundred pounds, and was used in Britain as a stationary power plant in mines and mills. A modified version of this engine, built for the U. S. Navy by Ericsson, utilized four 14-inch diameter pistons and delivered 300 hp at approximately 10 rpm. These Ericsson air engines were used for many years in this country for numerous marine applications -- particularly riverboats.

As explained in subsequent sections, it is mechanically difficult to reduce the Stirling cycle to practice. The extensive differences between early operating model cycles and the true Stirling cycles were such that the achieved thermal efficiencies were approximately 5 to 10 percent. Consequently, they were replaced by the more efficient Rankine (steam), Otto, and diesel engines as these engines became available.

In 1938, the N. V. Philips Corporation of Eindhoven, Holland, initiated a research program aimed at applying modern thermodynamic and heat transfer developments to engine design. In 1944, using air as the working fluid, the first closed cycle engine was operated successfully. Interest developed in several quarters after World War II, and in the United States the Navy conducted an evaluation program. However, the engines tested were undeveloped laboratory models and, in comparison with available diesel engines, did not exhibit significant advantages with respect to performance, weight, or operating characteristics.

In 1947, Philips developed a highly efficient liquefaction machine based on the Stirling cycle. Models of this device, currently available in the United States and Europe, are extensively utilized for the liquefaction of air, nitrogen, and similar gases. Based on the success of the liquefaction device, an intensive research and development program to improve the engine efficiency was undertaken by Philips and resulted in the development of a single-cylinder, 40 hp engine in 1954. This engine used hydrogen as the working fluid and closely duplicated the predicted 36 percent thermal efficiency. It has been operating since that time as a research and development unit, and various improvements (primarily in the regenerator) have increased the thermal efficiency to over 38 percent. Several hundred hours of testing have been conducted on the engine and, in conjunction with analytical evaluation of the test data, have resulted in various modifications of pistons, cylinders, and heat exchangers. Two development models of a four cylinder, 330 hp industrial engine have also been built and successfully tested.

With the release of data on the 40 hp engine, the General Motors Corporation took an active interest in the Philips engine program. Subsequent negotiations between General Motors and Philips culminated in an agreement in 1958 which assigned U. S. license rights for Stirling cycle devices, both heat engines and refrigeration equipment, to the General Motors Corporation.

All known developmental efforts that point toward utilization of the Stirling engine in space are being carried out by the Allison Division of General Motors Corporation.

1.0 THERMODYNAMICS OF THE ENGINE

The actual cycle of operation of the Stirling engine, like that of most modern engines, is considerably different from the ideal upon which it is based. The temperature diagram for the ideal Stirling cycle is shown in Fig. III-A-1, and the corresponding pressure-volume diagram is shown in Fig. III-A-2.

The ideal cycle consists of two isothermal and two constant volume processes. Heat is added to the cycle during the isothermal expansion (3, 4) and the initial constant-volume process (2, 3); it is removed during the isothermal compression (1, 2) and the final constant-volume process (4, 1). It is theoretically possible to equal the efficiency of the Carnot cycle with the Stirling cycle. To duplicate the Carnot efficiency, the heat which is normally rejected in the final constant-volume process (4, 1) must be stored and returned to the gas during the initial constant volume process (2, 3). Consider first the isothermal compression process (1, 2) in Fig. III-A-1 and Fig. III-A-2. Heat is removed during this process at a sufficient rate to maintain constant-volume process (2, 3), heat is added to raise the pressure to the higher level prior to expansion. This heat, in the ideal case, is supplied by the regenerator.

The expansion process (3, 4) occurs at constant temperature with heat energy added from an external source. In the final

HEAT IN = 1 BTU/SEC
HEAT OUT = .29 BTU/SEC.
HEAT STORED IN REGENERATOR 6.3 BTU/SEC

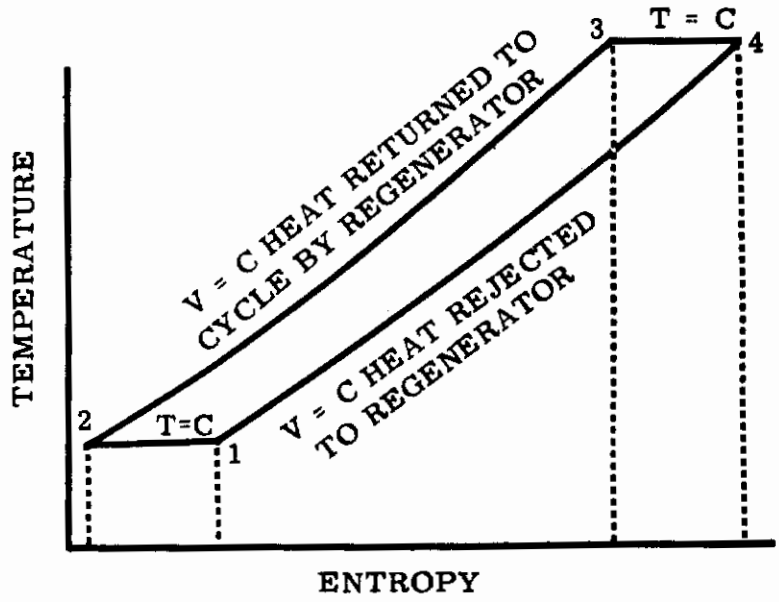

FIGURE III-A-1 TEMPERATURE-ENTROPY DIAGRAM, IDEAL STIRLING CYCLE

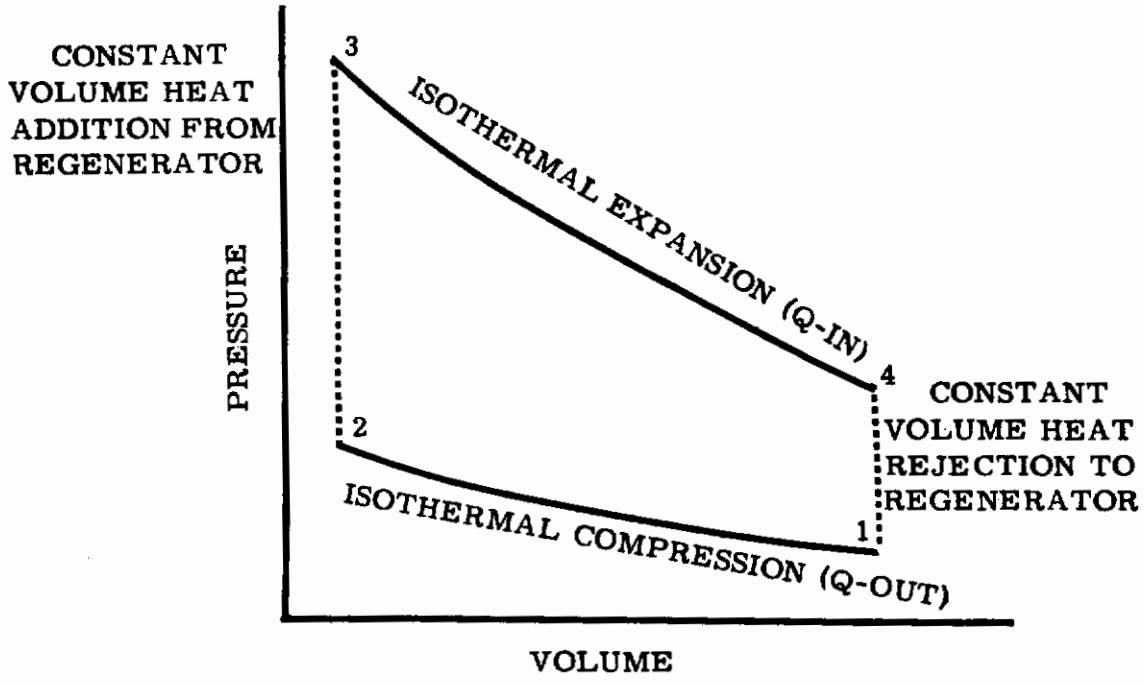

FIGURE III-A-2 PRESSURE-VOLUME DIAGRAM, IDEAL STIRLING CYCLE

constant-volume process (4, 1), heat is removed to lower the pressure and return the working fluid to the initial conditions prior to compression. This heat, in the ideal case, is stored in the regenerator.

The two effective processes from the work output standpoint are the compression process (1, 2) and the expansion process (3, 4). The constant-volume processes are merely intermediate steps to convert the working fluid from one pressure level to another.

The heat which is rejected during the final constant-volume process (4, 1) is equal to that which must be added in the initial constant-volume process (2, 3). This is readily shown. The heat added to or removed from a constant-volume process is the product of the specific heat (at constant-volume) and the temperature difference. The specific heat of the ideal gas is, of course, constant. Since both the initial and final constant-volume processes operate between the same isothermals, the temperature differences and, therefore, the heat involved are identical for both processes.

It is of interest to compare the amount of heat being handled at various points in the cycle. The ideal cycle has an efficiency of 71 percent at the conditions represented in Fig. III-A-1. Thus, for each unit of heat which is transferred into the system in the isothermal expansion process (3, 4), 0.29 units of heat are removed from the system during the isothermal compression process (1, 2). But, for each unit of heat introduced into the system, 6.3 units of heat are rejected during the final constant-volume process (4, 1) and must be stored and returned to the system during the initial constant-volume process (2, 3). The heat storage

capacity of the regenerator, then, must be 6.3 times as great as the quantity of heat which must be transferred into the system.

On the basis of this ideal analysis alone, it is quite clear that the regenerator assumes vital importance in the operation of the practical engine. Thus, the important key to the success of this cycle is a regenerator of extremely high effectiveness.

2.0 THE ENGINE

The requirements of the ideal Stirling cycle serve as a basis for establishing the prerequisite elements of an engine intended to follow the cycle. In order to pass through the desired cycle, the working medium within the engine must be heated, it must be cooled, it must store and remove energy from a regenerator, and it must be compressed and expanded at the proper times. These requirements then prescribe the five major components of the Stirling engine--the engine heater and a means of keeping it hot; the regenerator; the engine cooler and a means of keeping it cool; a displacer piston to control the movement of the working fluid through the heater, regenerator, and cooler; and the power piston to compress and expand the gas.

2.1 General Configuration

The arrangement of the engine elements is shown in the schematic diagram of Fig. III-A-3. The heater for the space version of the Stirling engine consists of thin-wall U-tubes which are uniformly spaced around the cylinder (see Fig. III-A-4). The heater shown in Fig. III-A-3 is that utilized for ground application in which combustible fuel is burned about the closely spaced, stainless steel tubes that are

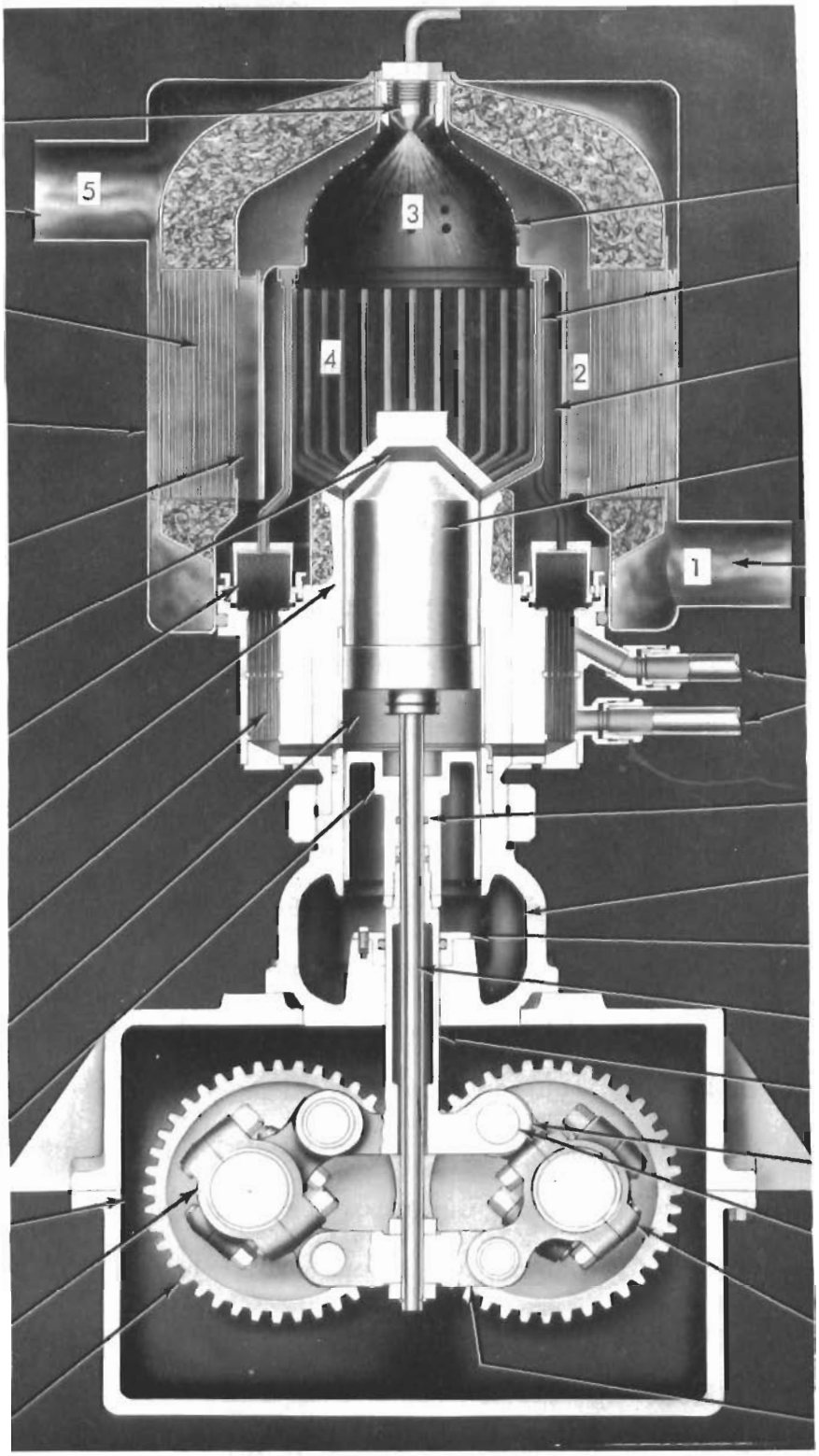

FIGURE III-A-3 STIRLING THERMAL ENGINE SCHEMATIC DRAWING

brazed into the cylinder head, as shown in that figure. In the space version, Figure III-A-4, the thin-wall, high-temperature steel tubes are enclosed in a stainless steel housing through which liquid metal is pumped to transfer heat to the heater assembly.

The regenerator, as shown in Figures III-A-3 and III-A-4, consists of cylindrical assemblies placed about the periphery of the cylinder wall containing stacks of 400-mesh, 0.0008-inch diameter stainless steel wire. The regenerator, one of the most critical engine components, must store approximately six Btu for each unit of heat input and must do it in a very short period of time with minimum pressure loss.

The cooler is located directly below the corresponding regenerator. The cooler assembly consists of many small diameter vertical tubes through which the working fluid flows. The tubes are located in an annulus through which the water coolant circulates.

The displacer piston is a hollow, stainless steel shell which fits loosely in the cylinder, its motion being controlled through the displacer piston rod connecting it to the drive mechanism in the crankcase. There is very little pressure difference between the top and bottom of the displacer piston, and small leakage of gas between the displacer and the cylinder wall can be tolerated. This piston, therefore, requires no piston rings or other means of sealing to the cylinder. Because the top of the displacer piston operates approximately at the temperature of the cooler, the piston walls are made as thin as possible to reduce conduction heat losses. Furthermore, the piston has two internal, horizontal baffles to reduce radiant heat losses through the piston.

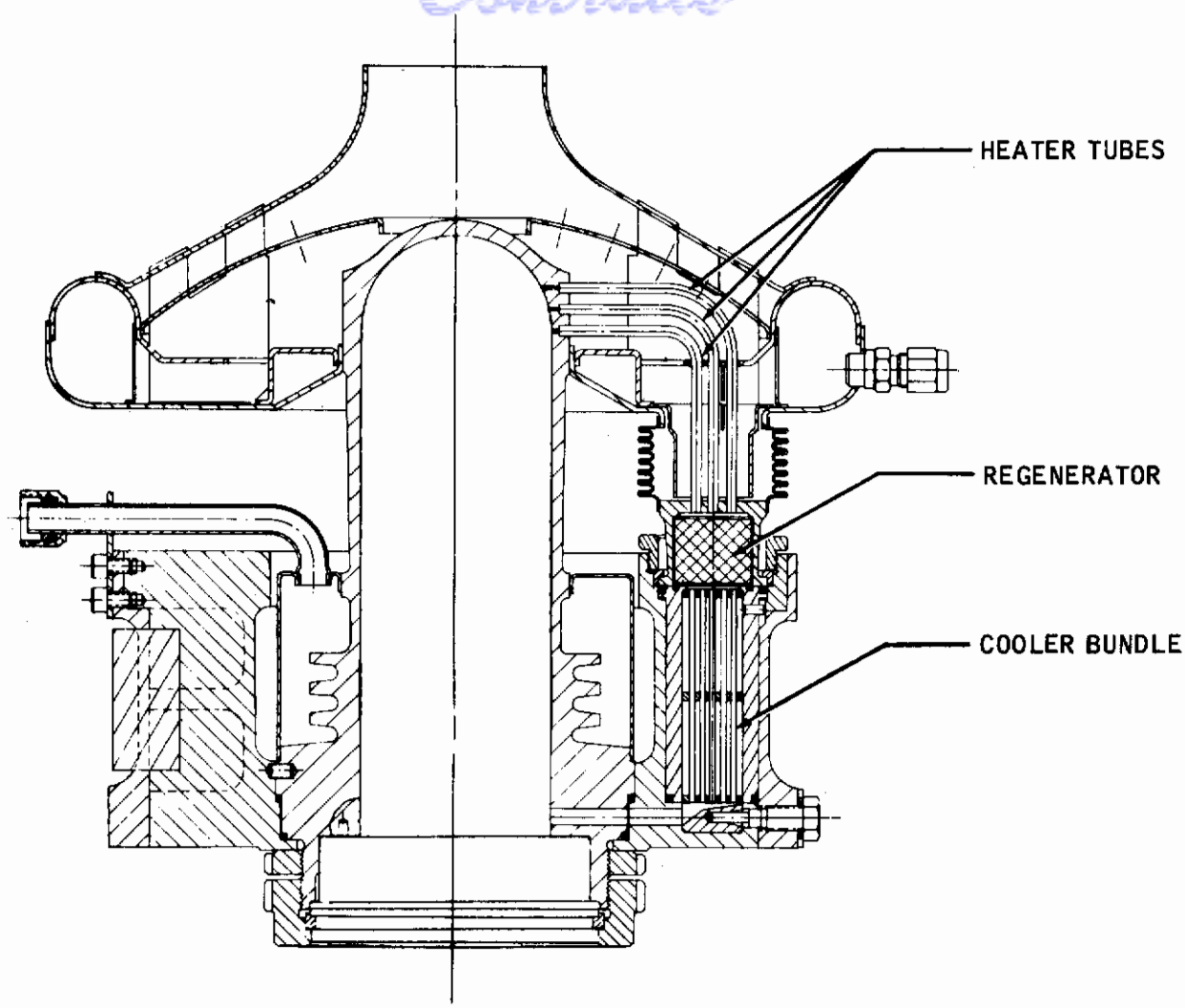

FIGURE III-A-4 STIRLING ENGINE HEAD ASSEMBLY

The power piston must provide the work of compression of the gas and must deliver the work of expansion, so it experiences considerable pressure differences between its upper and lower extremities. It therefore fits more closely into the cylinder and is equipped with rings or other sealing means to prevent gas leakage between the piston and cylinder wall. The location of the power piston in the cold zone of the engine allows more latitude in the selection of sealing means than is the case with usual engine pistons which experience high combustion temperatures. Forces are transmitted from the power piston to the Rhombic drive mechanism by means of the power piston rod as shown. The power piston rod is hollow, and the displacer piston rod passes through it. As shown in Figure III-A-3, a buffer space is located below the power piston and above the seal assembly at the top of the crankcase. The Stirling engine would generally have a low specific power output if it were operated at low mean cycle pressures. Accordingly the engine is designed to operate at higher pressures, and the buffer space is provided so that a thermodynamically inert volume of working fluid can be trapped below the power piston. The mean pressure of this gas in the buffer space is kept near the mean pressure of the working fluid above the power piston and serves to reduce the loads on the drive mechanisms. Present designs by the Allison Division of General Motors for space application utilize a buffer mean pressure of 1500 psi, and the fluctuations in the actual working medium above the working piston in this space model are $\pm$ 500 psi above and below this mean.

The motion of the two pistons is controlled by the Rhombic drive mechanism shown in Fig. III-A-3, which consists of two similar contrarotating shafts with one crank on each crankshaft. The shafts are timed together by a pair of helical timing gears; the power piston is connected to the cranks by the power piston rod, the power piston yoke, and the power piston connecting rods. A similar series of parts connects the displacer piston to the crankshafts of the lower yoke and connecting rod assembly. On each crank, there are actually two power piston connecting rods which are spaced by the yoke to serve as a single, split-connecting rod. The lower, displacer connecting rod then fits on the crank between the two power piston connecting rods. The Rhombic drive subassembly is shown in Fig. III-A-5. In the left of this figure, the two cranks are at their innermost points when the pistons are closest together, whereas on the right, the cranks are at their outermost points when the pistons are farthest apart. It is interesting to note that the pistons reach top dead center or bottom dead center when the crankshaft center, the crank pin center, and the yoke pin center are in a single straight line; and it is further to be noted that the positions of top dead center and bottom dead center of one piston are not 180 crank angle degrees apart. An important feature of this drive mechanism is its symmetry of construction which permits complete dynamic balancing of all the moving parts of the engine by suitably located and sized counterweights on the crankshafts.

2.2 Operation

The operation of the Stirling Thermal Engine is completely governed by the relative motion of the two pistons and is most easily described by considering these piston functions.

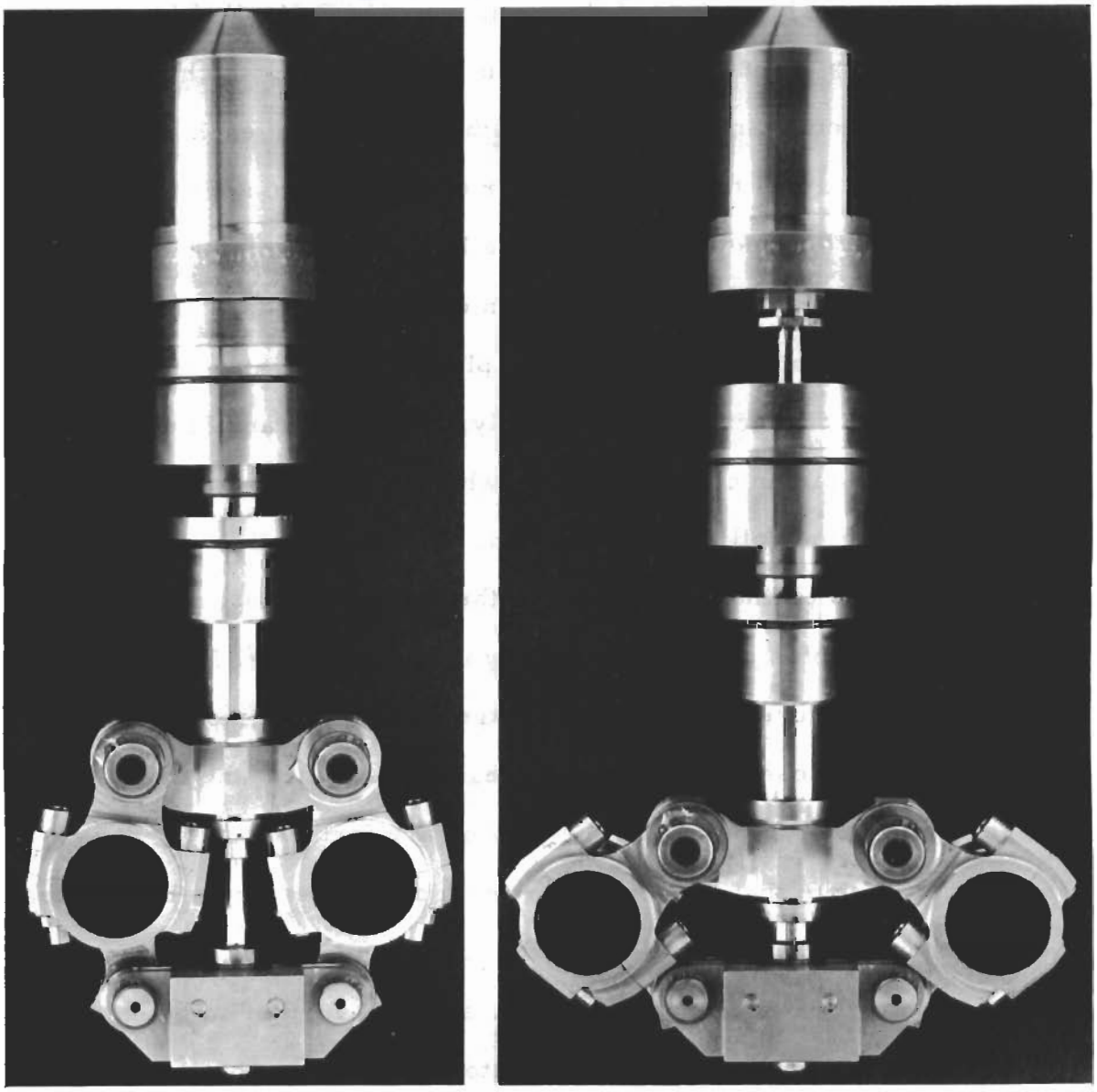

FIGURE III-A-5 RHOMBIC DRIVE SUB-ASSEMBLY

The basic functions of the pistons may be seen from an examination of Fig. III-A-3. First, it is evident that all of the working fluid is contained in the total volume that is the sum of the volumes of the engine's five working spaces and their short connecting passages. These five spaces are as follows: (1) the variable volume of the hot space in the cylinder above the displacer piston, (2) the internal volume of the heater, (3) the gas volume of the regenerator, (4) the internal volume of the cooler, and (5) the variable volume of the cold space between the pistons in the cylinder. The total volume occupied by the working fluid is therefore completely governed by the position of the power piston. Since the displacer piston always occupies the same volume, its position cannot change the total volume of the system. Thus, gas volume change to effect its compression or expansion is accomplished by motion of the power piston and is independent of the position or movement of the displacer piston.

On the other hand, the displacer piston serves to control the location of the gas within the total volume established by the power piston. When the displacer piston is at the top of the cylinder, most of the gas is in the cold spaces. Downward movement of the displacer piston forces the gas through the heat exchanger circuit upward through the cooler, regenerator, and heater into the hot spaces. The net effect of this downward motion of the displacer piston is to move most of the gas up from the cold space to the hot space. Moving the displacer piston down heats the gas. Reverse motion of the displacer piston upward from the bottom of its travel transfers most of the working fluid from the hot space downward through the heater, regenerator, and cooler into the cold space, thereby effecting a cooling of the gas.

Thus, the primary function of the power piston is to compress and expand the working fluid, and the primary function of the displacer piston is to heat and cool the working fluid. It must be emphasized that only the gas contained in the active spaces above the power piston goes through the thermodynamic cycle that converts part of the heat from the heater into work at the power piston. The gas contained in the buffer space below the power piston is the same kind of gas as the working fluid but accomplishes no thermodynamic purpose and serves only to balance the forces of the mean pressure of the supercharged working fluid.

The ideal Stirling cycle is usually described by the sequence of piston positions shown in Fig. III-A-6a. The ideal PV diagram is repeated as Fig. III-A-6b. In position 1, the power piston is at bottom dead center (BDC), and the displacer piston is at top dead center (TDC). Thus, the gas is contained in the cold space at maximum total volume. The first process in the ideal cycle is an isothermal compression from I to II that could be accomplished by movement of the power piston from BDC to TDC without moving the displacer piston. The next required process from II to III is a constant volume heating of the gas. This could be accomplished by moving the displacer piston from TDC to BDC without moving the power piston. The third process is an isothermal expansion from III to IV, and this could be accomplished by moving the power piston from TDC to BDC without moving the displacer piston. The cycle could then be closed by returning the displacer piston to TDC to cool the gas at constant volume.

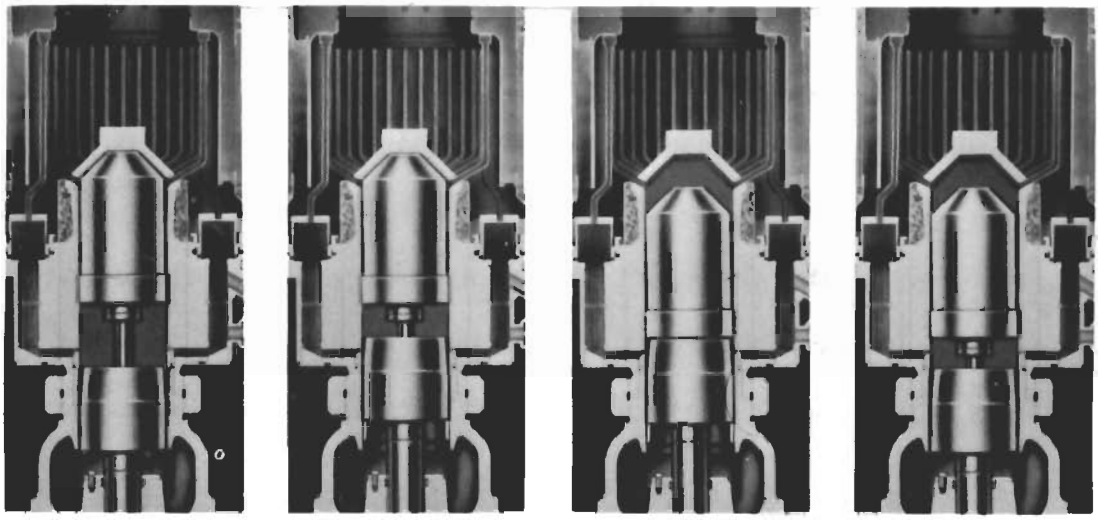

Piston Position Sequence

a

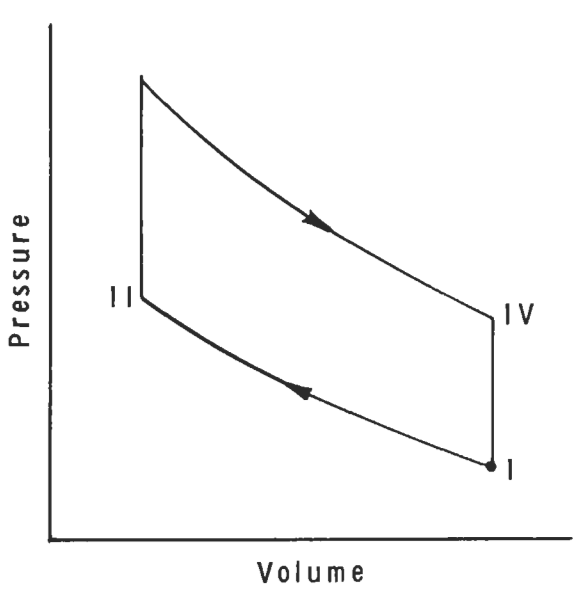

PV Diagram

b

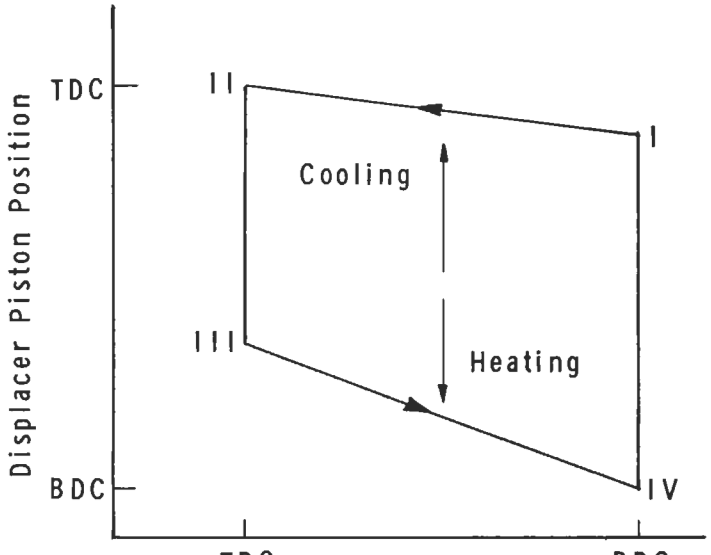

Piston Relative Motion Diagram

c

FIGURE III-A-6 IDEAL STIRLING CYCLE DIAGRAMS

The above ideal description of the piston motion is based on the postulate that heat is transferred into or out of the working fluid through the cylinder walls during the isothermal processes. It has already been shown, however, that the actual configuration of the engine is based on the premise that heating and cooling of the working fluid must be accomplished by suitable movement of the displacer piston. Recognizing this inherent characteristic of the engine, a more realistic picture of the piston motion required to produce the ideal Stirling cycle can be created by means of a piston relative motion diagram like that of Figure III-A-6c.

In this diagram the position of the displacer piston is plotted on the ordinate as a function of the position of the power piston as the abscissa. The TDC's are at the top and left, respectively. This diagram can be used to illustrate the individual effects of the piston motions when the pistons move simultaneously.

It is possible to construct an ideal piston motion diagram from the ideal PV diagram of the cycle. The first, isothermal compression, process must be accomplished by movement of the power piston from BDC to TDC to reduce the volume of the fluid and by an upward movement of the displacer piston to provide cooling equivalent to the work of compression performed by the power piston. Thus, the displacer piston cannot be at TDC at point I but must rise from some lower position to TDC during the compression process. The second, constant volume heating, process from II to III can be accomplished with movement of only the displacer piston, but it cannot move the full stroke to BDC since heating must also be done during the isothermal expansion stroke from

III to IV. After the constant-volume heating process, the isothermal expansion is accomplished by moving the power piston from TDC to BDC while the displacer piston finishes its travel to BDC. The final process is the constant-volume cooling from IV to I, which may be accomplished by motion of the displacer alone. The complete piston motion diagram is then as shown in Figure III-A-6c for the ideal cycle.

It is impossible to draw this diagram to any exact energy scale, because the quantitative relationship between the displacer piston position and the amount of heat transferred to the working fluid cannot be expressed directly. Nor is it possible to deduce the correct shape of the curves between the corners of the diagram. It is, however, possible to make some approximate statements about the over-all proportions of the diagram. First, the amount of heat transferred to and from the regenerators during the constant-volume processes is much greater than the amount of heat added during the expansion stroke or removed during the compression stroke. Also, the heat added during the expansion must be greater, by the amount of work produced per cycle, than the heat removed during the compression stroke. It is therefore to be expected that the ideal movement of the displacer piston will be less between I and II than it is between III and IV and that the movements between II and III and between IV and I will be greater than either of the two above.

The diagrams of Figure III-A-6 are duplicated in Figure III-A-7 using the actual engine parameters. A comparison of the actual PV diagram of Figure III-A-7b with the ideal diagram of Figure III-A-6b shows that the four ideal processes of the ideal cycle do not seem to be even closely approximated by the actual engine. However,

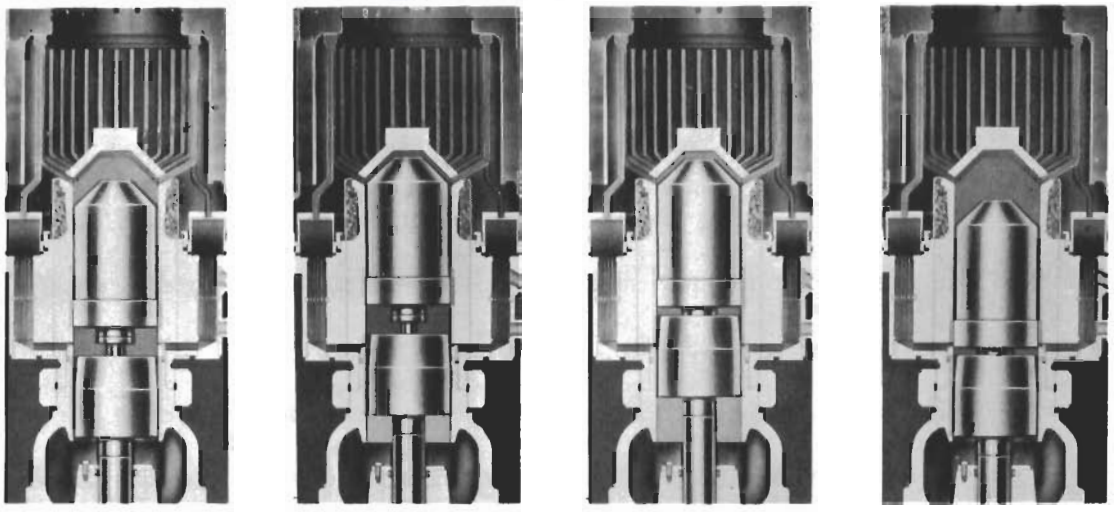

a

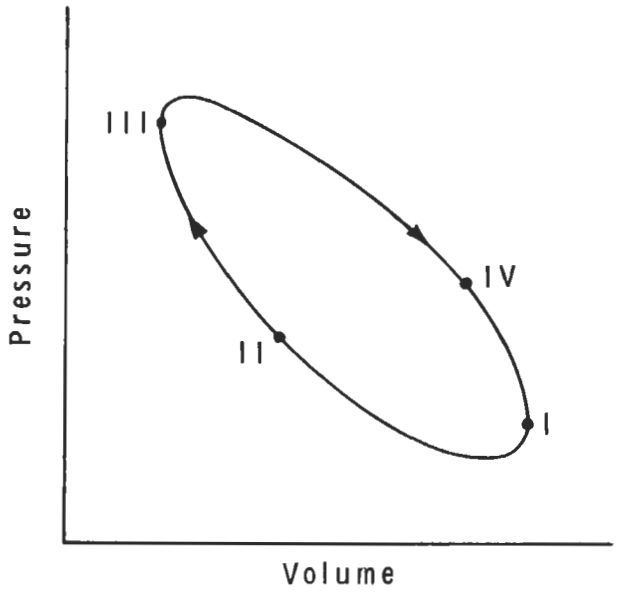

b

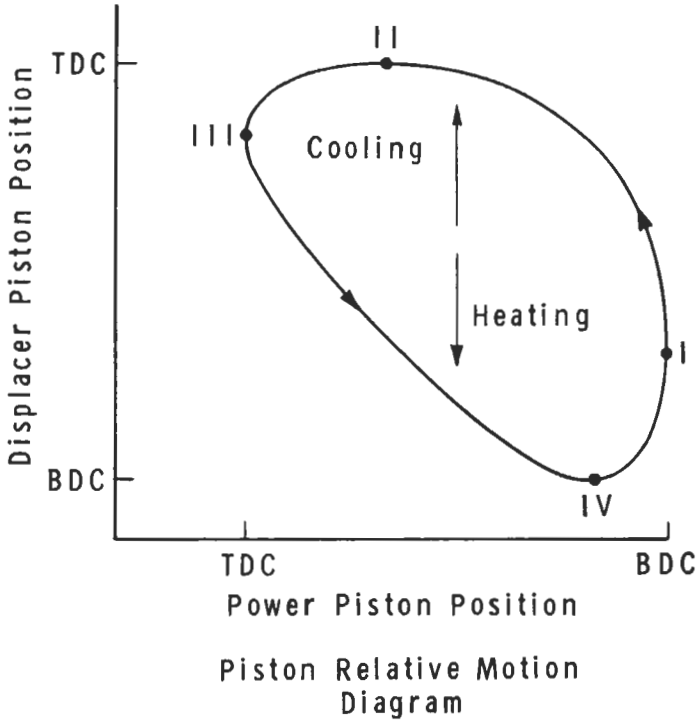

c

FIGURE III-A-7 ACTUAL STIRLING CYCLE DIAGRAMS

a comparison of the relative motion diagrams (III-A-7c and III-A-6c) shows that the positions of piston top and bottom dead centers are clearly defined for both the actual and ideal engines. This correlation of cycle events and mechanical piston events allows comparison between the actual engine operation and the ideal cycle. The ideal cycle thus becomes a cycle of four piston events rather than of four processes as shown on ideal PV diagrams. Four events follow in order for both ideal and actual engines: (I) BDC power piston, (II) TDC Displacer Piston, (III) TDC Power Piston, and (IV) BDC Displacer Piston. These four events are easily noted on the piston motion diagrams and can be noted accurately on the actual PV diagram by equivalent crankshaft positions.

It is now possible to examine Fig. III-A-7c and to observe the actual engine piston movements and some of the compromises that are imposed by the real drive mechanism. The first compromise which is evident results from the impracticability of allowing the power piston to completely stop for part of the cycle. It is theoretically possible to conceive a drive which would allow this discontinuity, but any reasonable mechanism will not permit it. Thus, the vertical lines of Figure III-A-6c have been eliminated. It would also be impossible to stop the displacer piston during part of the cycle, but this is not required even in the ideal instance as shown by the absence of horizontal lines in Figure III-A-6c.

Beginning at point I, the actual engine events can be traced on Figure III-A-7c. It is desired to accomplish isothermal compression from event I to event II. The figure shows that the displacer

piston moves in the cooling direction quickly at the beginning of this compression so that compression occurs with most of the fluid being cooled in the cold spaces, but cooling stops before the power piston reaches TDC. It is seen that the process from II to III is heating as in the ideal cycle, but that it is accomplished at decreasing gas volume rather than at the ideal constant volume. The expansion from III to IV, however, is quite similar to the ideal. The pistons are moving down together as indicated by the nearly straight, 45° portion of the curve; and the downward motion of the displacer tends to keep the gas in the hot spaces where it is heated while the downward motion of the power piston accomplishes the expansion or power stroke. The final, cooling process is accomplished by an upward movement of the displacer piston while the power piston completes its travel to BDC.

The actual engine operations during the expansion and compression strokes are quite like those anticipated from the ideal considerations with a relatively large time for heating during the expansion (III-IV) and a relatively small time for cooling during the compression (I-II). However, the long vertical lines which characterized the ideal diagram during the constant-volume, regenerative processes are not in evidence on the actual diagram. This difference is easily explained by examining the heat exchanger circuit in Figure III-A-3.

The figure shows the heater, regenerator, and cooler in a single continuous passage, so that gas passing from the cold space to the hot space, for example, must pass through all three heat exchangers. It has been stated that the net effect of moving gas from the cold space to

the hot space is to heat the gas. The truth of this statement is evident, and it is an adequate approximation of the major cycle event accomplished by downward motion of the displacer piston. It will be seen, however, that some of the heat introduced into the working fluid during its upward movement is recovered from the regenerator since the cold gas passes through the regenerator before it enters the heater. The converse of this heat transfer takes place during downward motion of the gas through the heat exchanger circuit when heat from the heater is stored in the regenerator before the gas passes to the cooler and the cold space of the cylinder.

The difference between the actual relative motion diagram and the ideal relative motion diagram (III-A-7c and III-A-6c) can thus be explained. In the ideal diagram, the regenerative processes were clearly shown, because it was presumed possible to stop the power piston while these constant-volume heat exchangers took place. In the actual diagram the vertical lines are absent, because the power piston does not stop; but the regenerative process still takes place during the entire upward or downward motion of the displacer piston while the net cooling or heating is being accomplished. Additional information regarding the various component operation may be had by referring to the list of references at the end of this section.

2.3 Controls

While there are numerous methods available for the control of the Stirling engine electrical output, it appears that there are three which are most relevant.

a. Introduction of a parasitic electrical load - when a constant power output for the engine is specified, it is possible to adjust for minor deviations either in the load requirements or engine output to the utilization of a parasitic load. For this type of power demand, the parasitic load appears to be the simplest and most reliable method of regulating power output. As described in Section 4, this is the control technique utilized in the space version of the Stirling cycle.

b. Control of the mean pressure of the working gas - changing the mean pressure of the Stirling cycle has no effect on the thermal efficiency of the engine, provided the cooler and heater temperatures remain unchanged. This technique can effectively vary the engine power output over the entire spectrum of its capability. There is a slight effect on the system efficiency as the power output is lowered, however, since the friction power requirement is essentially a function of engine speed only and will represent a higher proportion of the total internal engine power generated as this power is decreased. To satisfy the requirement of effectively varying the engine mean effective pressure, a separate regulator

is required. This regulator is described in detail in Reference III-A-1 and requires a number of separate control elements including an auxiliary accumulator and compressor. To utilize this type of control also requires that the buffer pressure be adjusted in approximately the same manner as the mean engine pressure.

c. Change in engine operating temperature -- by raising the rejection temperature of the working fluid or lowering the heater temperature or a combination of both, it would be possible to effectively decrease the work output of the Stirling engine. This would be done, however, at the expense of an efficiency drop. This drop is obvious from examination of the temperature entropy diagram of engine operation. This mode of engine control would probably not be recommended if extended operation of the engine were required considerably below the design point.

3.0 SPACE CONFIGURATION

As mentioned previously, all known efforts toward developing the Stirling cycle engine for space application are presently being performed by the Allison Division of the General Motors Corporation. Allison efforts are partially sponsored by the Advanced Research Projects Agency through contract with the Wright Air Development Division (AF 33(616)-6771). Their efforts are now concentrated toward the design,

fabrication, and performance testing of an advanced Stirling cycle engine suitable for application in a flight prototype system. This flight system incorporates two similar contrarotating generators which are completely enclosed in the engine crankcase. This arrangement cancels the gyroscopic torques which would exist if a single generator were used. The general specifications for this power system are given below in Table III-A-1:

TABLE III-A-1

ENGINE GENERATOR SPECIFICATION

Rated Power	3 kw * (400 cycle, 220 volts, 3 phase, ac)
Speed	3000 rpm (engine and generators)
Rated Engine Efficiency	30.5 percent (brake thermal)
Rated Generator Efficiency	80 percent
Heater Temperature	1250°F liquid metal inlet temperature
Cooler Temperature	150°F coolant water inlet temperature
Mean Cycle Pressure	1500 psi
Working Medium	Helium
Weight	285 lb** (engine and generators)

* Engine is capable of 5 kw output.

** Estimated weight of prototype engine. Considerable reduction in weight is anticipated for the fully developed flight configuration.

The following subsections will briefly describe the various components selected for this engine.

3.1 Drive Mechanism

The Rhombic drive, used to move the pistons with proper phasing, has been selected by Allison as that drive which gives the most highly desirable characteristics for Stirling engine operation. Among these desirable characteristics are the following:

a. Phasing of the pistons for optimum thermodynamics can be realized by selecting the proper distance between the crankshafts and lengths of the connecting rods, crank throws, and cross heats.

b. There are no side loads on the pistons.

c. A single cylinder engine can be completely balanced.

d. The linear motion of the piston shafts makes it possible to seal the working cycle from the crank case.

Extremely tight tolerances are required to insure precise linear movements of the pistons necessary in order to realize high efficiency. The mass and center of mass of all parts are carefully determined and adjusted to give complete balance of the unit. The calculated weights of the parts of the Rhombic drive mechanism have been determined from layout drawings, and adjustments have been made to meet conditions of complete balance. Extensive dynamic and static force analyses have been made to insure both complete engine balancing and integrity of all stressed units (e.g., Reference III-A-7). Due to the symmetry of the connecting rod arrangements, all x-component forces exerted by the connecting rods on the power piston are balanced, and the net force on the power piston is in the y direction only.

Evaluations of system imbalancing due to tolerances have caused the Allison Division to feel that if the present exacting tolerance limits can be held, serious performance degradation due to a combination

of tolerance errors will not occur. An investigation of system dynamics has shown that the critical speed is 7,100 rpm, well above the 3,000 rpm design point. Vibration amplitudes of less than 80 μ are anticipated.

3.2 Engine Head Assembly

The cylinder, heater tubes, and regenerator cups of the engine under development by Allison are made of Hastelloy and are brazed into a single assembly (see Figure III-A-4). The sheet metal duct work and manifold which direct the flow of the liquid metal heat source over the heater tubes are brazed to the cylinder heat. Bellows sections connect the duct to the top of regenerator. Flexing of the bellows and the heater tubes occurs because of the difference in thermal expansion of the cylinder head and the cooling water jacket which holds the regenerators fixed. A split ring and nut arrangement secures each of the regenerator cups to the cooling jacket directly over the cooler bundles. The cooling jacket (one of two employed in the engine) is a fabricated piece -- copper brazed together -- that holds the bundles of cooler tubes and forms the passage of the cooling water. The bottom of this cooling jacket, drilled for a gas passage from the cylinder cold space to the bottom of the cooler bundles, is shouldered against the cylinder and secured by a spanner nut. A second water jacket is provided to maintain dimensional stability and cooling of the cylinder wall in the region of the displacer piston seal.

3.3 Crankcase

The crankcase for this engine will be a simple cylinder with domed ends to withstand the high gas pressure. Bulkheads

across the case carry the main bearings of the crankshafts on removable covers. Between the bulkheads, a compartment which is isolated from the rest of the crankcase by the shaft seals, is used as the buffer space under the work piston. The bulkheads also carry the generator stators.

A gear pump, driven from one of the crankshaft synchronizing gears, is provided for the pressure lube system. A filter, oil cooler, and pressure regulator are included in the lube system. The large helium-oil separator mounted on the outside of the crankcase is an off-the-shelf, high-pressure filter. No attempt has been made to design a thin wall unit which could be installed inside the crankcase. During testing with the present setup, it should be relatively simple to inspect the hard-wound filter core to determine the amount of oil removed from the gas that is vented from the crankcase to the buffer space. A check valve prevents flow back through the filter when the buffer space pressure is higher than crankcase pressure.

3.4 The Control System

For the Stirling cycle engine presently being developed by Allison, a constant load duty cycle is specified. Studies by Allison have indicated that a parasitic electrical load device and control would result in the lightest system weight with the highest response. The specifications necessary for this regulator are as follows:

1. Generator power - - 120/208 volts, 400 cps, 3 phase, 2 generators of 2.5 kva each.
2. Frequency control - - $\pm$ 1 percent; voltage control -- $\pm$ 1 percent.

3. Generator power output -- 5.5 kva output capability; constant load -- 5.0 kva; waste power load for 500 watts for speed and frequency regulation.

The basic diagram for the proposed control system is shown in Fig. III-A-8. From this diagram, it can be observed that the proposed regulators are composed of two basic systems -- one for voltage regulation of the generator output and the other for alternator frequency control. These two systems are similar in the manner in which output power is controlled to either the field windings or the waste power load. The primary difference is the mechanism. In one case, voltage is sensed and field current is controlled; and, in the other case, frequency is sensed and generating load is controlled. These two systems are described in considerably greater detail in Reference III-A-1.

3.5 The Working Fluid

The performance of the Stirling engine is closely related to the working fluid. The volume of gas in the heat exchangers (cooler, regenerators, heater) is "dead" volume and must be kept to the absolute minimum consistent with heat transfer requirements. The high volumetric heat capacity of hydrogen, its high heat transfer coefficient, and high gas constant, are very desirable working fluid characteristics. The serious deficiency of hydrogren, however, is its tendency to diffuse through metals at high temperatures. The use of barrier metal coatings such as molybdenum will greatly reduce this diffusion. However, it is felt that the inherent difficulties imposed on an extended, unattended life operation limit the feasibility of hydrogen utilization, especially in light of the availability of helium, for which diffusion is not a serious problem.

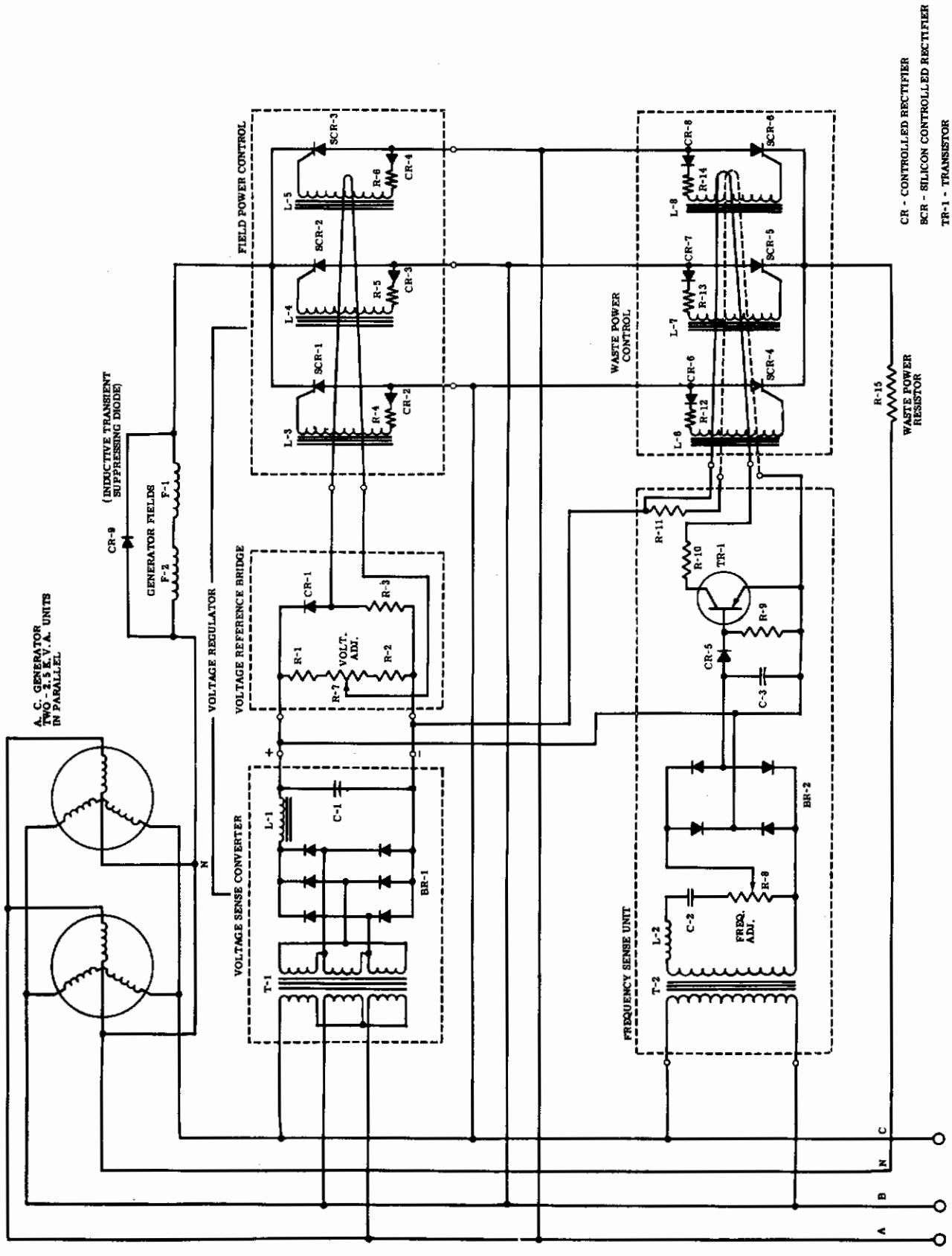

FIGURE III-A-8 GENERATOR VOLTAGE AND FREQUENCY REGULATOR SYSTEM

The thermodynamic properties of helium are nearly as good as those of hydrogen, and these properties, coupled with a low diffusion rate, make helium the preferred working fluid.

Allison has determined that the generally less desirable thermodynamic characteristics of air are not satisfactory where high efficiency is required. Table III-A-2 presents the estimated relative efficiency of the Stirling engine operating on air, helium, and hydrogen between the temperatures specified in Table III-A-1.

TABLE III-A-2
EFFECT OF WORKING FLUID
ON ADVANCED STIRLING CYCLE PERFORMANCE

Working Fluid	Estimated Efficiency
Helium	30.5 percent
Hydrogen	34.5 percent
Air	25.5 percent

3.6 Engine Performance

The performance estimates of the power plant are based on test data of the 40 horsepower advanced Stirling engine. These estimates are corrected to the operating conditions which are established by the system weight analysis and are based on helium as the working fluid. Allowance has been made in these calculations for the effect of size factors on performance. Estimated engine performance data over

a range of operating conditions for the engine presently under development are presented in Fig. III-A-9 - 12 for variations in the heater temperature, cooler temperature, mean pressure, and speed, respectively. The design point conditions are indicated by a circled point in these figures.

3.7 Engine Weight and Dimensions

The estimated weight and dimensions of the engine and generators, are shows in Table III-A-3 below for a range of power ratings.

TABLE III-A-3

ESTIMATED ENGINE-GENERATOR ASSEMBLY WEIGHTS AND DIMENSIONS

Power-KW	Weight LB	Dimensions (Inches) Height	Length	Width
1.0	83	14.5	18.8	11.0
4.0	186	20.0	23.0	13.5
10.0	330	25.0	27.4	16.2
15.0	420	27.3	30.0	17.8
20.0	500	29.5	32.1	19.1
30.0	630	33.0	35.8	21.2

4.0 DEVELOPMENTAL STATUS

The space version of the Stirling engine described previously is scheduled for its first performance test in the latter part of August 1960. Following the performance test, a calibration test will be conducted by Allison. Depending upon the successful outcome of these initial programs, endurance developmental testing will commence immediately thereafter to

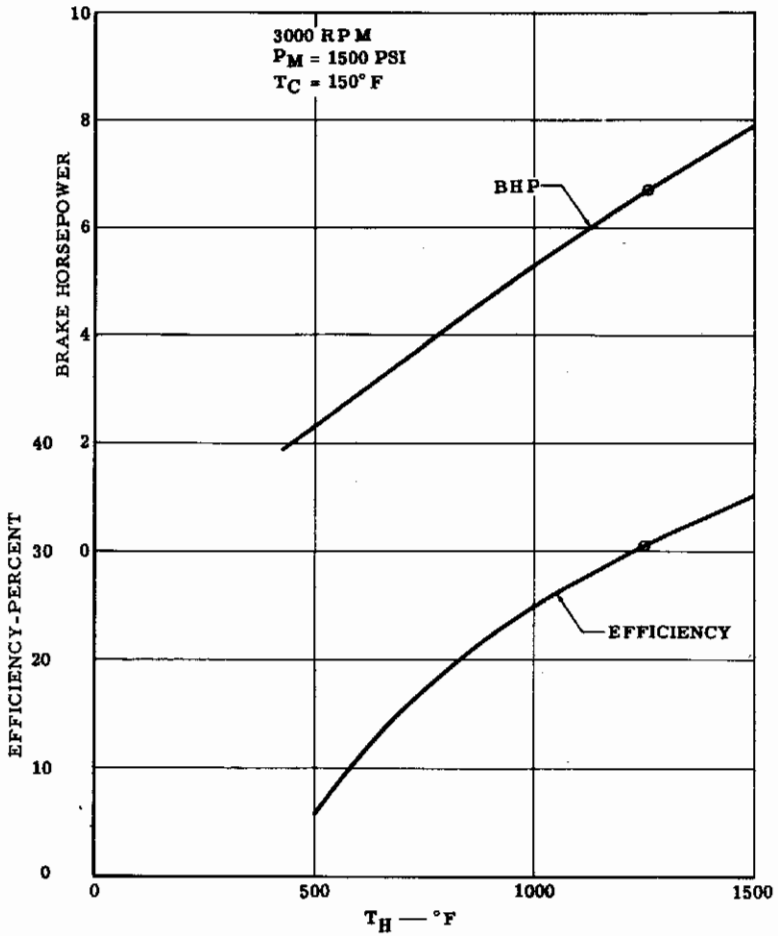

FIGURE. III-A-9 ESTIMATED EFFECT OF HEATER TEMPERATURE ON POWER AND EFFICIENCY OF THE ALLISON ADVANCED STIRLING ENGINE

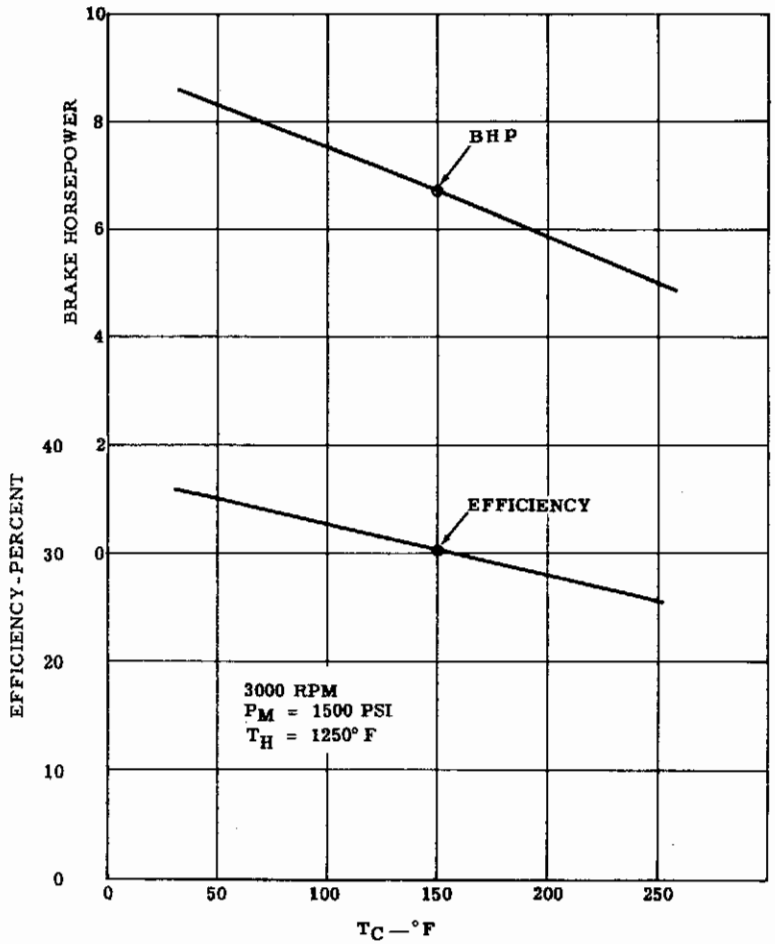

FIGURE III-A-10 ESTIMATED EFFECT OF COOLING TEMPERATURE ON POWER AND EFFICIENCY OF THE ALLISON ADVANCED STIRLING ENGINE

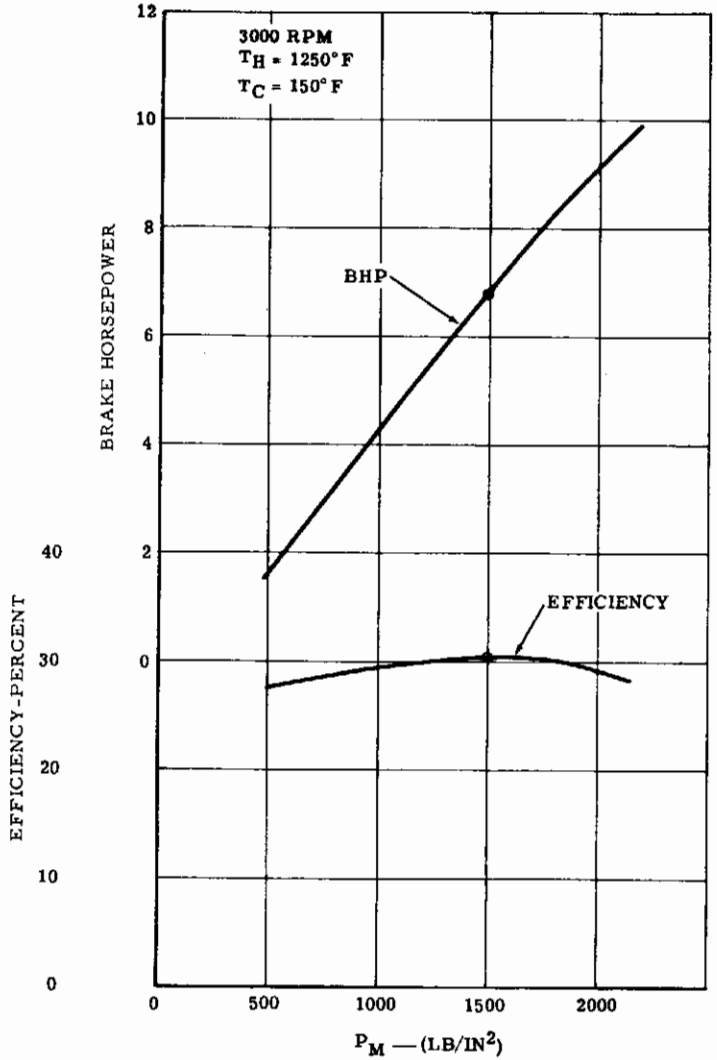

FIGURE III-A-11 ESTIMATED EFFECT OF MEAN CYCLE PRESSURE ON POWER AND EFFICIENCY OF THE ALLISON ADVANCE STIRLING ENGINE

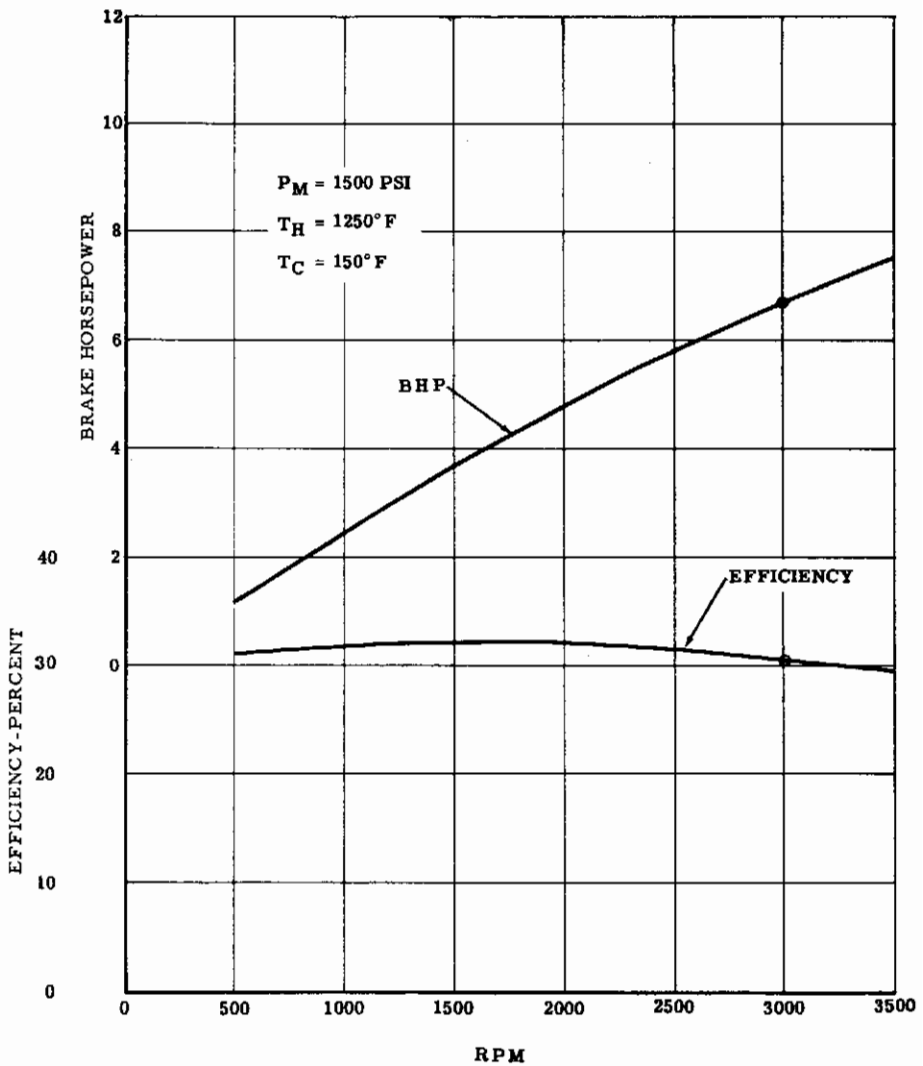

FIGURE III-A-12 ESTIMATED EFFECT OF SPEED ON POWER AND EFFICIENCY OF THE ALLISON ADVANCE STIRLING ENGINE

experimentally verify the predictions regarding engine performance, reliability, and suitability as a long-lived, unattended, space power system.

Until the endurance test program has been completed, it will not be possible to determine more definitely the feasibility of the Stirling engine for space application. The effect of certain sensitive areas must be determined prior to such a decision. The following subsections will delineate those portions of the Stirling engine which might possibly pose as major developmental areas to be resolved in the operating Stirling engine.

4.1 Seals

As mentioned previously, the regenerator is perhaps the most important system component to be considered in determining the actual operating efficiency of the Stirling engine. The fact that it stores six Btu per each Btu added externally during each cycle, causes any degradation in regenerator performance to degrade engine efficiency seriously. It appears that the major source of poor regenerator performance would be fouling by crankcase lubricant which might find its way to the area above the power piston. The most obvious areas for leakage of this lubricant to occur would be around the power piston-cylinder wall seal and the seal between the power piston and the displacer piston connecting rod.

Of these two possible sources of leakage, it appears that the more serious is that of the power piston-displacer piston connecting rod seal. Extensive testing is presently being performed by Allison to achieve absolute integrity of this seal, but a more quantitative estimate of its actual suitability must await the endurance development tests.

4.2 Zero Gravity Lubrication

Very little information is available regarding lubrication problems which might be imposed by a zero gravity environment. It is anticipated that a spray-mist type crankcase lubrication system will be utilized in the first Stirling cycle prototype, and concurrent theoretical and experimental evaluations will be made of this type lubrication to determine its applicability to the zero gravity environment. If it is determined that this type lubrication system is not feasible, it appears that a pressure type lubrication system, although perhaps somewhat more complex and heavier, would not encounter the zero gravity restrictions.

4.3 Vibration

Through extensive study and analysis, Allison feels confident that vibration problems will not be present in the existing engine. Tolerances of all engine parts have been held to 0.0001 inches. In addition, because of the intrinsic static and dynamic balancing capability of the Rhombic drive, it is felt that severe vibration problems will not occur. With any dynamic system, however, the possibilities of vibrations and unbalanced torque are present. The magnitude of these disturbing forces must be determined and matched to specific mission allowances prior to system selection.

REFERENCE LIST

III-A-1. Meijer, R. J. "The Philips Hot Gas Engine with Rhombic Drive Mechanism," Philips Technical Review, May 1959.

III-A-2. Flynn, Gregory, Jr. et al. "GMR Stirling Thermal Engine." Presented at the SAE Annual Meeting, January 1960. SAE Preprint No. 118A, January 1960.

III-A-3. Finkelstein, Ted. "Generalized Thermodynamic Analysis of Stirling Engines." Presented at the SAE Annual Meeting, January, 1960.

III-A-4. Finkelstein, Ted. "Optimization of Phase Angle and Volume Ratio for Stirling Engines." Presented at the SAE Annual Meeting, January 1960.

III-A-5. Staff of the Allison Division of General Motors. "Technical Proposal for Development of a Satellite Solar Secondary Power Plant," January 1959.

III-A-6. Staff of the Allison Division of General Motors. "Technical Proposal for Sunflower I Solar Power System," December 1959.

III-A-7. Allison Division of General Motors. "Design and Development of a 3 KW Stirling Cycle Solar Power Plant." First Semiannual Technical Summary Report, Engineering Report No. 1628.

ENERGY CONVERSION SYSTEMS REFERENCE HANDBOOK

Volume III - Dynamic Thermal Converters

Section B

TURBINES

R. Spies
Energy Research Division
ELECTRO-OPTICAL SYSTEMS, INC.

Manuscript released by the author
September 1960 for publication in this
Energy Conversion Systems Reference Handbook

WADD Technical Report 60-699

C O N T E N T S

CONTENTS (Cont.)

ILLUSTRATIONS

I L L U S T R A T I O N S (CONT'D)

I L L U S T R A T I O N S (CONT'D)

TABLES

B. TURBINES

In this section, attention is focused on the turbine engine, which is the primary converter in a power plant consisting of a heat source, a turbine for converting the energy to shaft work, an alternator for converting the shaft work to electrical energy, various condensers and heat exchangers, and controls. Figure III-B-1 is a schematic diagram of such a system.

1.0 THERMODYNAMIC CYCLE

The turbine may be employed in three types of systems. These are:

a. Open working cycle using a chemical energy source (e.g., hydrogen and oxygen) where the combustion products are eliminated overboard.

b. Semiclosed working cycles using a chemical energy source (e.g., hydrogen and oxygen) to heat the working fluid (e.g., a liquid metal) which passes through the turbine. These are often referred to as closed cycles, but it must be noted that the combustion products are still eliminated overboard.

c. Closed working cycles using nuclear or solar energy to heat the working fluid. Nothing is eliminated overboard. Either single or double loop systems may be employed. In the former, the working fluid of the turbines passes directly through the reactor core or solar absorber. In the latter, two loops are employed where the energy is transferred to the working fluid through a heat exchanger.

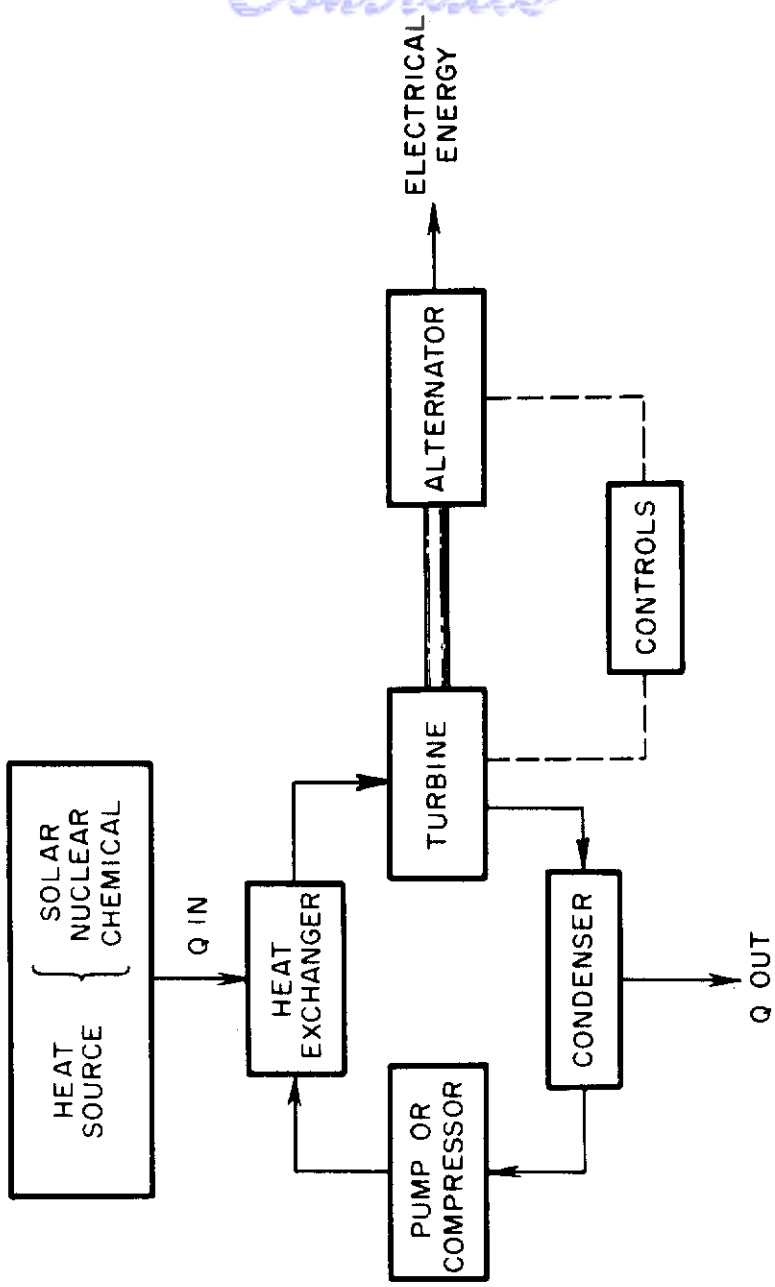

FIGURE III-B-1 TURBINE SPACE-POWER PLANT SCHEMATIC DIAGRAM

In the open cycle, the products of combustion are high energy, high-pressure gases which are expanded through a turbine. The system is sensitive to the exhaust pressure; and, in a vacuum, the

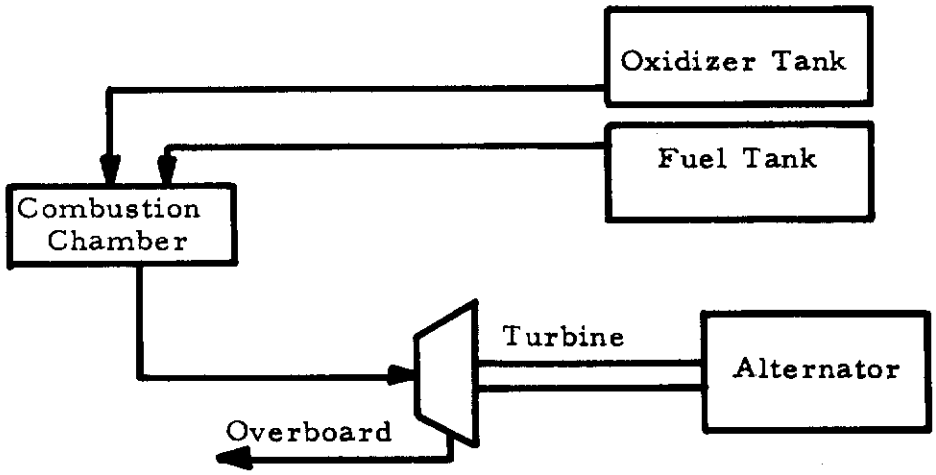

gas velocity in the turbine will be large because the expansion ratio is large. Basically, this cycle is useful in short term APU applications, as discussed in Volume VI.

Energy utilization in the open cycle is limited by the temperature at which the high-speed turbine can operate. If the cycle is modified by incorporating the turbine in a second closed loop, the combustion temperature can be greatly increased because the turbine working fluid can be much cooler to keep stresses low. The system is now a semiclosed one comprising an open chemical cycle and a closed working-fluid cycle. The combustion process now involves the evolution

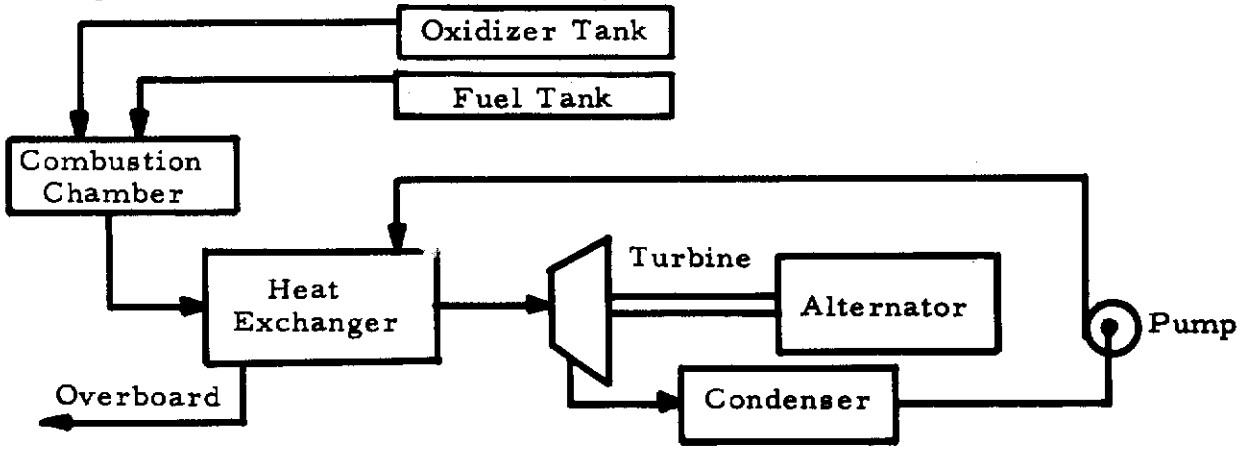

of heat rather than the creation of high-energy gasses; therefore selection of fuel and oxidizer may be different than from that in the open cycle. Any one of many fluids may be used in the closed loop section, although it is probable that a liquid metal suitable to work in a Rankine cycle would be employed.

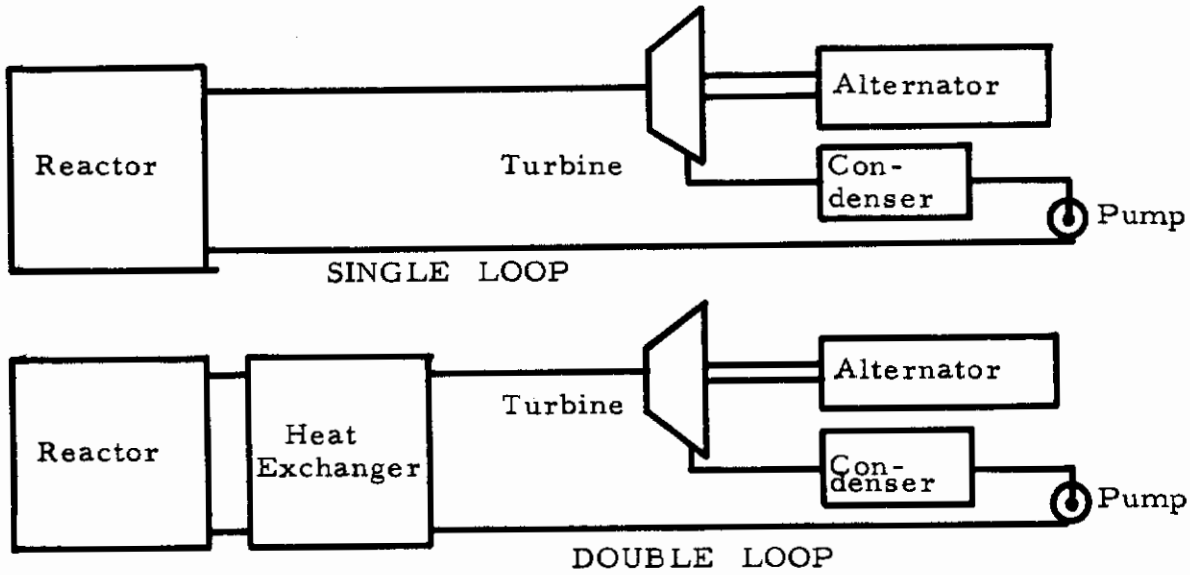

In space applications the problems are such that Rankine cycles seem more useful than Brayton cycles. Two basic variants of the Rankine cycle can be used, i.e., those with and without superheat. The choice is based mostly on whether expansion from the saturated state will yield a quality too low for efficient

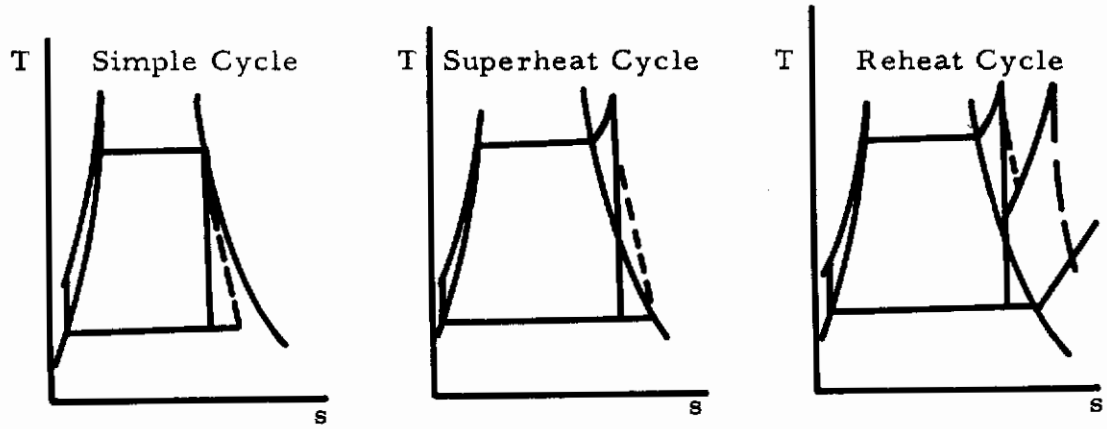

turbine operation because of droplet impingement. It should be noted that superheat must reduce the cycle efficiency, since all of the heat is not added at the peak cycle temperature. The temperature can be kept more uniform by staging the turbine (may not be desirable) and reheating. The problem of superheat and reheat is complicated by the need for an additional heat exchanger where energy can be added to the vapor. The heat-transfer coefficient will be low and large surfaces may be needed. While most space-power systems large enough to warrant a dynamic system will require a staged turbine, the heat exchanger weight may limit the utility of the superheat or reheat cycle. Heat exchangers are discussed in detail in Volume VII. Ref. III-B-1 has a detailed comparison of Rankine and Brayton cycles as they apply to turbine engine for space-power systems.

2.0 WORKING FLUIDS

Once it has been determined that the Rankine cycle is to be used in the space-power plant, the choice of working media narrows to fluids which are condensable at reasonable radiator-condenser temperatures. Liquid metals and certain types of organic compounds have been suggested, including the following:

a. Mercury

b. Rubidium

c. Potassium

d. Sulfur

e. Aluminum Bromide

f. Sodium

Figure III-B-2, taken from Refs. III-B-2 and III-B-3 shows a comparison of cycle efficiencies for some of these vapors.

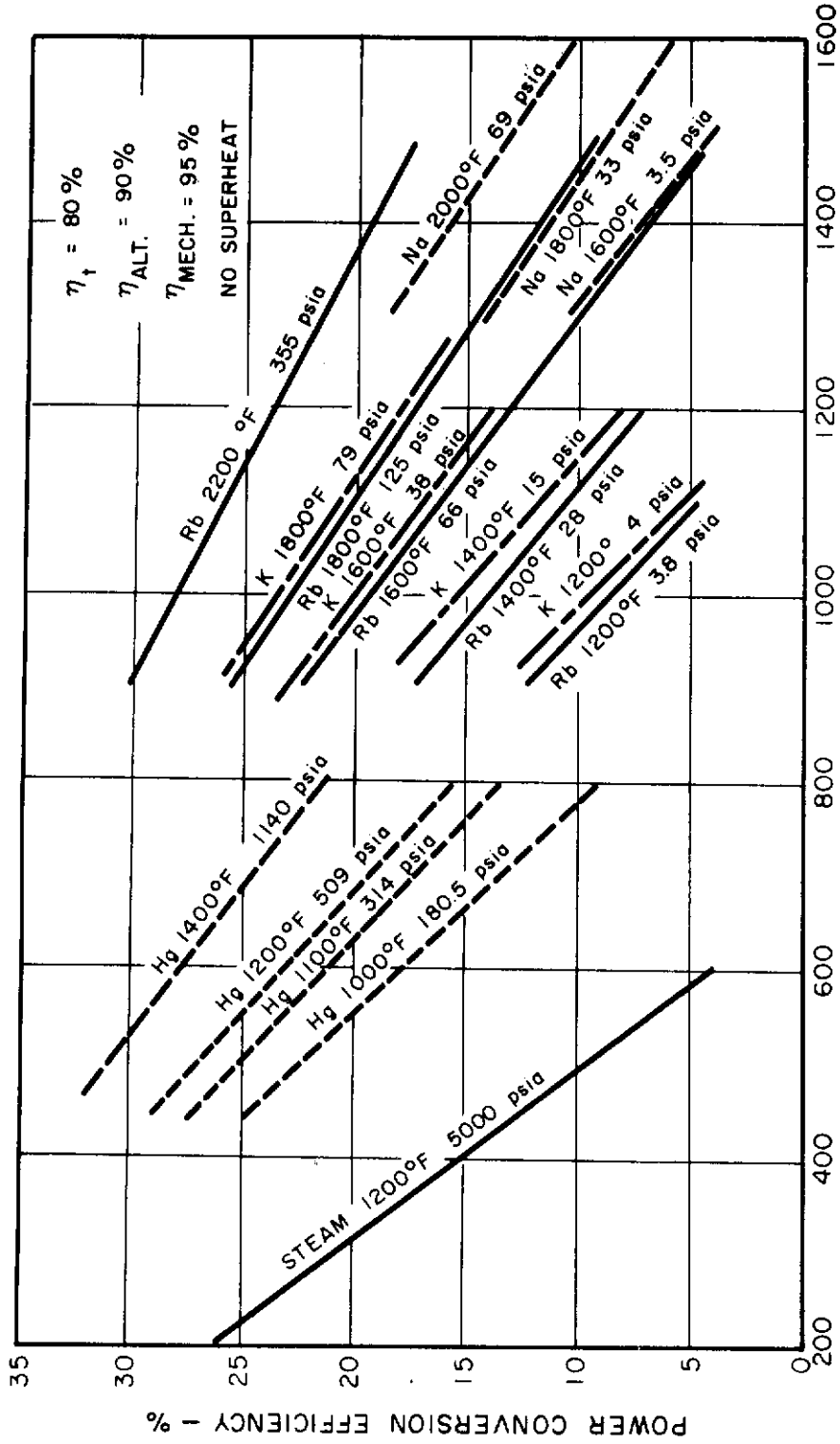

FIGURE III-B-2 COMPARISON OF RANKINE CYCLE WORKING FLUIDS

For efficient turbine performance, the ideal characteristics of the working fluid are as follows:

a. Referring to Figure III-B-3, it can be seen that it would be desirable to have the slope of the vapor dome nearly infinite, so that the normal expansion process would be along a line of constant quality. In this way, expansion from the saturated state results in a high quality at the exhaust, eliminating wet-vapor losses and erosion. If the slope is positive, superheated vapor results but there are some thermodynamic losses.

b. The vapor pressure should be low so that the stresses in the condenser and boiler tubes are low. The latter may result in some cavitation problems in the pump but these can be solved by jet pumps and inducers. (Volume VIII)

c. The specific heat of the liquid should be low. Since heat addition across a large temperature difference is highly irreversible and so associated with losses, the condensate should be raised to boiling temperature with a minimum of heat addition.

d. The fluid should be noncorrosive and nonpoisonous, so that it can be handled easily, storable for long durations, and relatively inexpensive.

The physical properties of various fluids usable for space applications are currently under investigation. Ref. III-B-4 is probably the most complete and up-to-date reference available. Corrosion studies are also being undertaken by various companies, but very few results have been published in the open literature. These properties are further discussed in Volume VII.

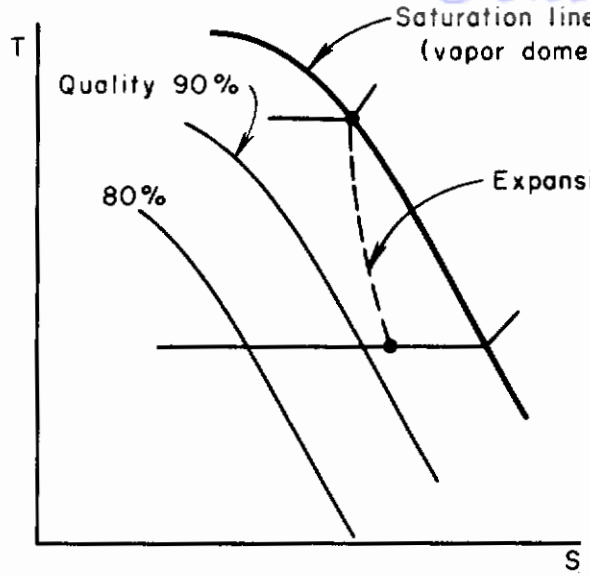

a. EXPANSION WITH FLAT VAPOR DOME. RESULTS IN LOW QUALITY.

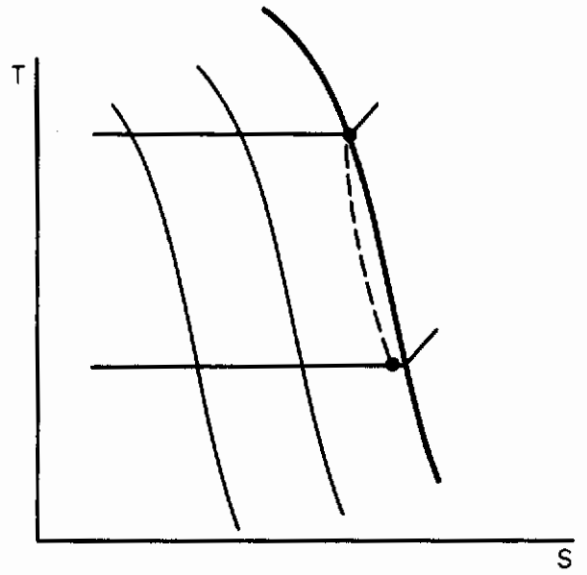

b. EXPANSION WITH STEEP VAPOR DOME. RESULTS IN HIGH QUALITY.

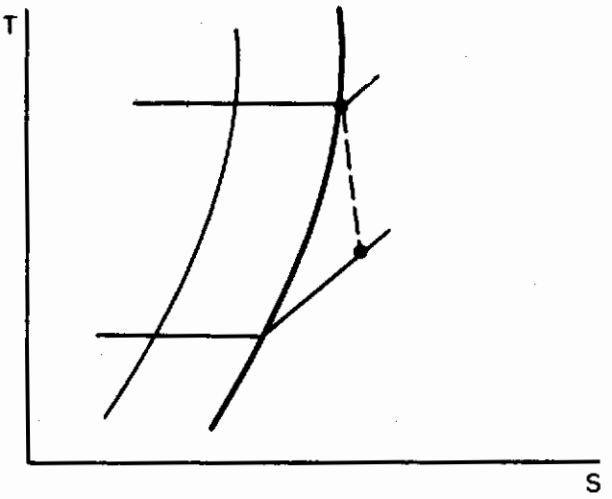

c. EXPANSION WITH VAPOR DOME WITH POSITIVE SLOPE. RESULTS IN SUPERHEAT.

FIGURE III-B-3 EFFECT OF VAPOR DOME SHAPE ON VAPOR QUALITY

3.0 TURBINE ENGINES

Since turbines have been built for many years, the basic art is well developed. However, in space systems some problems arise which have not been encountered before, and their solution requires unique turbines which have not been fully developed previous to the appearance of space-power systems. In the following subsections, each turbine type will be discussed with reference to space application. First, however, the various types of turbines which exist will be reviewed.

3.1 Turbine Types

It is usual to classify turbomachines by the principal direction of the flow through the machines. Thus, in particular, turbine types are classified as either axial-flow, radial-flow, or tangential-flow. Axial-flow turbines, which are by far the most common, are composed of two broad classes: reaction turbines and impulse turbines. As a general definition, reaction turbines expand the working fluid in both the stator and the rotor, whereas impulse turbines restrict the fluid expansion to the stator. Turbines may also be staged, i.e., two or more turbines may be used in series. Two types of staging are used--velocity staging and pressure staging. The impulse turbine may have stationary nozzles over the whole periphery or over only part of the periphery, i.e., full admission and partial admission.

The radial-flow turbine is a type of reaction turbine and may be either radial inflow or radial outflow. Of turbines designed in this manner, radial inflow is more common, since flow separation within the rotor passages is less likely to occur.

Tangential flow turbines are also known as drag, vortex, or regenerative turbines. The flow is admitted at one port located along the

periphery and flows primarily in a tangential direction around the turbine to an exit port located about 300° from the inlet. A block seal separates the inlet and outlet ports. Drag turbines are named after their originators, e.g., the Tesla Turbine, the Balje Turbine, and the Silvern Turbine.

3.1.1 Axial-Flow Turbines

In the impulse turbine, the expansion of the working fluid takes place in a stationary nozzle generating a high-speed jet. This jet is ingested by a rotating blade row and turned through an angle of 120 to 140 degrees. In the true reaction turbine, the expansion takes place in a rotating nozzle mounted on the rim of the turbine wheel. In practice, neither pure impulse nor pure reaction turbines are used, but expansion takes place in both a stator and a rotor. The relative amount of expansion occurring in the rotor is termed the percent reaction, defined as

$$\text{Percent R} = \frac{\text{Static enthalpy change across rotor}}{\text{Total enthalpy change across turbine}} \times 100.$$

From this definition, it is clear that a pure impulse turbine has zero percent reaction and that a pure reaction turbine has 100 percent reaction. It can be shown that, for a given head to be expanded (i.e., enthalpy change across the turbine), the wheel tip speed needed for peak efficiency is increased as the reaction increases. However, the value of the peak efficiency also improves as reaction is increased. In selecting a turbine design, the mechanical considerations due to high tip speed must be balanced against the performance gain to be obtained by increasing reaction.

When the power output is small and available enthalpy drop large, the volume-flow rate is usually small. The required flow area is, therefore, small--meaning that the height of the blade row and the diameter of the wheel are reduced. There is, of course,

a practical limit to this reduction. As the turbine size decreases, clearances reach a minimum value governed by fabrication considerations, and any further decrease in size will cause a decrease in efficiency because of increased leakage. Another technique for reducing the flow area is therefore used. In partial admission turbines the number of nozzles is reduced, and flow is admitted over only a portion of the wheel's periphery. However, partial admission introduces other types of losses. Basically, these are associated with the need to accelerate the fluid trapped in the blade passages as this relatively stagnant fluid re-enters the nozzle arc. References III-B-5 through III-B-9 discuss these losses and show how to analyze partial-admission turbines.

Partial-admission turbines must be of the pure impulse type. Since there is no flow through the blades over part of the wheel's periphery, no pressure difference can be sustained across the turbine wheel. Expansion in the moving blades is, therefore not possible.

3.1.2 Radial-Flow Turbines

In the radial-flow turbine, the flow is introduced at the rim of an impeller and ducted radially inward to a center eye, where it leaves the wheel. In effect, this turbine looks and acts like a centrifugal compressor operating in reverse. Although it is possible to design a turbine with the flow directed radially outward, separation of the flow from the blade passage walls is more likely to occur; therefore, the inflow configuration is preferred.

The main attribute associated with this turbine type is its ability to operate effectively over a wide range of flow rates, a characteristic which makes this turbine attractive for application where

off-design operation is important. Figure III-B-4, taken from Reference III-B-10, shows this effect as the nozzle area is varied. However, in present space-power systems, the operation should always be near the design point. Consequently, the use of the radial-flow turbine is currently limited. As more sophisticated power systems are needed in space, radial-flow turbines will be used more widely.

The general operating regime for radial-flow turbines is similar to that for the 50-percent reaction turbine. These turbines, therefore, are less suitable at power levels and conditions which are proper for impulse turbines, although their use is often advocated. In Reference III-B-11, it is shown that the radial-flow configuration would have a wheel diameter approximately 12 percent greater than that of the comparable axial-flow machine. This characteristic is a disadvantage, because space-power systems are usually limited in the volume available. Since the number of blades is small, radial-flow turbines are unsuitable for partial-admission applications, unless the ratio of outer-to-inner diameter is nearly unity. In that case, they can be analyzed much like axial-flow machines. Details of radial-turbine performance can be found in References III-B-10 through III-B-16.

3.1.3 Tangential-Flow Turbines

When the flow rate is low and the available energy large, none of the turbine types discussed above are useful. For example, the losses in the partial-admission turbine become so large that the efficiency is prohibitively low. In contrast, however, the tangential-flow turbines are particularly useful in this range.

Until very recently, the design of this turbine type was mostly empirical. In fact, the exact mechanism of the energy

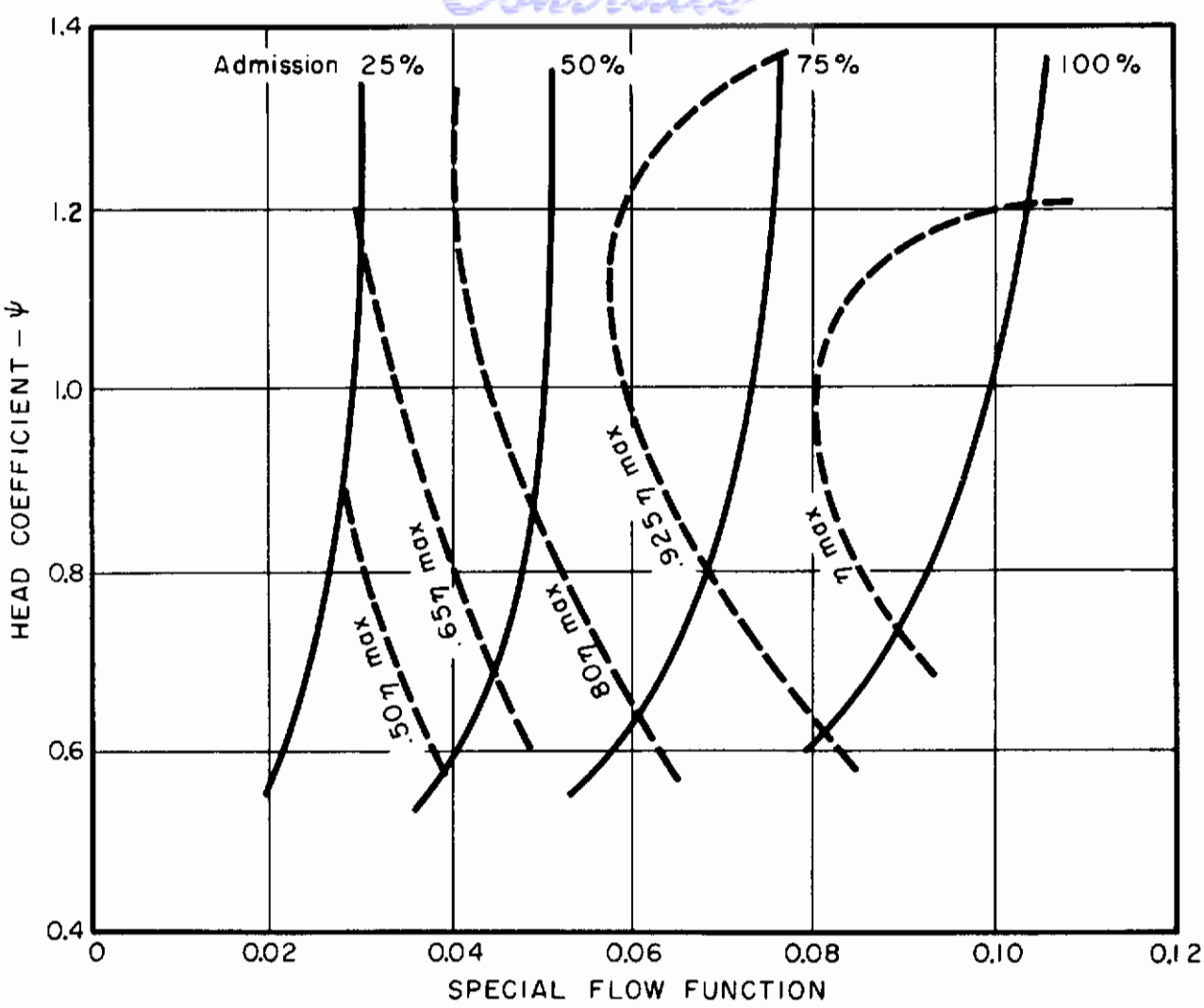

FIGURE III-B-4 PERFORMANCE CURVE FOR RADIAL-FLOW TURBINE

transfer from the fluid to the wheel was not well understood. In the simplest designs (Fig. III-B-5), the fluid injected into the turbine case flows in the peripheral direction and emerges from a port located approximately 300 degrees from the inlet. A block seal separates the inlet and outlet. As the fluid traverses the periphery, it drags the turbine wheel along with it. Thus, this turbine was often called the drag turbine. This description of the turbine is, essentially, one dimensional. The drag can therefore be expressed as a fraction of the relative velocity past the rotor defining an equivalent friction coefficient (Ref. III-B-17). Spies showed in Ref. III-B-18 that both the torque and the pressure distribution in the turbine could be predicted in this way and that, using a compressible fluid, it is beneficial to expand the throughflow area in the turbine to keep the throughflow velocity constant. The efficiency is improved quite markedly by this technique.

In an effort to increase the power output from this turbine, different "blade" shapes were tried by many investigators. The conclusion was that the rounded blades shown in Fig. III-B-6 (which compares various blade shapes tried) were best (Ref. III-B-19). It is to be noted that all these results are empirical and many are based on labyrinth-seal theory. As a result of studies undertaken under ONR contract NOnr 2292(00), the development of the tangential-flow turbine has been extended. Silvern (Ref. III-B-20) analyzed the flow, not on the basis of the one-dimensional flow model but in the light of the complex recirculatory flow which was found to be present and which had been predicted by Wood in Ref. III-B-21. A new variation of the tangential-flow turbine built on this principle was tested and showed very high efficiency. Full details on this turbine may be found in Ref. III-B-22.

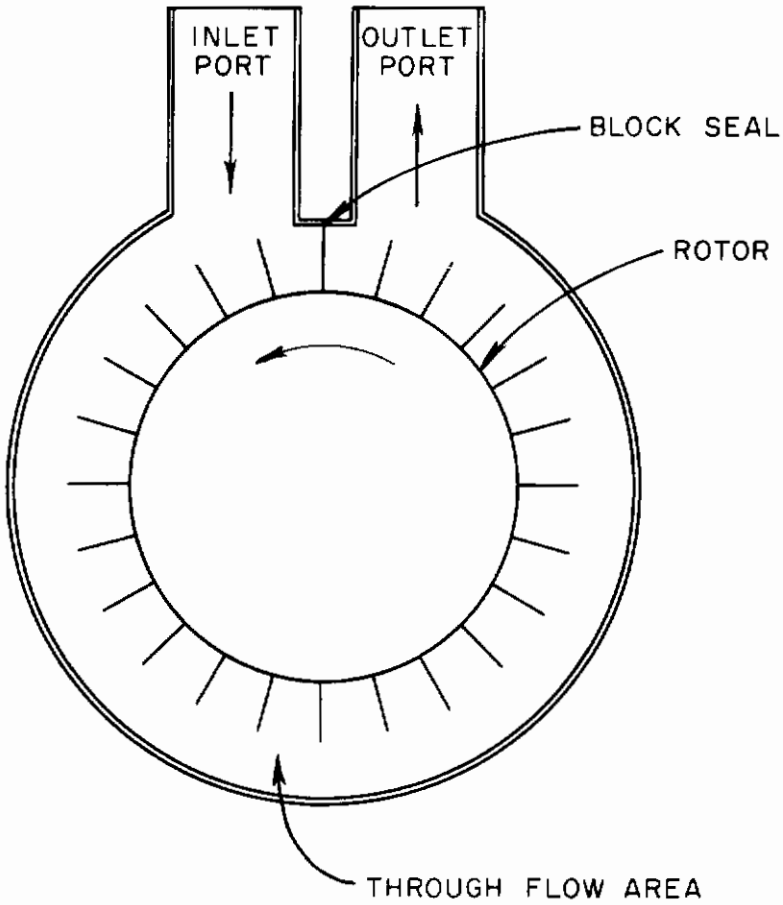

FIGURE III-B-5 TANGENTIAL-FLOW SCHEMATIC OF TURBINE

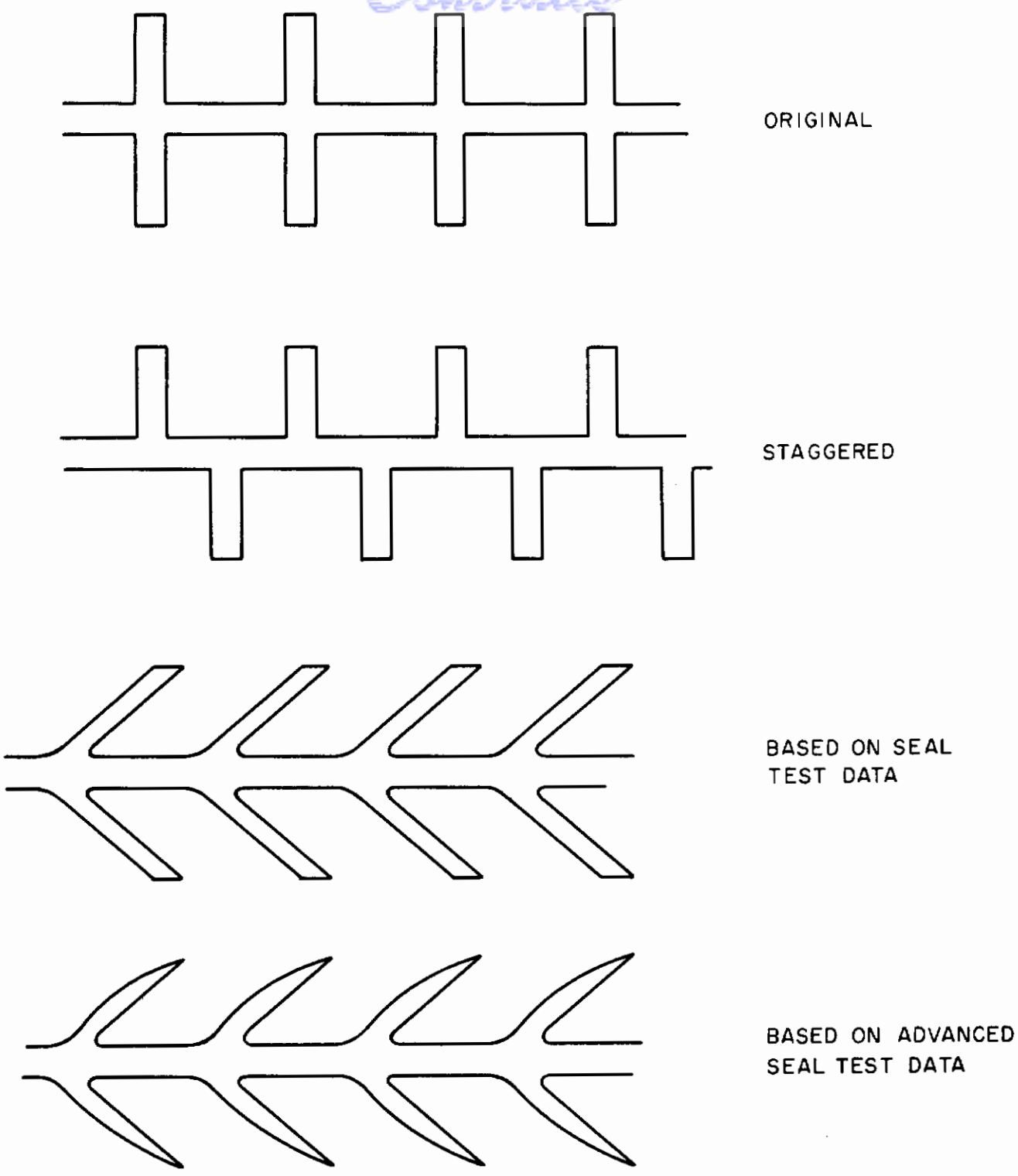

FIGURE III-B-6 DRAG TURBINE BLADE DEVELOPMENT

For space applications, the power range over which a tangential-flow turbine operates best is outside the regime in which single-stage turbomachines may be expected to be employed. However, application may be found as one stage of a multistaged space turbine. Tangential-flow turbines have also been proposed as an answer to the problem of wet-vapor operation. Ordinarily the expansion of a vapor in a turbine may result in droplets of condensed liquid. These drops could cause blade damage and/or efficiency loss. In the tangential-flow turbine, a particle of fluid exchanges momentum with the wheel many times, and as a consequence the turbine is, in effect, pressure staged. As the droplets form, they may be centrifuged to the other rim of the turbine where they can be collected and removed, thereby preventing further damage due to their presence. This feature is discussed in detail in Ref. III-B-23 where some experimental verification of this theory is presented. If the theories stipulated can be verified completely, tangential-flow turbines may find application in space power systems using vapor.

3.2 Method of Performance Presentation

The performance of a particular turbomachine is usually presented by showing how some function of the head expanded or produced varies as the flow changes at constant rpm. For pumps, head and capacity are plotted directly; for compressors and turbines, non-dimensionalized head and capacity coefficients are used. Very often compressor and turbine maps are presented by plotting pressure ratios, p/p_{∞} against a "nondimensional" flow rate (the quantity has dimensional units even though specified as nondimensional) $\frac{\dot{w}\sqrt{T_{\infty}}}{p_{\infty}}$ or corrected flow rate $\frac{\dot{w}\sqrt{\theta}}{\delta}$, where θ is the corrected temperature

and δ is the corrected pressure. Usually lines of constant efficiency can also be shown. For turbines, the flow is limited when the nozzle chokes, and so the use of flow for the abscissa must be restricted to subsonic turbines to be significant.

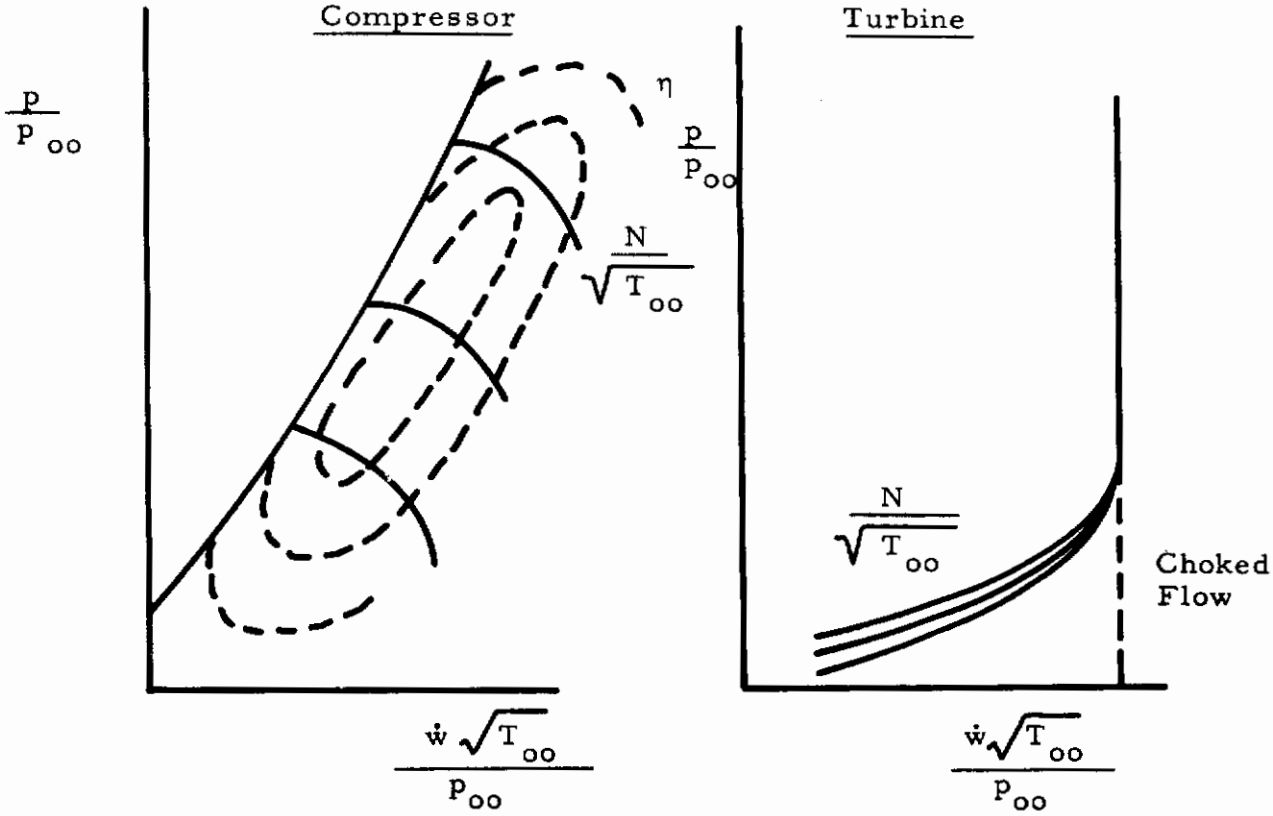

Various other combinations are therefore used for the presentation of performance of a particular turbine. Most usual among these is a graph of turbine efficiency against the velocity ratio u/c_o where u is the wheel-tip velocity and c_o is the theoretical spouting velocity of the gas.

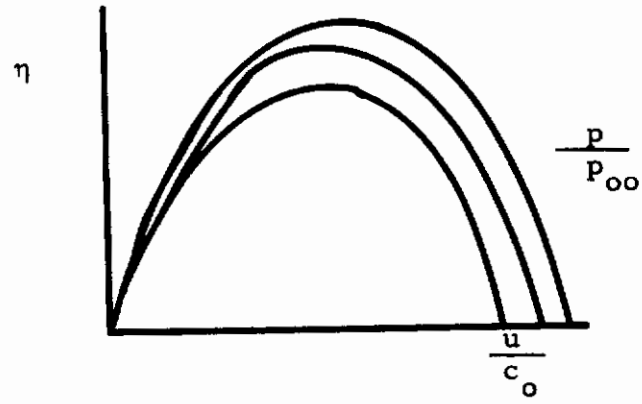

$$c_o = \sqrt{2 g H}$$

where H is the head due to isentropic expansion. Usually the efficiency depends on the pressure ratio.

It is important to recognize that various definitions of efficiency are employed in turbine performance presentations. The terms "total-to-static efficiency" and "total-to-total efficiency" are often found. Efficiency, by its very meaning, is the ratio of something achieved to what could have been achieved in an ideal process. In the case of a turbine, the efficiency is the work actually obtained divided by the work obtained in an ideal (adiabatic, reversible) expansion. The latter is, of course, dependent on the pressure ratio. Adiabatic head determined from the ratio of the actual total pressure will differ from that determined from the ratio of actual static exhaust to total inlet temperature. The use of total-to-total efficiency is justified only if the turbine has a pressure equal to the total pressure at the exhaust (i.e., when the kinetic energy of the leaving gas is converted to pressure in a suitable diffuser). If a diffuser is not used, total-to-static efficiencies are more meaningful. The difference between the two efficiencies can be seen in Fig. III-B-7 where they are shown as a function of specific speed which is defined below.

When the interest shifts from a study of a particular machine to a whole class of machines, similarity parameters are used. In Ref. III-B-20, a dimensional analysis is performed which shows that the significant parameters are as follows:

Specific Speed, N_s

Specific Diameter, D_s

Mach Number, Ma

Reynolds Number, Re

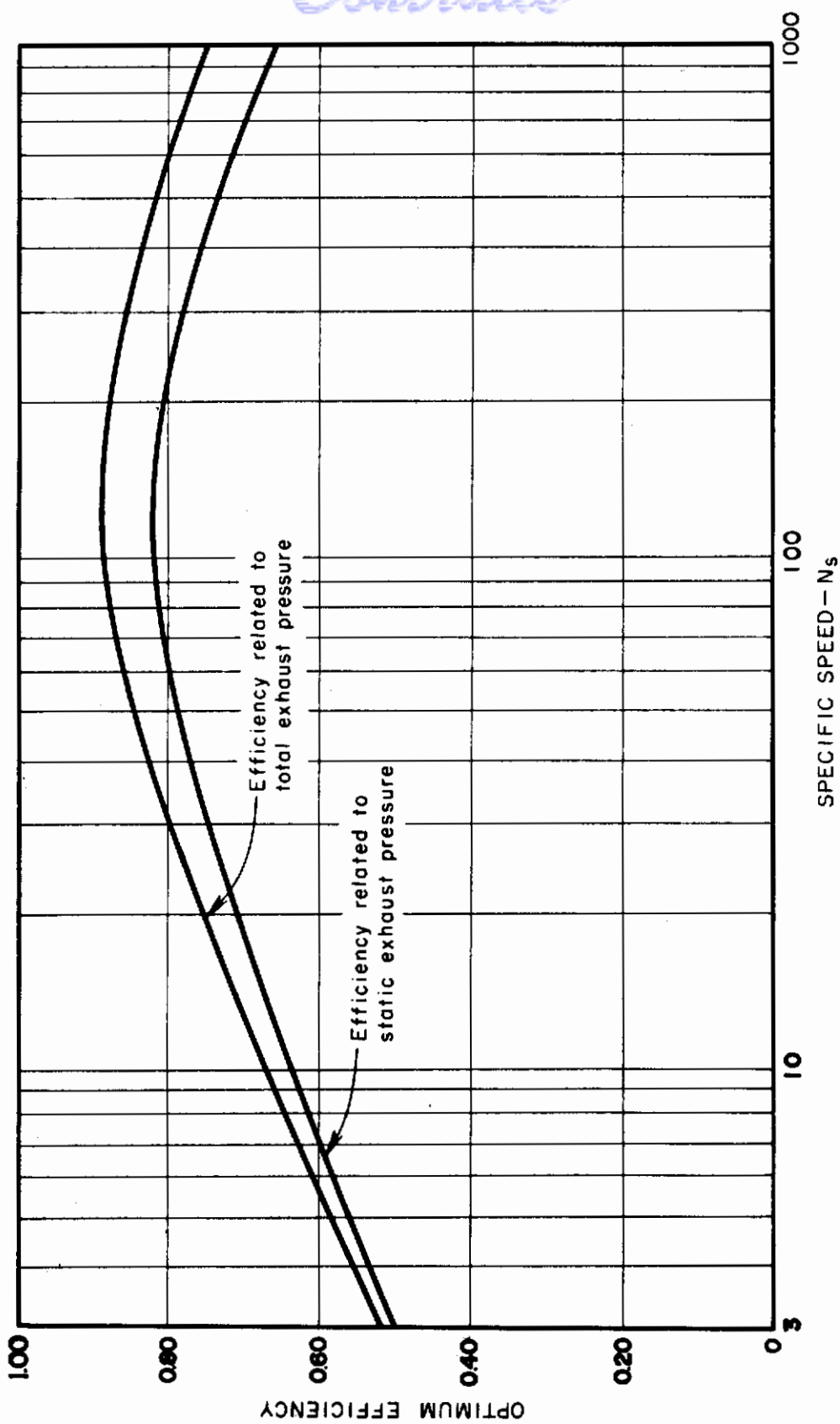

FIGURE III-B-7 OPTIMUM EFFICIENCY, AXIAL-FLOW TURBINE

For machines handling incompressible fluids, the ThomaParameter, σ, replaces the Mach number. Specific speed and specific diameter are defined as

$$N_s = \frac{N\sqrt{Q}}{H^{3/4}}$$

$$D_s = \frac{D\,H^{1/4}}{\sqrt{Q}}$$

where

N = rotative speed, rpm

Q = maximum volume - flow rate, cu ft/sec

H = head due to isentropic expansion (or compression), ft

D = wheel diameter, ft

Specifically, Linhardt and Silvern show in Ref. III-B-9 that upon analysis of all the losses, the maximum efficiency for partial admission impulse turbines is

$$\eta_T = \frac{N_s D_s}{77}\underbrace{\left\{1+\psi_R\left(1-D_s^2 \sin \frac{2\psi_N\sqrt{2g}}{D}\frac{h}{D}\frac{\pi}{2Z}\right)\right\}\left\{\psi_N \cos\alpha_2 - \frac{N_s D_s}{154}\right\}}_{\text{Hydraulic Efficiency}} -$$

$$\underbrace{\frac{N_s^3 D_s^5}{154^3}\,1.4\sqrt{2g}\left(\frac{c}{D}\right)\left(\frac{h}{D}\right)}_{\text{Scavenging Loss}} - \underbrace{\frac{2N_s^3 D_s^5}{154^3}\left\{K_W + K_p\left(1-\frac{1}{D_s^2\, h/D\,\pi \sin\alpha_2 \psi_N\sqrt{2g}}\right)\left(\frac{h}{D}\right)^{1.5}\right\}}_{\text{Disc Friction and Pumping Loss}}$$

It is easily seen that the maximum turbine efficiency is a function of N_s, D_s, factors dependent on Ma and Re, and the geometric ratios. For this reason, it is possible to show a diagram (Fig. III-B-8*) giving all the

* Only skeleton diagrams are shown in this report. For design purposes, reference to the original material is recommended.

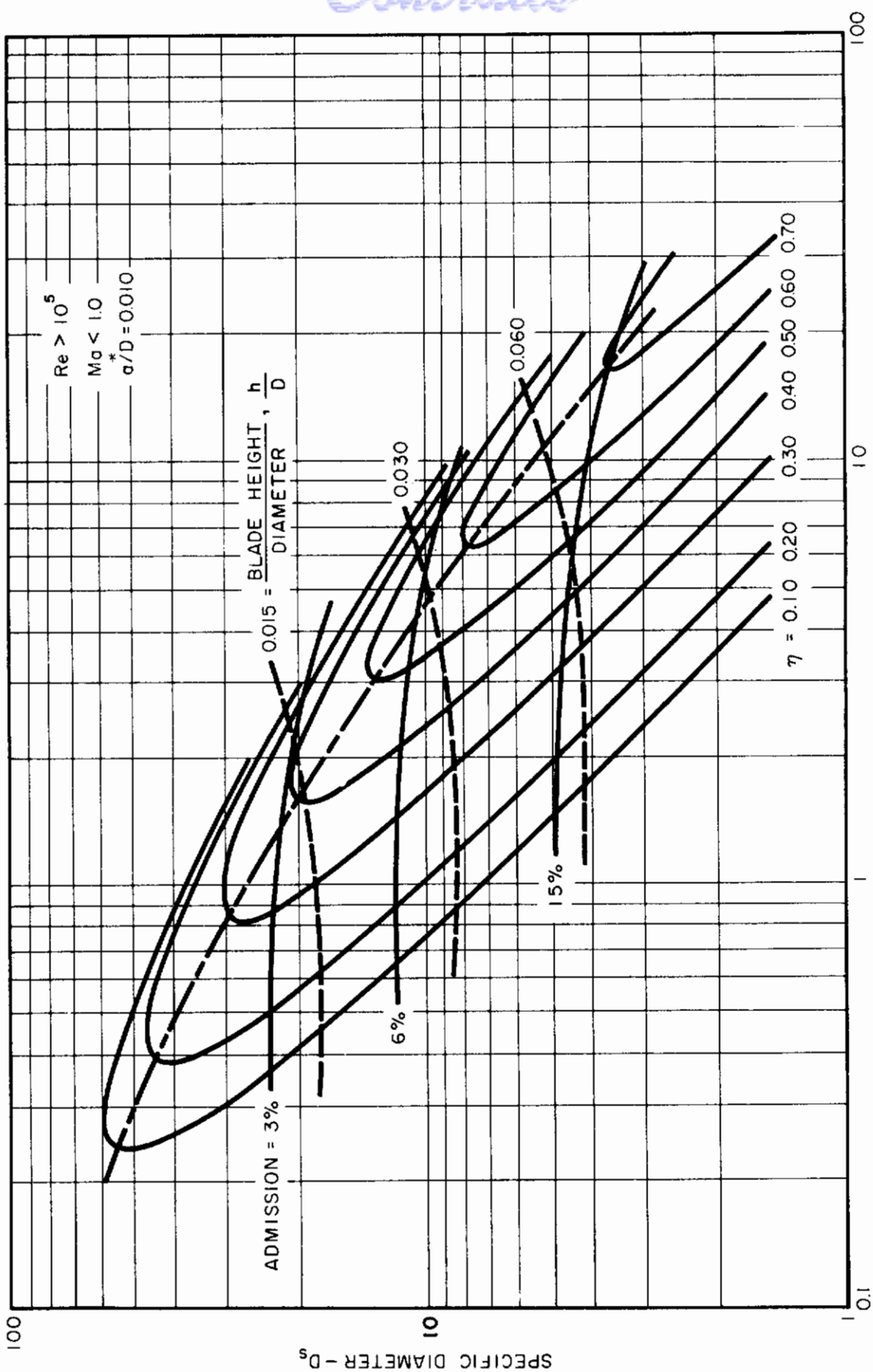

FIGURE III-B-8 N_S-D_S DIAGRAM FOR PARTIAL-ADMISSION, AXIAL-IMPULSE TURBINE

geometric ratios and the maximum efficiency for various values of N_s and D_s. It must be remembered that this diagram is for a class of similar machines (similarity parameters are used), and that other N_s - D_s diagrams must be drawn for other turbines, e.g., drag turbines, reaction turbines, etc. A comparison of the various diagrams should then reveal the best turbine to use in any application.

Upon inspection of the N_s - D_s diagram, it is found that for each value of specific speed there exists a particular value of the specific diameter where the efficiency is greatest. This, then, is the point defining the geometry of the best turbine for that specific speed. The line connecting these optimum points can be cross-plotted on coordinates of η vs. N_s, which will show the regimes of operation for various turbine types. Figure III-B-9 gives such a comparison.

The value of data presentation on N_s - D_s coordinates is in the availability to the designer of a chart which shows him the geometric values (e.g., blade height/diameter or percent admission) to use in a design. The charts are valid as long as the loss coefficients used in their derivation are valid. When the values of the loss coefficients are better defined, better N_s - D_s diagrams can be drawn.

3.3 Selection and Design of Space Turbines

The aim of the turbine designer is the same for space application as it is for ground application. He must select a specific type and then design an effective turbine to produce power for a specified time. For space application, the designer will emphasize size and weight rather than cost or, perhaps, efficiency.

3.3.1 Selection of a Turbine Configuration

The selection of a specific turbine configuration

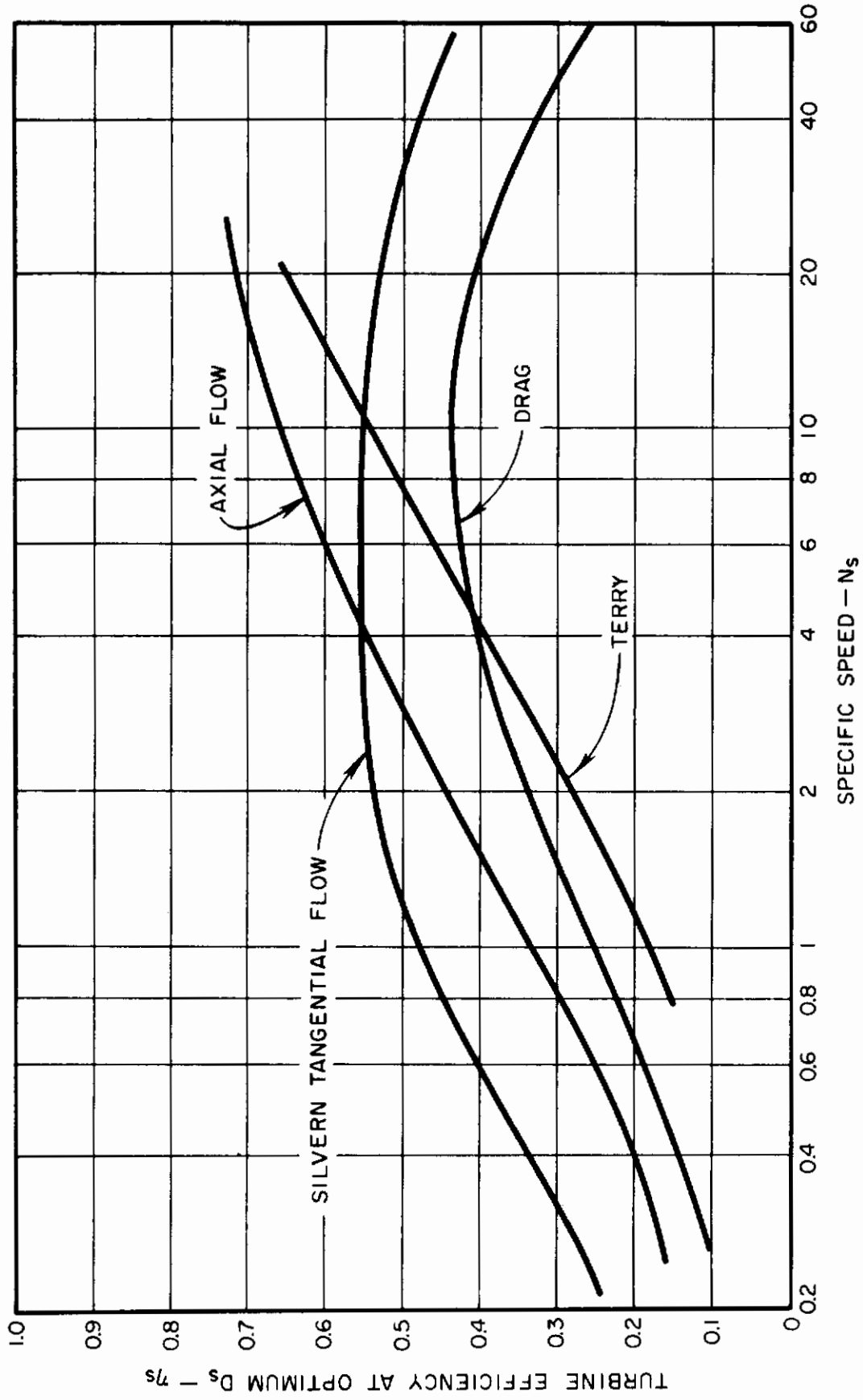

FIGURE III-B-9 MAXIMUM EFFICIENCY FOR OPTIMUM TURBINE DESIGNS

is based not only on considerations of power and speed but also on many factors involving the working fluid and the available energy. In all applications other than those involving very low power levels, the use of staged turbines will be required. It has already been shown that the efficiency of all turbines is dependent on the ratio of wheel-tip speed to spouting velocity, u/c_o. A performance summary is presented in Figure III-B-10 taken from Ref. III-B-8 for various turbines with friction losses and a nozzle angle of 20^o. When the available energy per pound of working fluid is large, the spouting velocity is large. Therefore, because the tip speed is often limited by stress considerations, the ratio u/c_o may, of necessity, be limited to a value of 0.2 or less. When this limitation occurs, multi-stage turbines can be used to improve efficiency. If pressure staging is used, the enthalpy drop in each stage is a fraction of the over-all enthalpy drop for the turbine, and the u/c_o for each stage is higher than the u/c_o for a single-stage turbine. Figure III-B-11 shows, as an example, that the optimum efficiency for an axial-staged turbine increases as u/c_o is raised, so that the efficiency of the staged turbine may be expected to be increased.

In velocity staging all the enthalpy drop is taken in the first stage, but the use of two or more wheels allows the tip speed to be reduced. This reduction means that even though the turbine is operating at a u/c_o much less than that of a single-stage turbine, some of the energy which would be lost at the exit is recovered and the efficiency is kept high. In Figure III-B-12, the velocity diagrams for the staged turbines may be compared to the single-stage case for equal over-all enthalpy drop at peak efficiency. The effect on u/c_o is evident.

It might be noted in Figure III-B-10 that the peak efficiency of the staged turbine is less than the peak efficiency of the single-stage machine--a result of the increased losses associated with flow through more than one blade row.

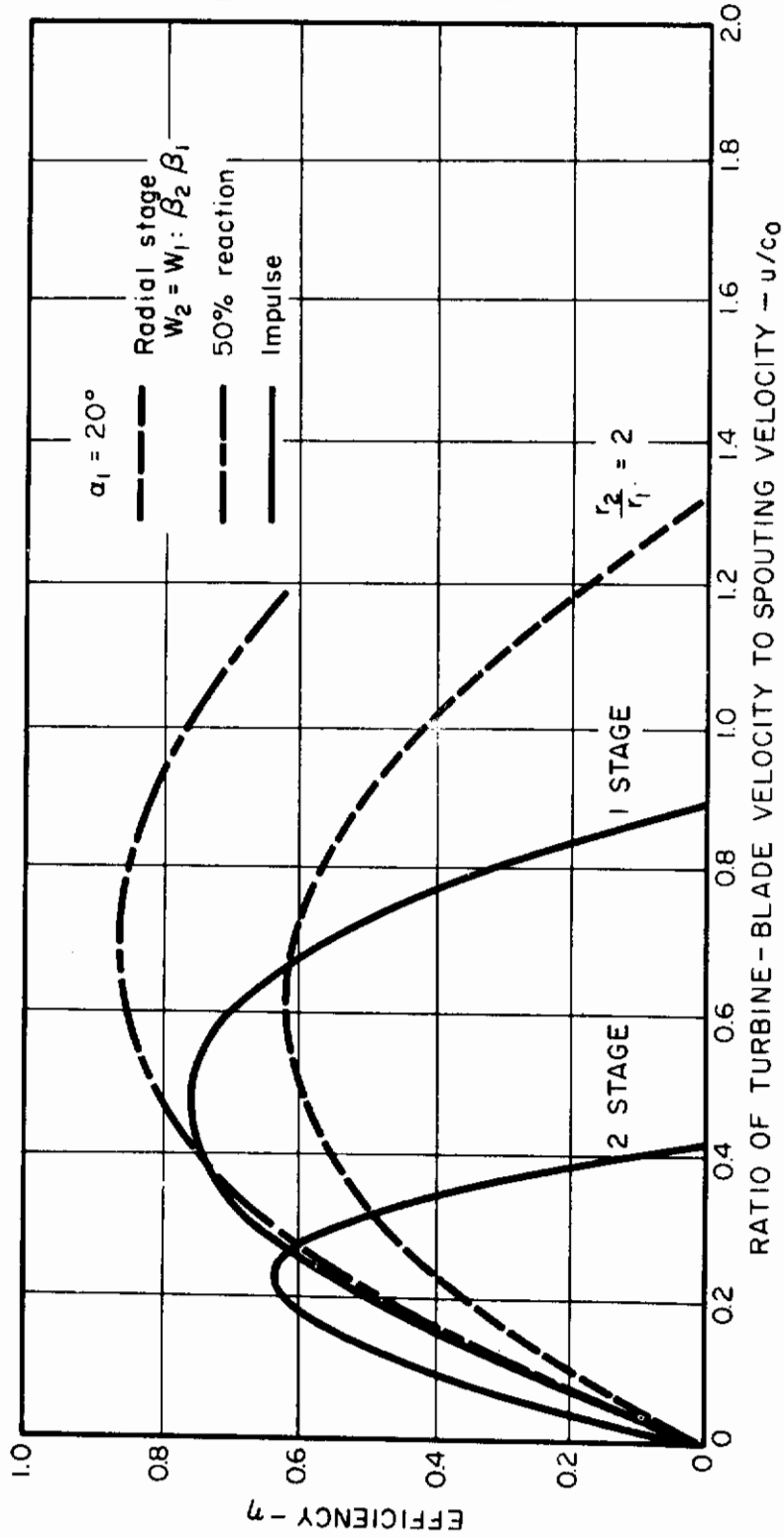

FIGURE III-B-10 EFFICIENCY FOR SEVERAL TURBINE TYPES WITH NOZZLE ANGLE OF 20° AND FRICTION LOSSES

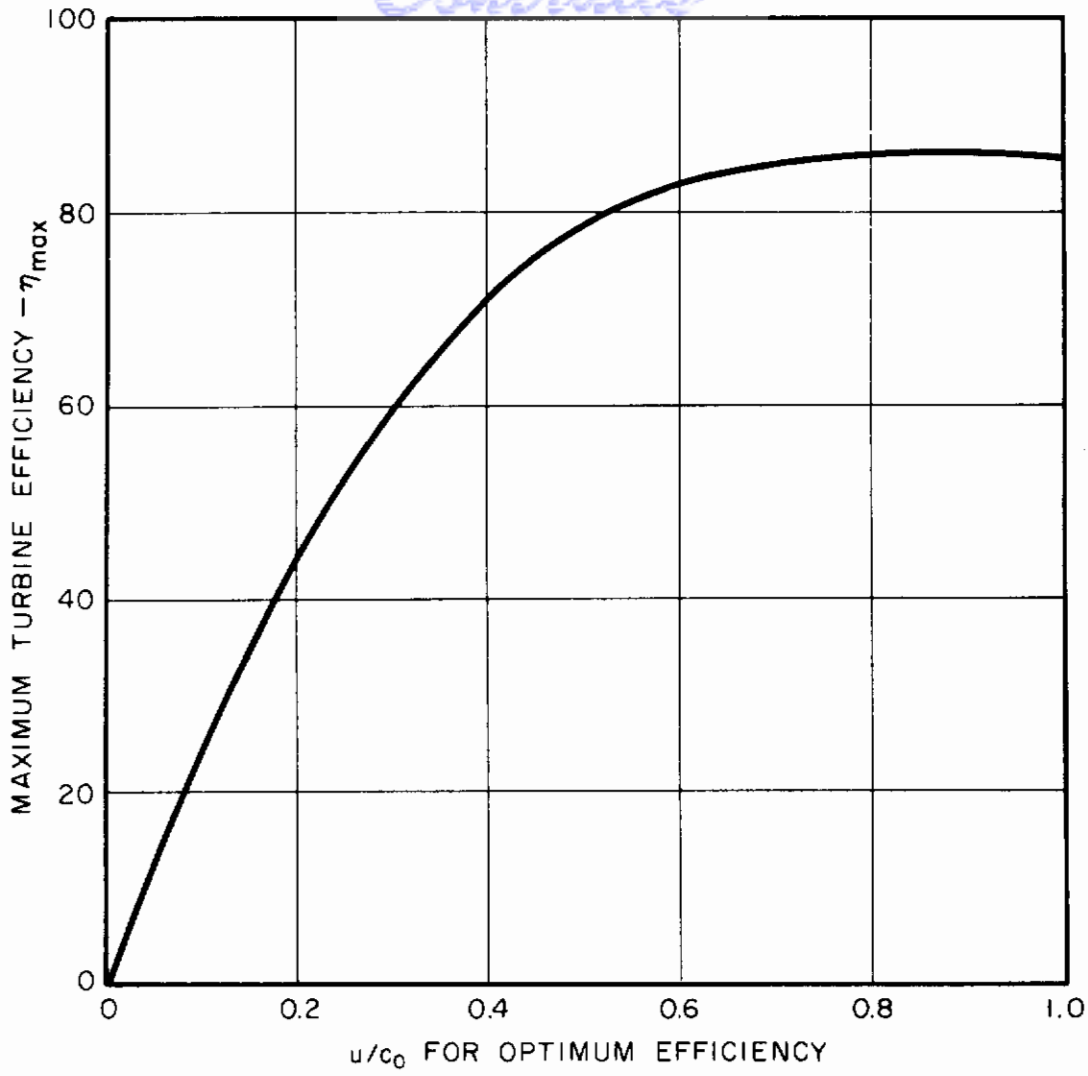

FIGURE III-B-11 MAXIMUM EFFICIENCY ATTAINABLE AT ANY SPEED RATIO - AXIAL-FLOW TURBINES - SINGLE DISC

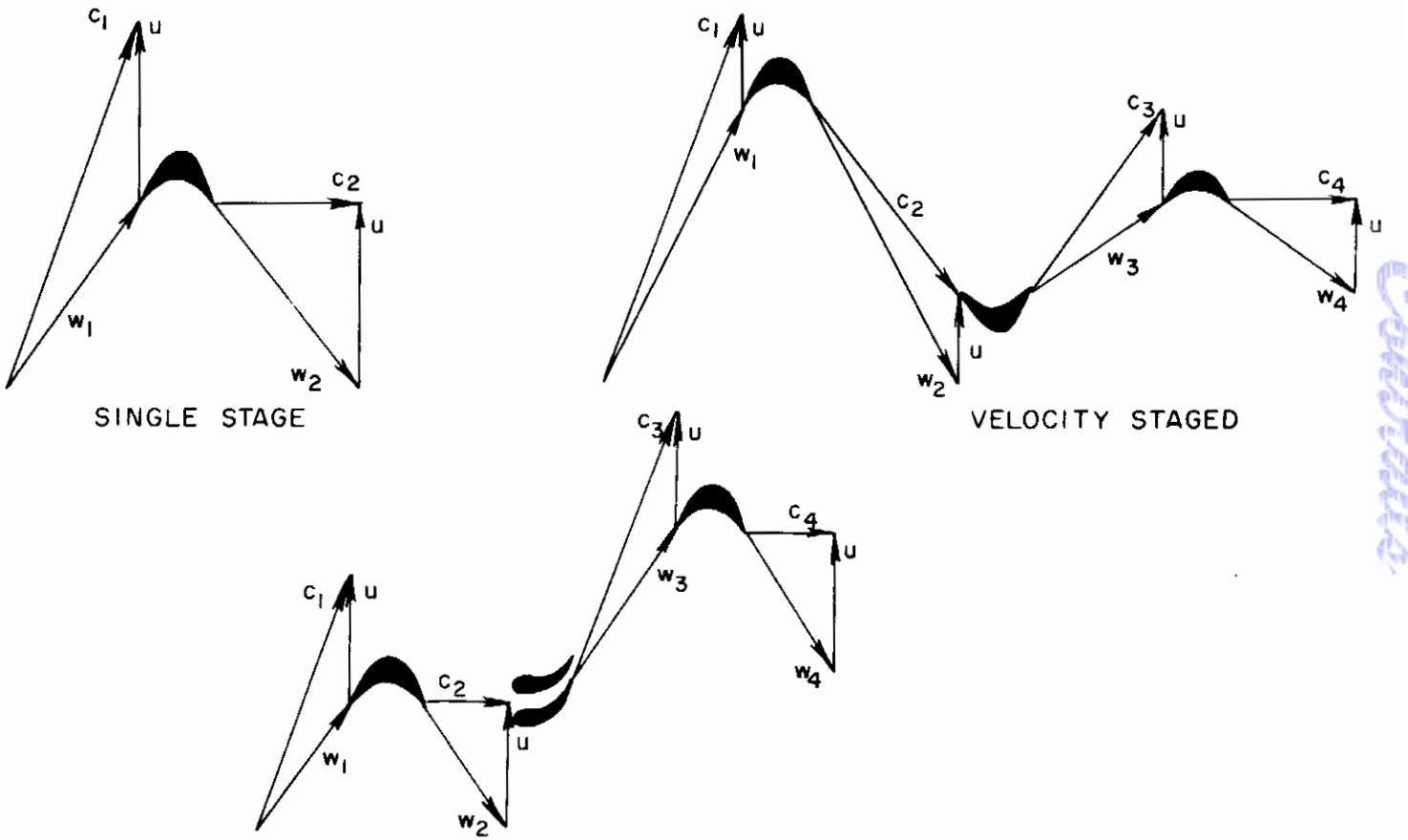

FIGURE III-B-12 VELOCITY DIAGRAMS FOR STAGED TURBINES TOTAL ENTHALPY DROP CONSTANT

If the flow rate is low enough, each of the stages of a multistaged turbine may require only partial admission. In that case, some losses can be eliminated if one wheel is multistaged by letting the flow re-enter. This turbine type has been analyzed in Reference III-B-9, and the expected efficiency is shown in Figure III-B-13. The distribution of enthalpy drop between the stages was also investigated. Its effect on efficiency is shown in Figure III-B-14.

A special type of velocity staged turbine is the Terry turbine, which is described in detail in Reference III-B-20. It incorporates partial-admission using a single nozzle which directs a jet against the rim of the disc into circular buckets. A significant feature of this turbine type is the directing of the fluid through additional buckets as it is redirected by stationary buckets in the housing into a helical path around the wheel. It is this feature which provides the velocity staging.

When a turbine is to operate in a Rankine cycle, expansion in a single stage may reduce the quality of the vapor to unacceptable limits. Wet-vapor operation, which is discussed in detail in subsection 3.4 can cause both lower performance and structural damage. If wet-vapor operation is anticipated, the turbine must be staged and either reheat or separation of liquid must be provided.

It follows that the turbine type for a particular application must be selected with care. Table III-B-1 shows the operating regimes of the various types.

A typical design example can be used to demonstrate the factors which may govern the choice of turbine configuration. As a

TABLE III-B-1

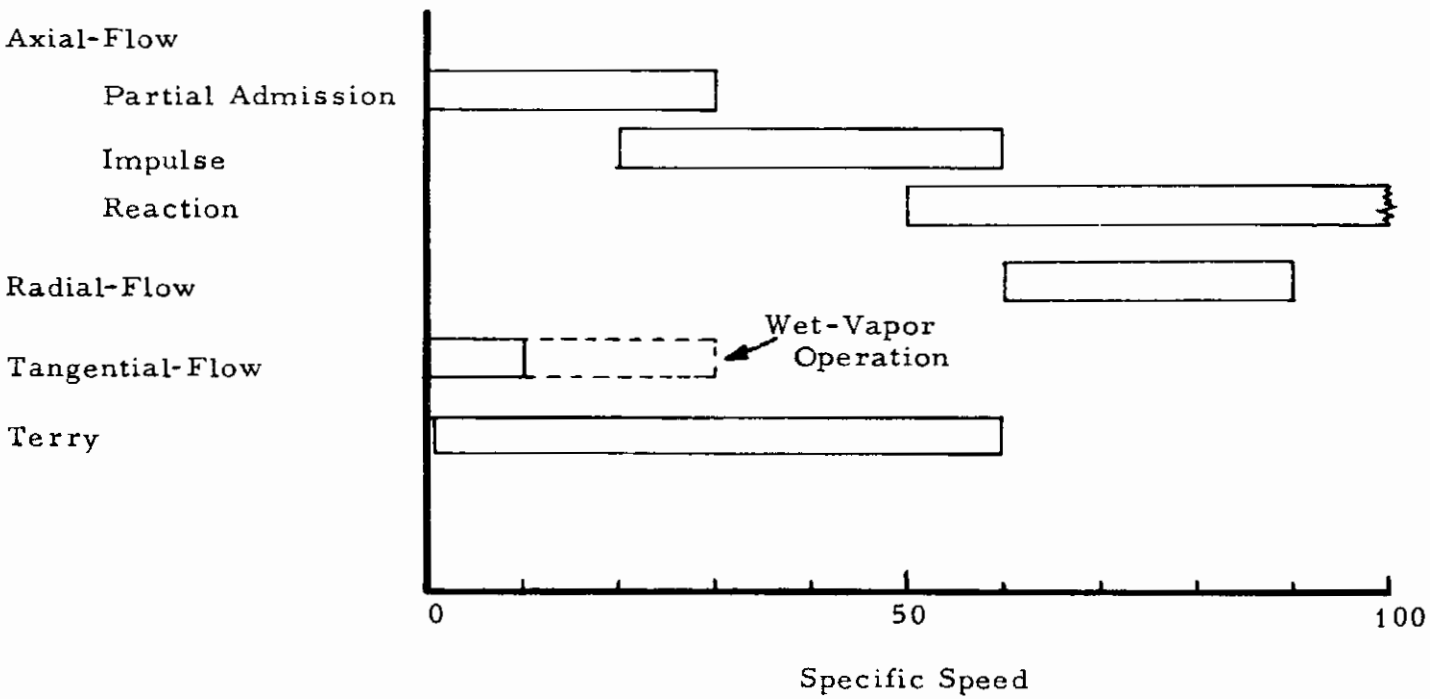

OPERATING REGIME OF VARIOUS TURBINE TYPES

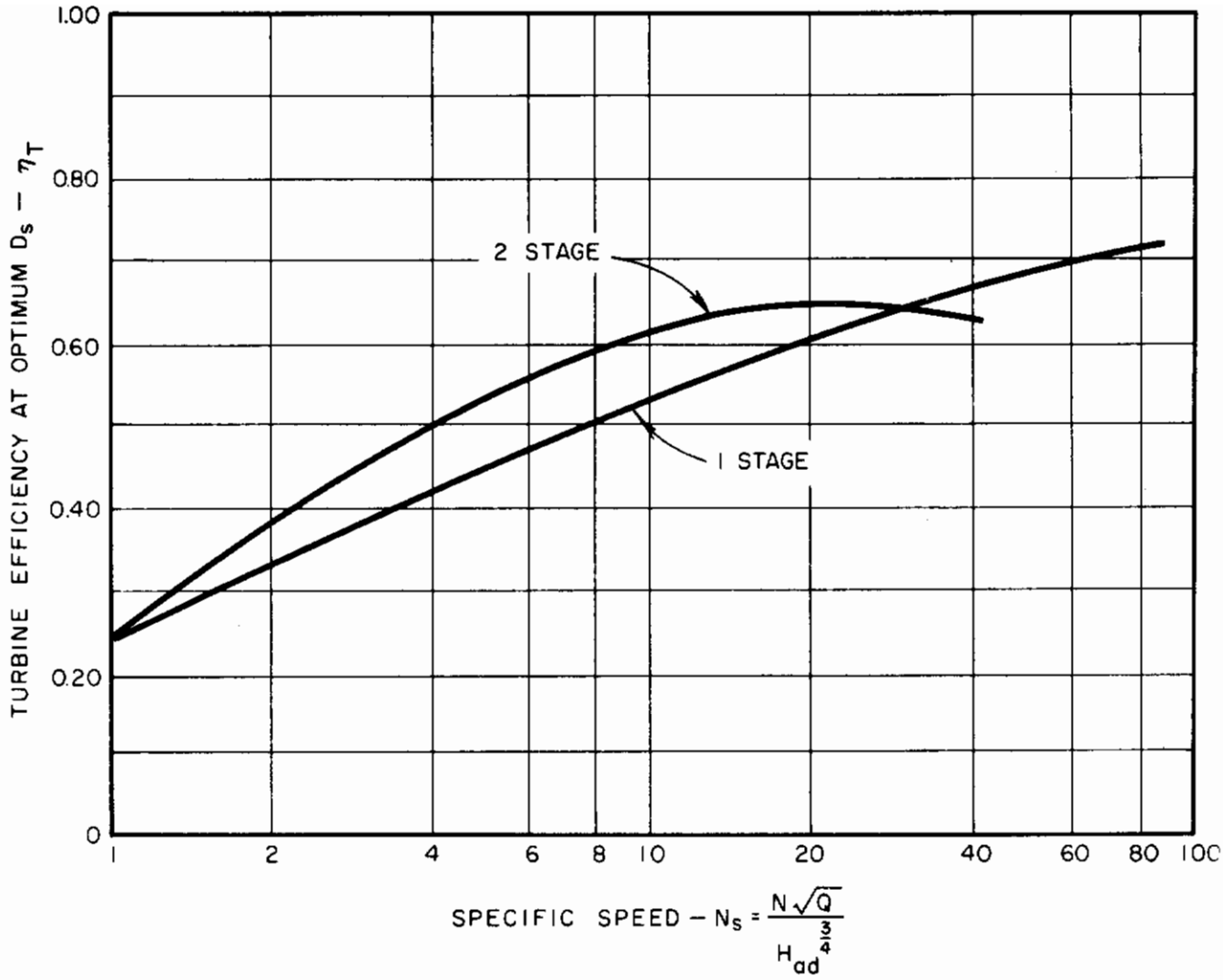

FIGURE III-B-13 COMPARISON OF SINGLE STAGE AND TWO STAGE RE-ENTRY TURBINES

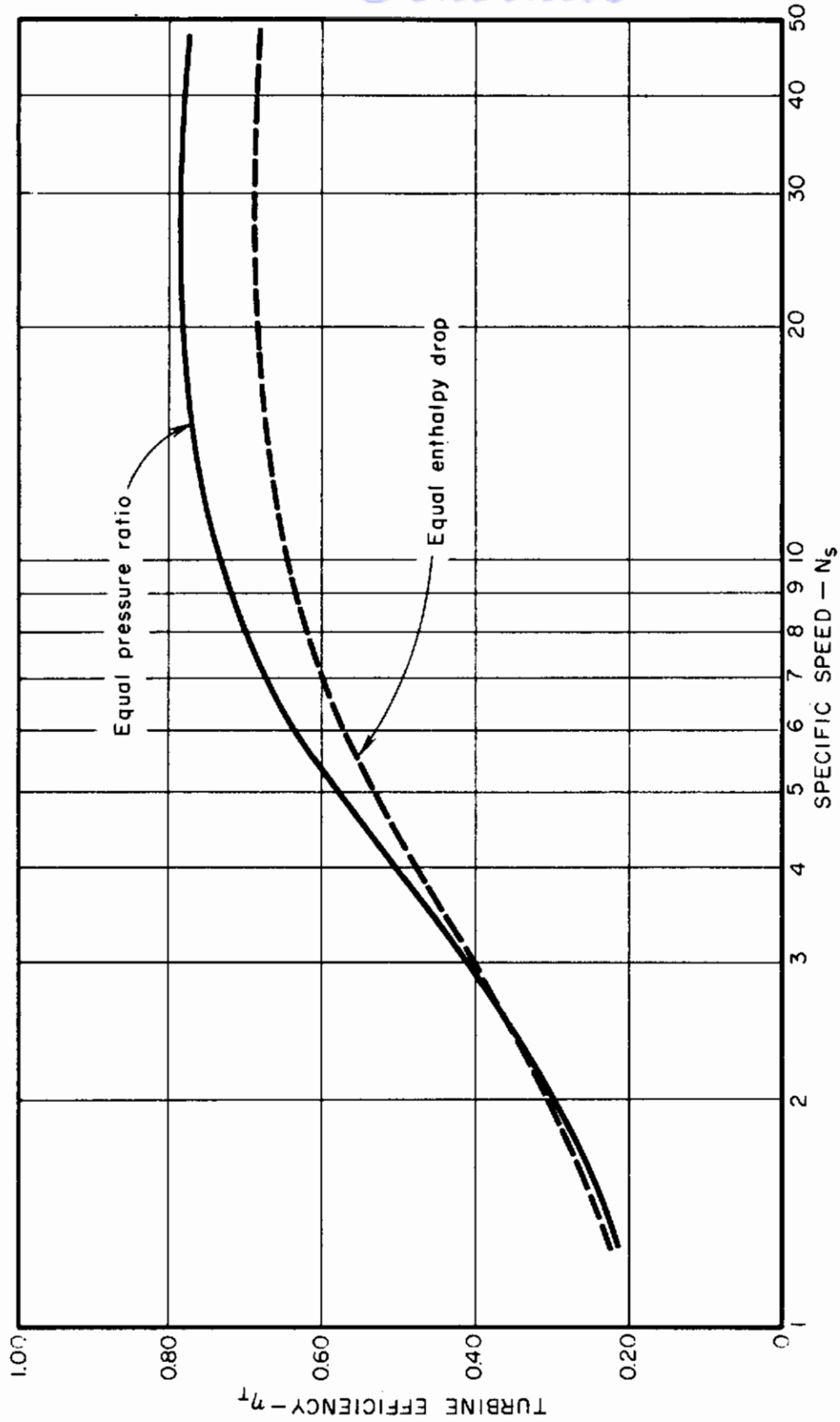

FIGURE III-B-14 COMPARISON OF OPTIMUM DESIGN POINT PERFORMANCE OF EQUAL HEAD AND EQUAL PRESSURE RATIOS IN BOTH STAGES OF A TWO-STAGE REENTRY TURBINE - TOTAL PRESSURE RATIO - 300:1

basis for this discussion, the work reported in Reference III-B-20 will be used. All losses in the turbines were analyzed, and the turbine design was optimized on the basis of the best available loss data. The referenced report is particularly useful, because test data are given to substantiate the rather complete analysis (Figure III-B-15).

Two hypothetical examples will be used. The first involves superheated mercury vapor, and the second, saturated rubidium vapor. Table III-B-2 lists the conditions chosen.

Table III-B-2

SAMPLE WORKING CONDITIONS

	Example No. 1	Example No. 2
Working Fluid	Mercury	Rubidium
Inlet Pressure, psia	100	160
Inlet Temperature, ^{o}F	1150	1860
Degrees Superheat, ^{o}F	250	0
Pressure Ratio	16	16
Net Power Level, hp	5	5

For Example No. 1, Figures III-B-16 through III-B-20 are derived from the curves in References III-B-20 and III-B-22 in order to show how some of the more important design variables change with specific speed. Once the best specific speed for the turbine is found, these curves will help in the choice of the turbine and the critical dimensions.

The design starts with the determination of the specific speed which can be found from the relation

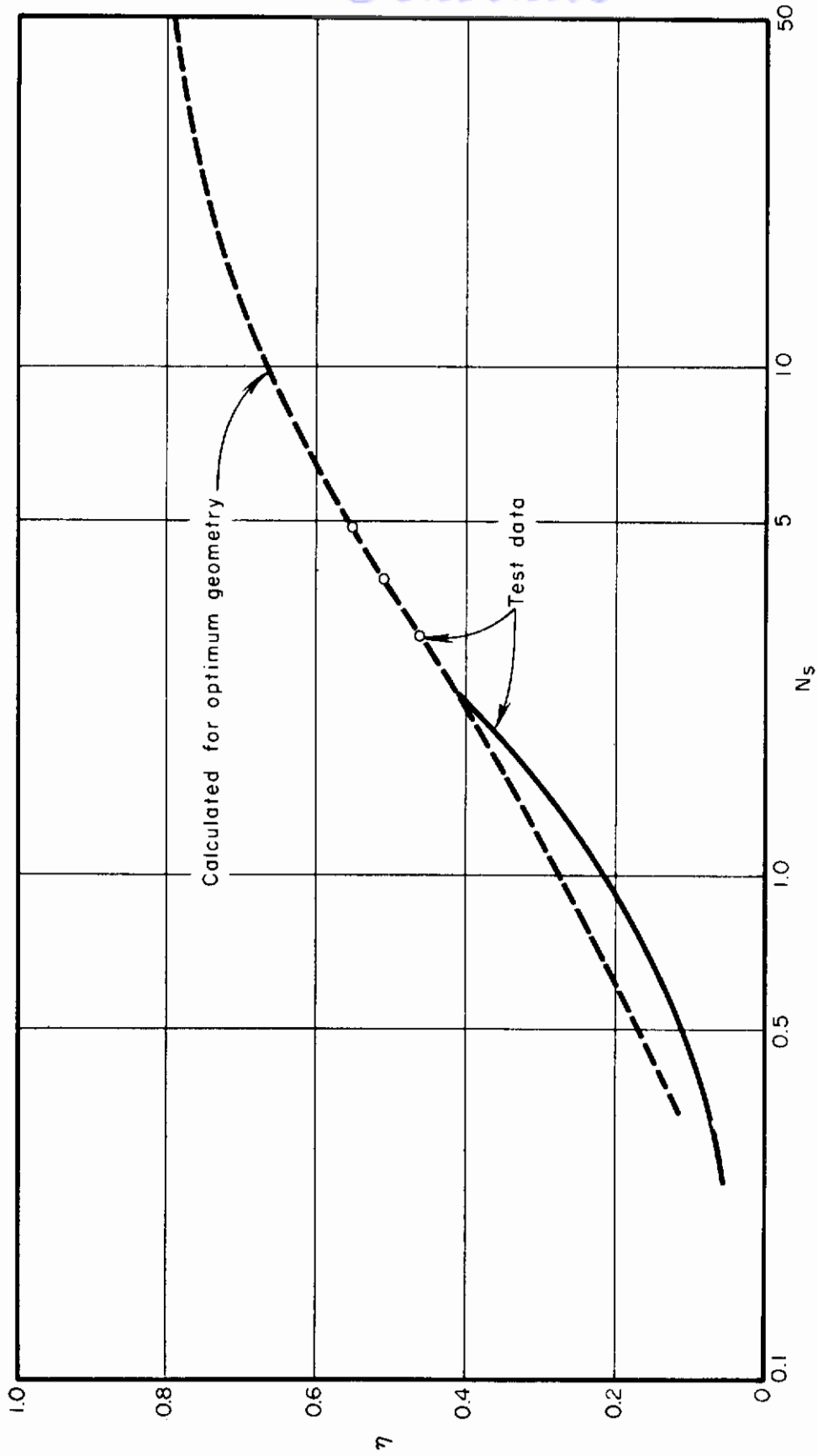

FIGURE III-B-15 COMPARISON OF TEST DATA WITH THEORY OF LOW SPECIFIC SPEED AXIAL TURBINES

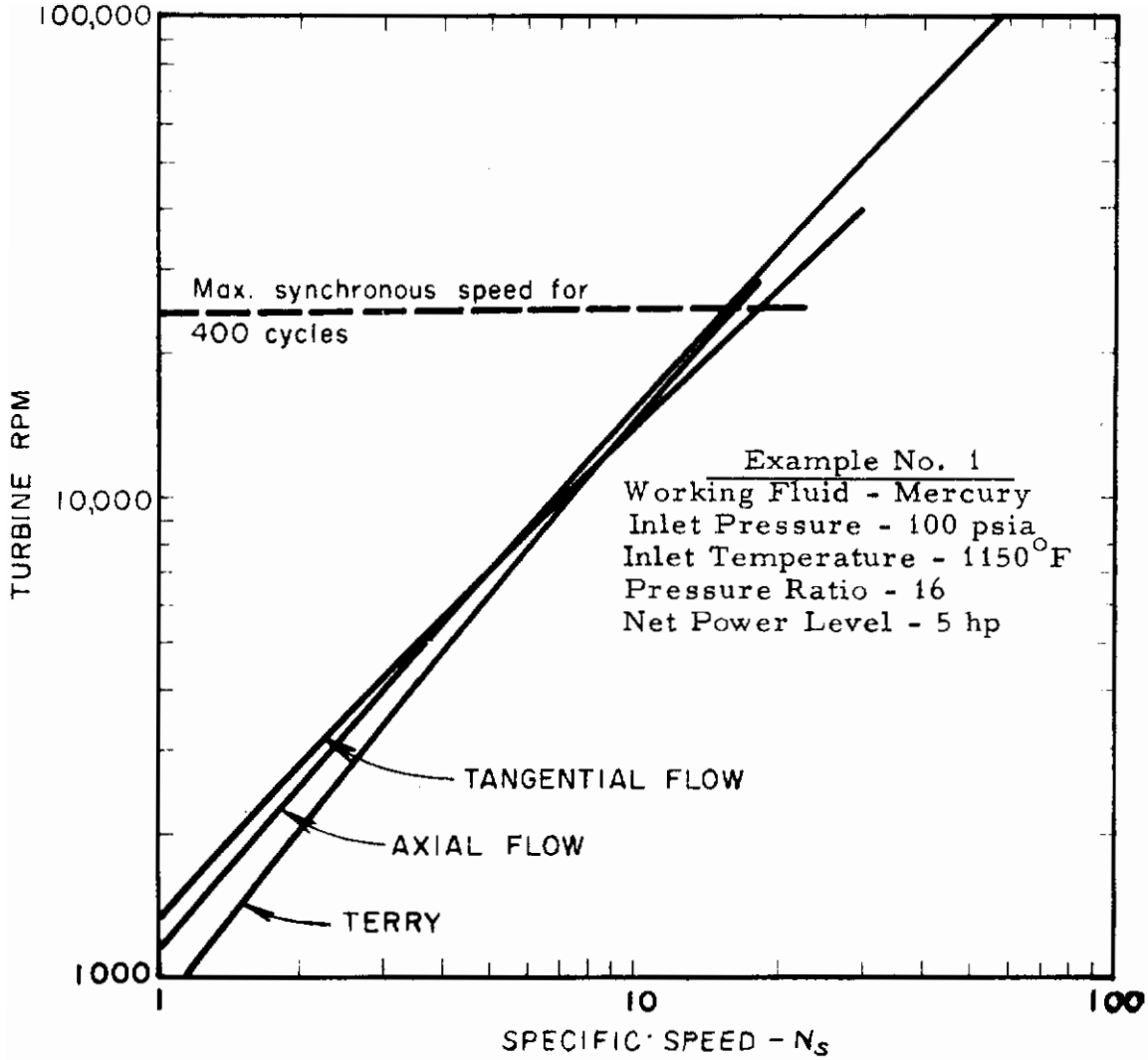

FIGURE III-B-16 TURBINE SPEED FOR VARIOUS TURBINES EXAMPLE NO. 1

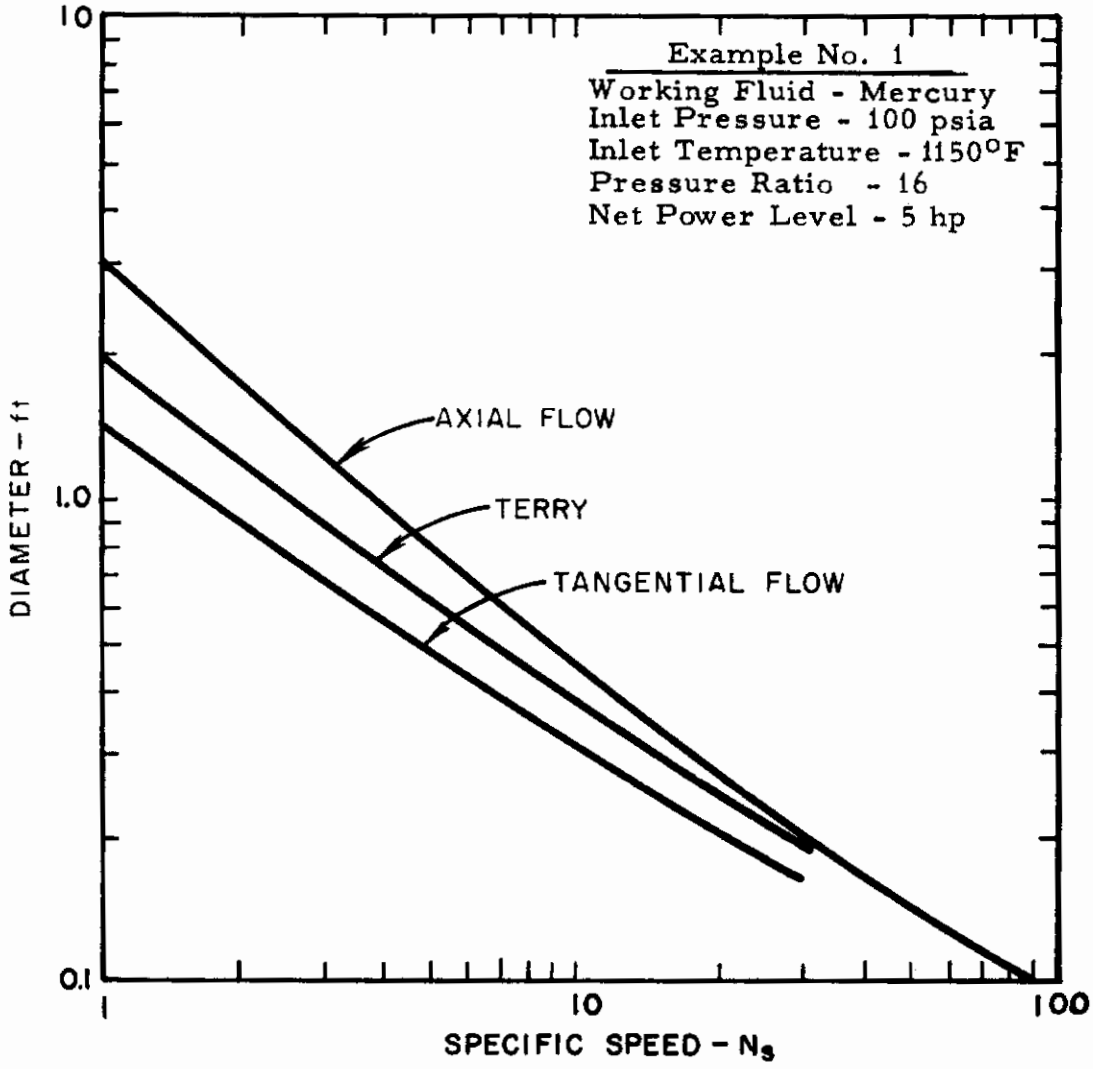

FIGURE III-B-17 TURBINE DIAMETER FOR VARIOUS TURBINES EXAMPLE NO. 1

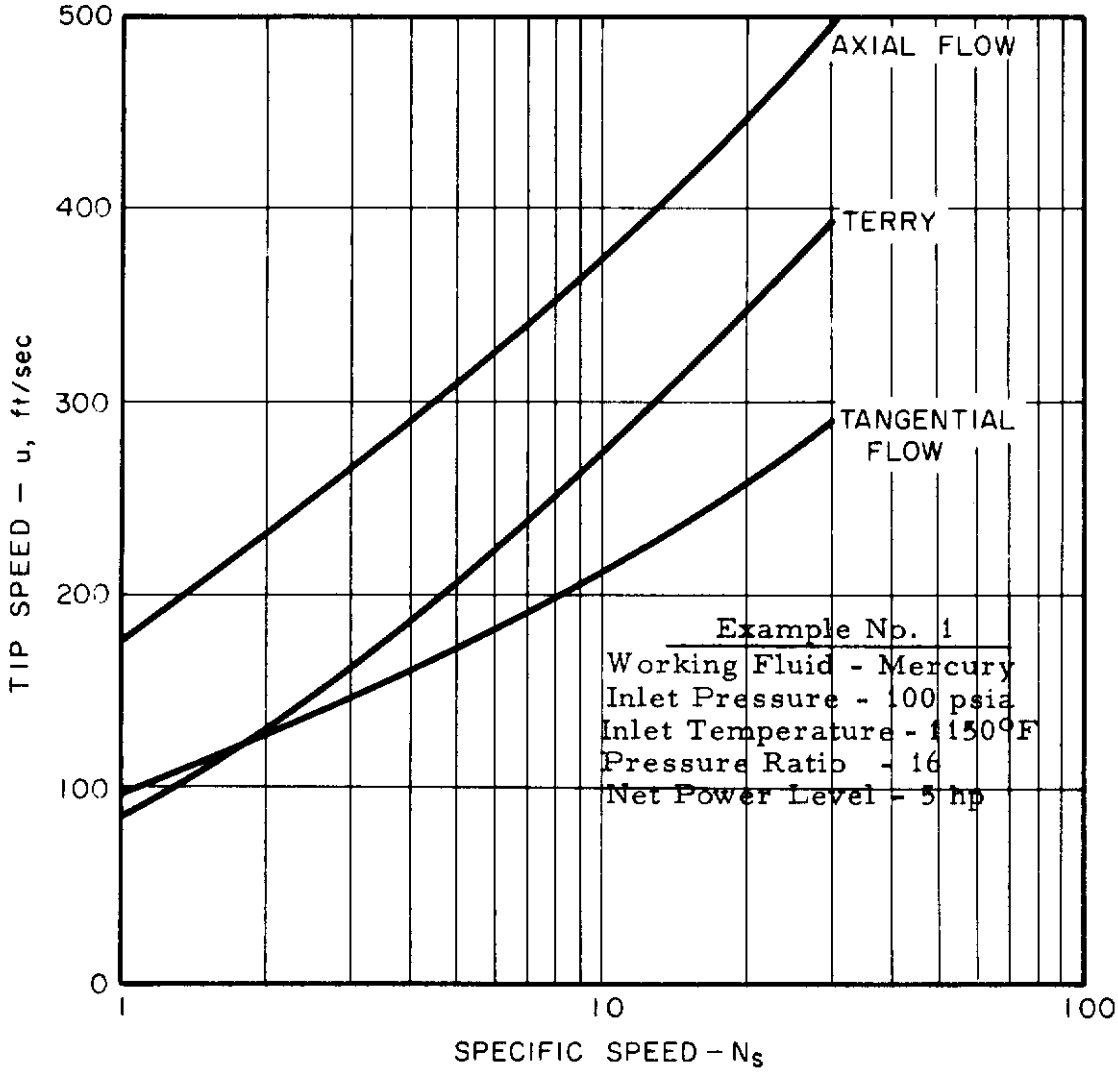

FIGURE III-B-18 TURBINE TIP SPEED FOR VARIOUS TURBINES
EXAMPLE NO. 1

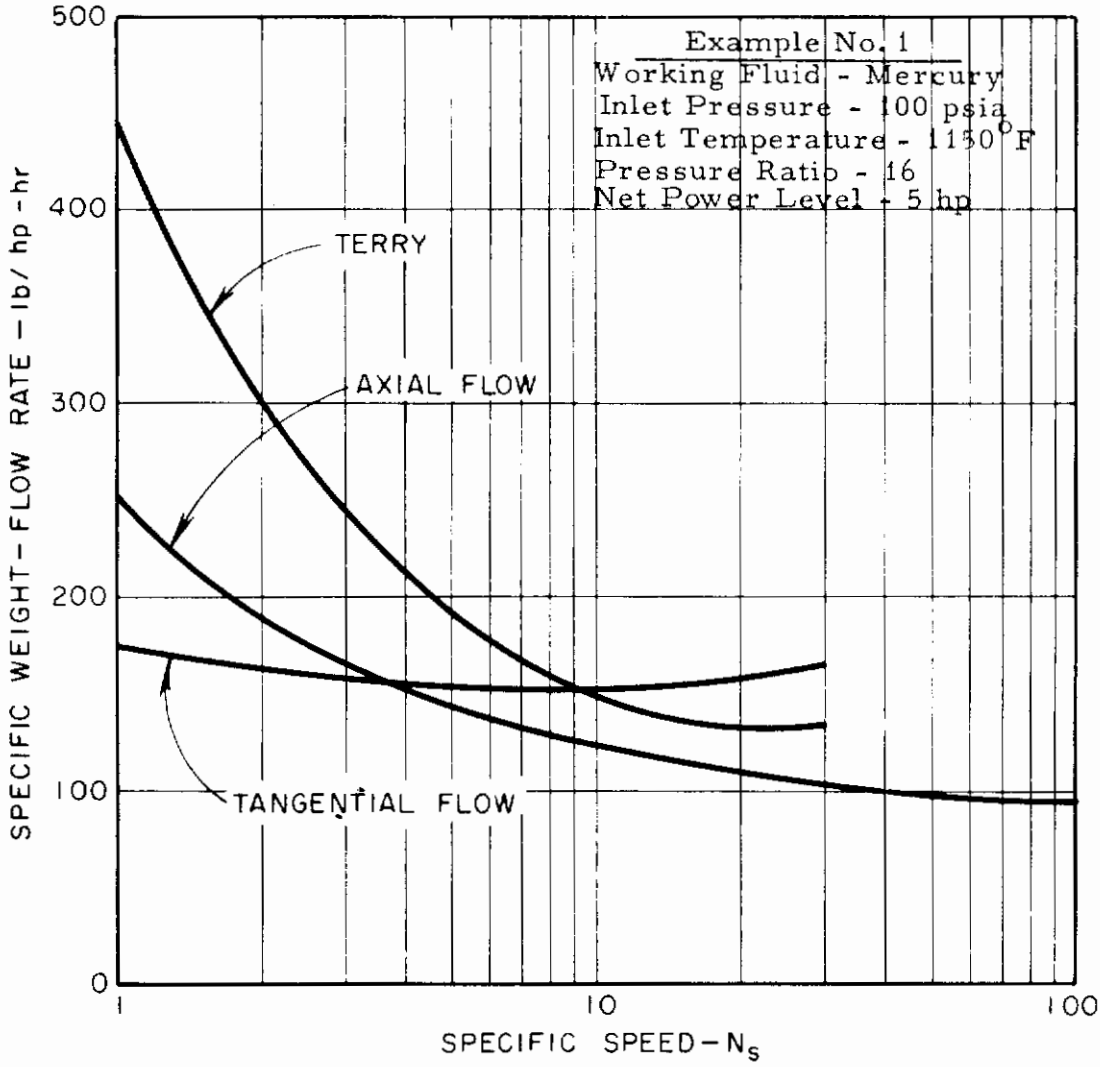

FIGURE III-B-19 REQUIRED WEIGHT-FLOW RATE FOR VARIOUS TURBINE TYPES

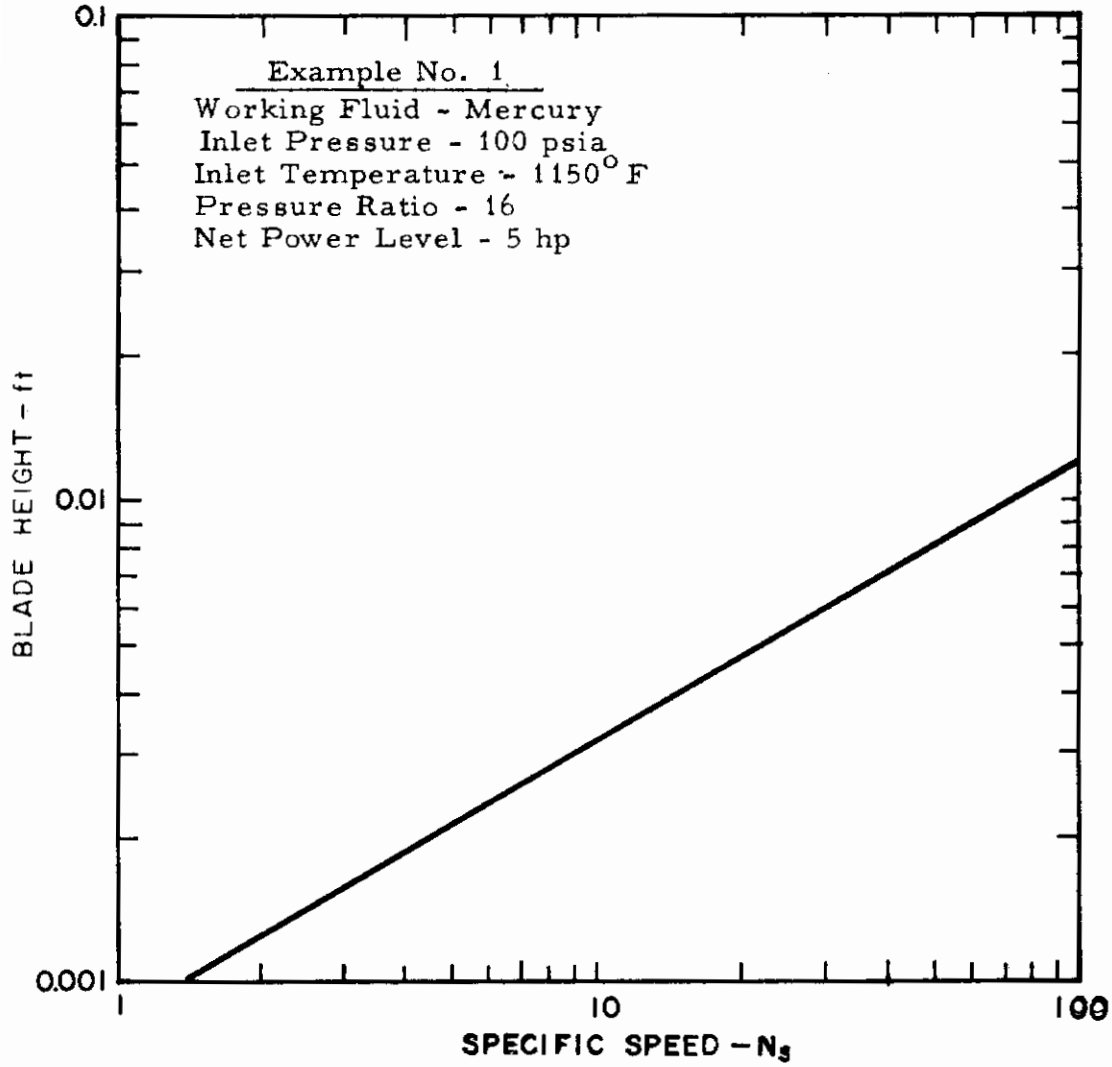

FIGURE III-B-20 TURBINE BLADE HEIGHT FOR VARIOUS TURBINES EXAMPLE NO. 1

$$N_s = \frac{N\sqrt{HP}}{H^{5/4}} \sqrt{\frac{550}{\eta \rho}}$$

where

N = rotational speed, rpm

HP = power level, hp

H = head due to isentropic expansion, ft

η = anticipated turbine efficiency

ρ = density of exhaust products, lb/ft^3 .

The value is not arbitrary, because each of the quantities is fixed by the particular application. Thus, the head, which is the available enthalpy drop, is fixed by the inlet state of the working fluid and the pressure ratio by

$$H = J\Delta h = \left(\frac{\gamma}{\gamma - 1}\right) RT_{in} \left[1 - \left(\frac{p_{out}}{p_{in}}\right)^{\frac{\gamma - 1}{\gamma}}\right]$$

for a perfect gas or by the change of state as shown on the Mollier diagram for the vapor.

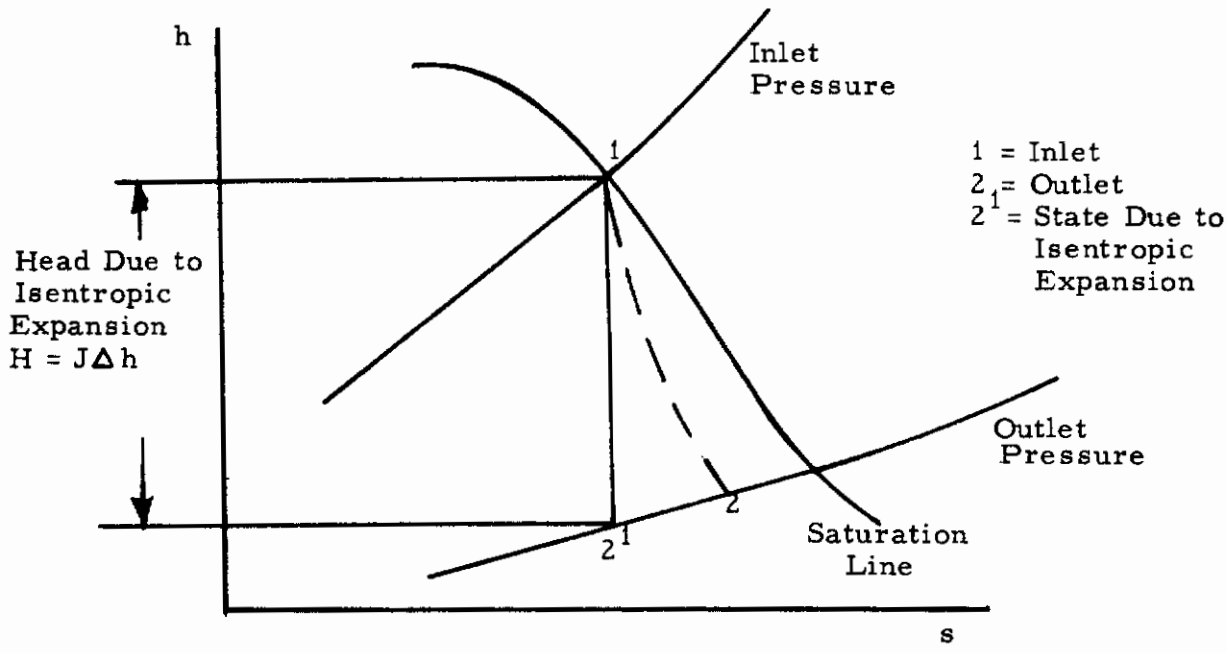

The density of the exhaust products is again fixed by the working fluid: the power level is a design criterion: and the efficiency can be estimated and later checked from the N_s - D_s diagram. The rotational speed is governed by considerations involving the turbine and the alternator. In general, the turbine designer will want to keep the rpm as high as the stress limitation will allow, but the alternator speed is governed by the synchronous speed necessary to achieve the proper frequency. Thus, if 400-cycle power is to be used, the alternator speed cannot exceed 24,000 rpm since

$$N = \frac{120\,f}{p}$$

where

N = synchronous speed, rpm

f = frequency, cycles/sec

p = number of poles

and the minimum number of poles is two.

In general, it is undesirable to place transmissions of any kind in a space-power package. As discussed in subsequent paragraphs, the problems of sealing for space applications are such that the working fluid is employed as a lubricant in bearings. Since the lubricating qualities of the working fluid are usually limited, every effort should be made to eliminate the need for additional lubrication, such as that needed in gear trains. Transmissions involving belts are difficult to apply in space because of the high speeds required. In general, it is highly desirable to have the turbine and alternator on the same shift, a situation referred to as "close-coupled."

For a speed of 24,000 rpm, the curves of Figure III-B-16 show that the tangential-flow turbine has a specific speed of 17.5 for maximum efficiency, that the Terry turbine has a specific speed of 16, and that the axial-flow turbine has a value of 15. The required diameters, tip speeds, and specific weight flow are listed in Table III-B-3.

TABLE III-B-3

DESIGN DATA-MERCURY-24,000 RPM

			D	u	swf
Turbine Type	N_s	η	ft	ft/sec	lb/hp-hr
Axial-flow	15	70%/o	0.330	415	116
Terry	16	62%/o	0.275	324	135
Tangential-flow	17.5	54%/o	0.208	260	158

Since the efficiency and specific weight flow are best in the axial-flow turbine, this type is most suited to space application, as long as the size and stress level are acceptable. The turbine tip speed is only 415 ft/sec, which is acceptable at the temperature level being used (see Section 4.1). The diameter of 0.33 ft(4 in.) is not excessive and should be usable in most space-power packages.

If the axial-flow turbine is chosen, the blade height for maximum efficiency would be 0.004 ft as can be seen in Figure III-B-17. Because such a blade is obviously too small for reasonable machining practice, it is necessary that partial admission be considered. From Figure III-B-8, it is evident that the best value of percent-of-admission is 15 percent, i.e., 54° of arc should be nozzles. From the design curves found in Reference III-B-20, the best number of blades and other design data can now be found.

For Example No. 2, the results using the same procedure would be as listed in Table III-B-4.

TABLE III-B-4

DESIGN DATA - RUBIDIUM - 24,000 RPM

Turbine Type	N_s	η	D	u	swf
			ft	ft/sec	lb/hp-hr
Axial-Flow	6.0	60 %	0.556	700	38.9
Terry	6.8	48 %	0.400	500	49.9
Tangential-Flow	6.2	56 %	0.328	410	44.1

It may well be that a turbine wheel nearly 7 inches in diameter (which is required for the axial-flow case) is too big, in which case the choice of the somewhat less efficient but smaller tangential-flow turbine is indicated. This type would be only 4 inches in diameter.

It must be re-emphasized that the design of the turbine is governed by many things and that the choice of turbine type cannot be generalized in terms of power level. However, unless the power level results in a specific speed less than 20, the axial-flow turbine is usually the logical choice.

As the power level increases, the design specific speed will also increase. Above a value of 30, full admission will become possible; above a value of 50, reaction turbines should be considered.

3.4 Wet-Vapor Operation

One of the problems encountered when operating a turbine in a Rankine cycle is operation with wet vapor. In subsection 1.0, the choice of a working cycle was discussed, and the possibility of superheating and/or reheating in the Rankine cycle was mentioned. Unless

sufficient superheating occurs, the expansion will result in the formation of wet vapor, i.e., an intimate mixture of condensed liquid and saturated vapor, the quality of which is defined as the weight ratio of the uncondensed vapor flow to the total mass flow. Any standard thermodynamics text may be consulted for an analysis of this phenomenon.

The formation of the water drops has a dual effect on the turbine. First, because the condensed drops move slower than the vapor, the relative velocity of the drops may be such that they strike the convex surface of the blades, physically slowing them and decreasing the efficiency. Second, the drops hitting the blades may cause structural damage known as blade erosion. Because of these effects, the practice in steam power plants has been to maintain the quality of the vapor above 85 percent.

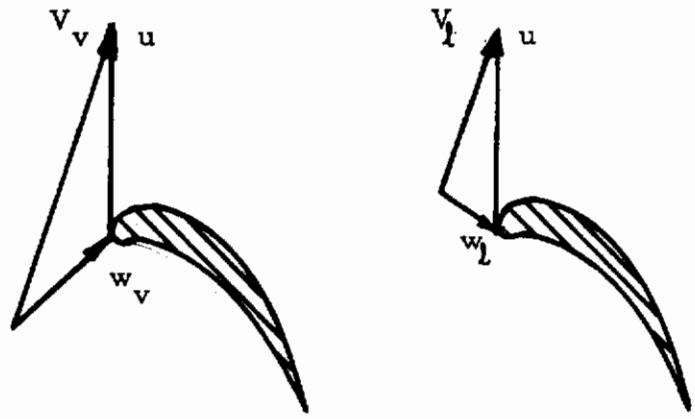

VAPOR LIQUID

Sometimes a turbine which would appear to operate in the "safe" zone is found to have erosion. Referring again to the rubidium cycle of Example No. 2, the quality of the vapor leaving the turbine is about 90 percent.

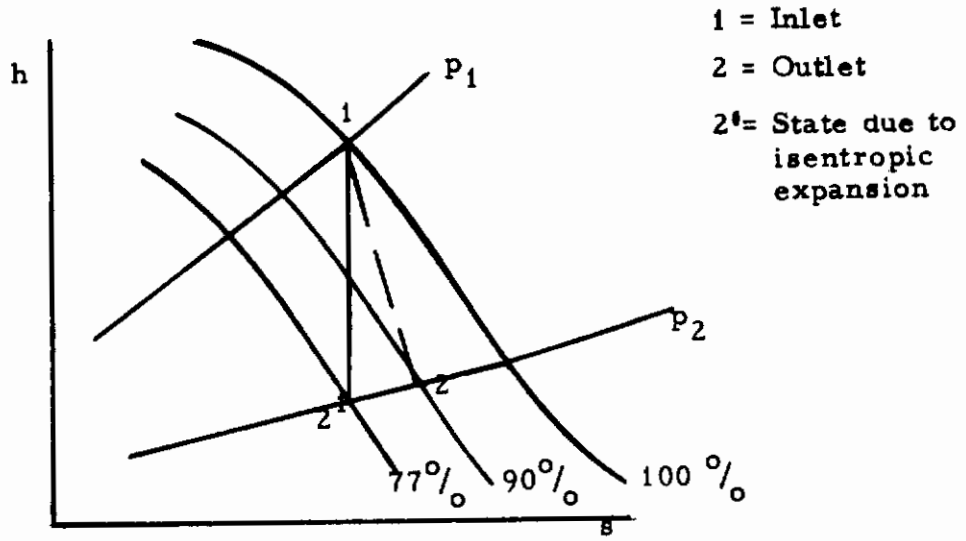

OVER-ALL EXPANSION

However, it must be remembered that the turbine is the impulse type: i.e., all the pressure drop occurs in a stationary nozzle. Since nozzles have an efficiency of approximately 95 percent, the quality of the vapor leaving the nozzle may well be 80 percent. By the standards of the steam turbine

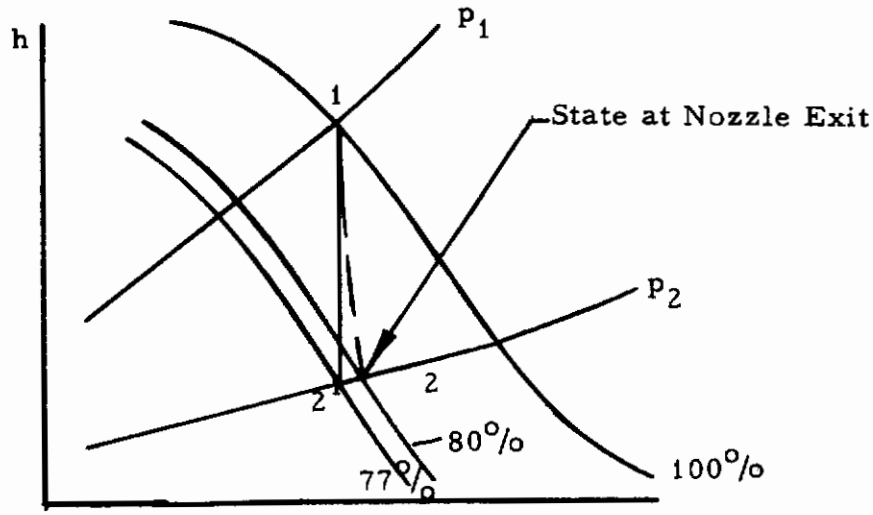

NOZZLE EXPANSION

technology, this would be too wet, and it becomes necessary to either superheat or stage and reheat. The former will prevent low quality since a much higher initial enthalpy will be used; whereas, as discussed

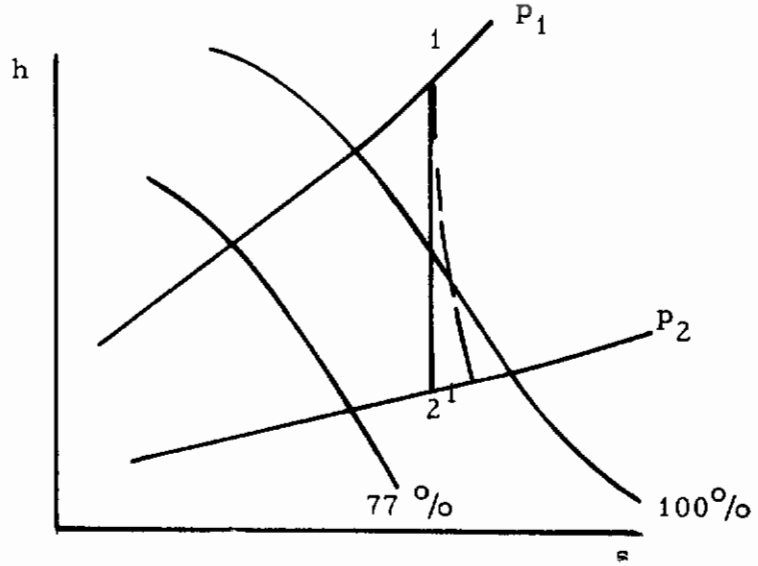

EFFECT OF SUPERHEAT

in subsection 3.3.1, the latter will keep the enthalpy change per stage to a lower value and thereby keep the quality higher.

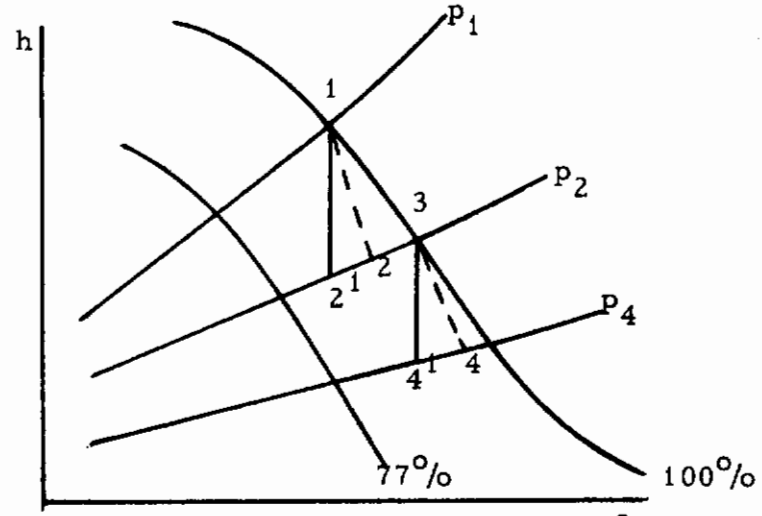

EFFECT OF STAGING

One of the proposed solutions to the problem of wet-vapor operation has been the use of a tangential-flow turbine. The flow in this machine is quite complex and, according to References III-B-20 and III-B-22, should be helical. If this is the case, droplets formed during the expansion might be expected to be centrifuged from the blades

when the fluid makes short-radius turns. This problem has been studied in detail, and the results are presented in Reference III-B-23. It was shown that a substantial increase in performance was possible if provision was made for draining the condensed droplets. This result verified that the droplets were separated in the turbine.

The problem of wet-vapor operation of space-power plants may not be as acute as it is in the stationary steam power plant. In a technical note being prepared for publication III-B-24), it is pointed out that suction-side impingement occurs only if the droplets are moving at a velocity less than a critical value. As can be seen from the velocity diagrams, this value is given by

$$\frac{V_\ell}{V_v} = \frac{1}{\psi \cos a} \quad \frac{u}{c_o}$$

where

V_ℓ = velocity of liquid drops

V_v = velocity of vapor

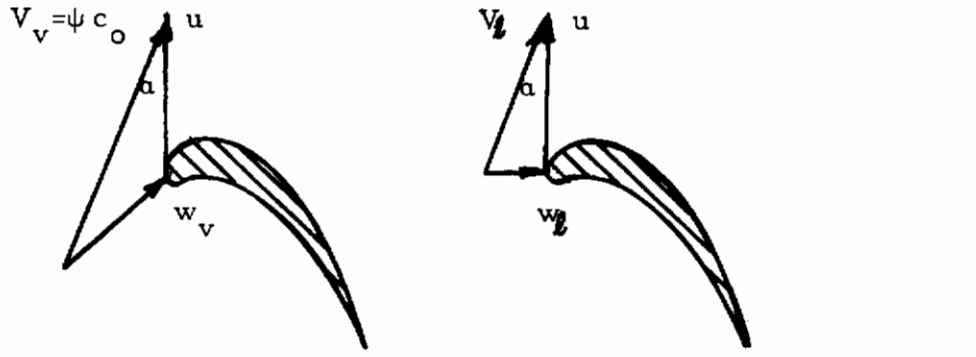

VAPOR LIQUID IMPINGING ON SIDE

ψ = velocity coefficient

α = nozzle angle

u = wheel tip speed

c_o = spouting velocity

In steam turbines, wet-vapor operation is usually associated with reaction turbines where the design u/c_o is about 0.8. In space applications, impulse turbines are more likely, so that u/c_o will be about 0.4. Furthermore, the use of vapors like mercury will mean that the drag on droplets is much greater, making the attainment of higher liquid velocities much more probable. For these reasons, it is concluded that by proper design, the loss due to wet-vapor operation can be made less than that found in conventional turbines. This contention is confirmed by limited tests (Reference III-B-24) which show that there is no change in efficiency when a small, partial-admission, impulse turbine is run with air, nitrogen, and wet steam. The long duration achieved at Thompson Ramo-Wooldridge on the SNAP I turbine operating with wet mercury vapor also indicates that wet-vapor operation is possible without erosion.

4.0 MECHANICAL CONSIDERATIONS

In considering the mechanical aspects of turbine design for a space-power plant, one might be tempted to carry over the large body of technology which has accrued in the design of jet-power plants for airplanes. Some significant differences exist, however. First, the jet power plant operates on an open Brayton cycle, not a closed Rankine cycle. This means that a gas, not a vapor, is being used and that a compressor is a vital part of the system which will influence its design greatly. Second, the power level is much larger, and the temperature may be quite different. Third, the jet engine must be designed to be flexible enough to operate over a wide variety of conditions.

A large body of experience has also been accumulated on auxiliary power units, and the temptation to use this material might be great. Again, the working fluid is a gas not a vapor, so vital differences exist. Furthermore, the duty cycle for an APU is usually short, so that mechanical compromises can be made.

The major design areas which are of interest are the materials problem and the accompanying stress, the creep problem with its effect on clearances, the seals, and the bearings. Each is discussed in relation to space below.

4.1 Stress

Because a turbine wheel rotates at high speed and is subject to high temperature, the stress problem is quite important. A combination of centrifugal stress, thermal stresses, and fatigue loading is to be expected. For space turbines, the wheel configuration will usually be a solid disc,

profiled to reduce centrifugal stress and operating at a steady state over most of its life cycle. It is quite logical to assume that the wheel will operate at a constant temperature and that thermal stresses will be small except at start up. Conversely, the high centrifugal stress will impose severe limitations on the tip speed.

One way used to lower the maximum stress level in a wheel is to reduce the wheel's thickness in the radial direction, since the centrifugal stress, which is the major component, depends on the mass distribution. Careful design will result in a disc which has constant stress. Figure III-B-21 shows how the stress level can be reduced by profiling. It is seen that a profiled wheel with $h_o/h_a = 6$ operating with a tip speed of 1,600 ft/sec has a stress level equal to that of a constant-thickness disc operating at only 1,000 ft/sec. Conversely, at the same tip speed and temperature, the constant-stress disc has only 39 percent of the stress of the constant-thickness disc, making it possible to operate this wheel for much longer durations. For the same life span, it can operate at a temperature of 200 to 300 degrees greater than that found in the constant-thickness disc.

It must be noted that a disc whose h_o/h_a is greater than 1 will be heavier than the constant-stress disc. The weight penalty incurred is shown in Figure III-B-22. However, since the disc weight is a small fraction of the system weight, this penalty is not too significant. Some of the weight penalty can be removed by designing the disc by the "Method of Inversion" described in Ref. III-B-25.

The stress at the root of the turbine bucket is also quite high. Figure III-B-23 shows the stress level for various blade heights. In space-power turbines, the rotational speed will be high but the blade height will be small, making r/r_o high (>0.8) so that stresses at the blade root will not exceed wheel stress. (It might be noted that the stress level for $\frac{r}{r_o} = 0.8$ corresponds,

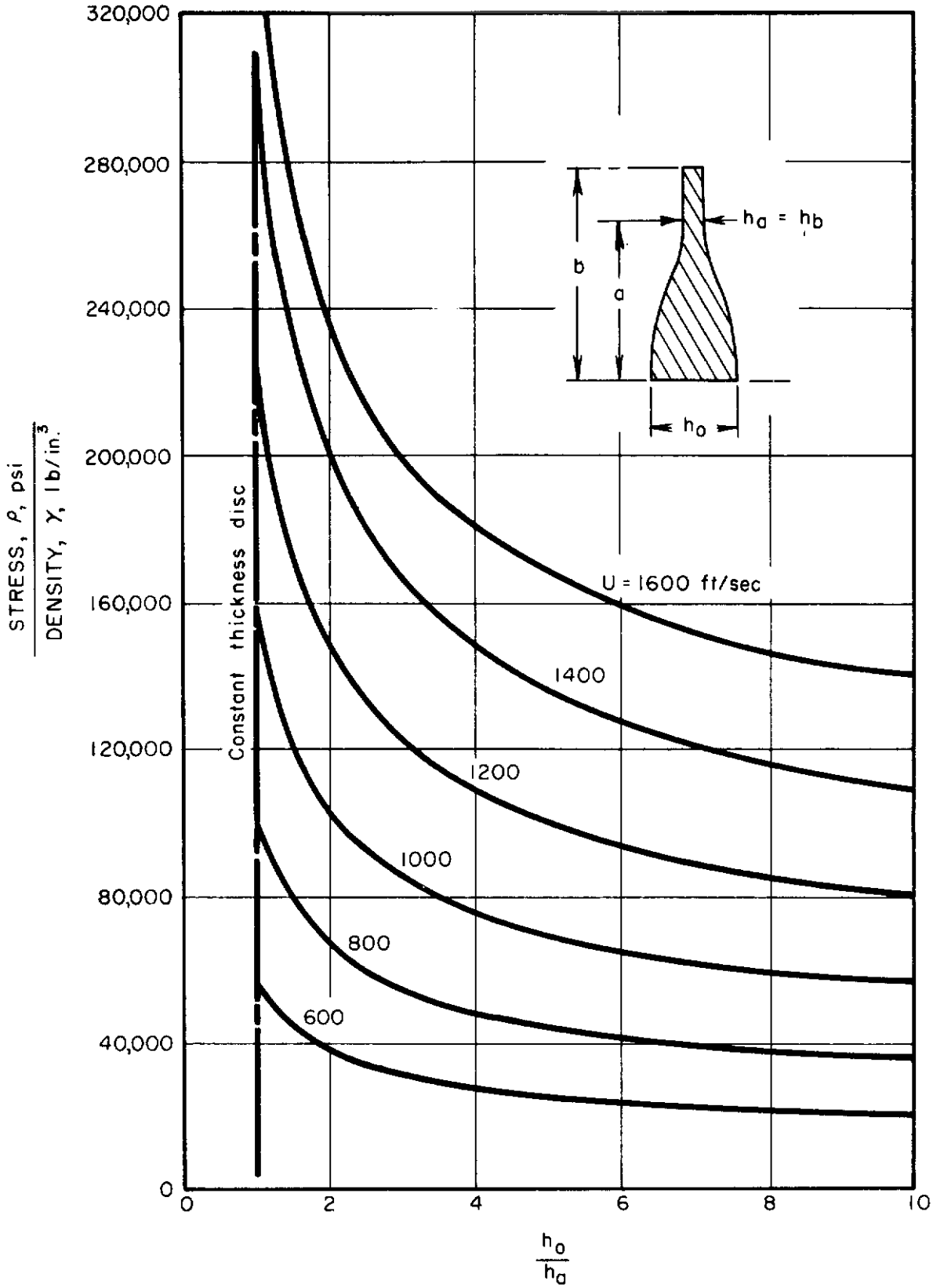

FIGURE III-B-21 DESIGN CURVES FOR CONSTANT-STRESS TURBINE DISCS

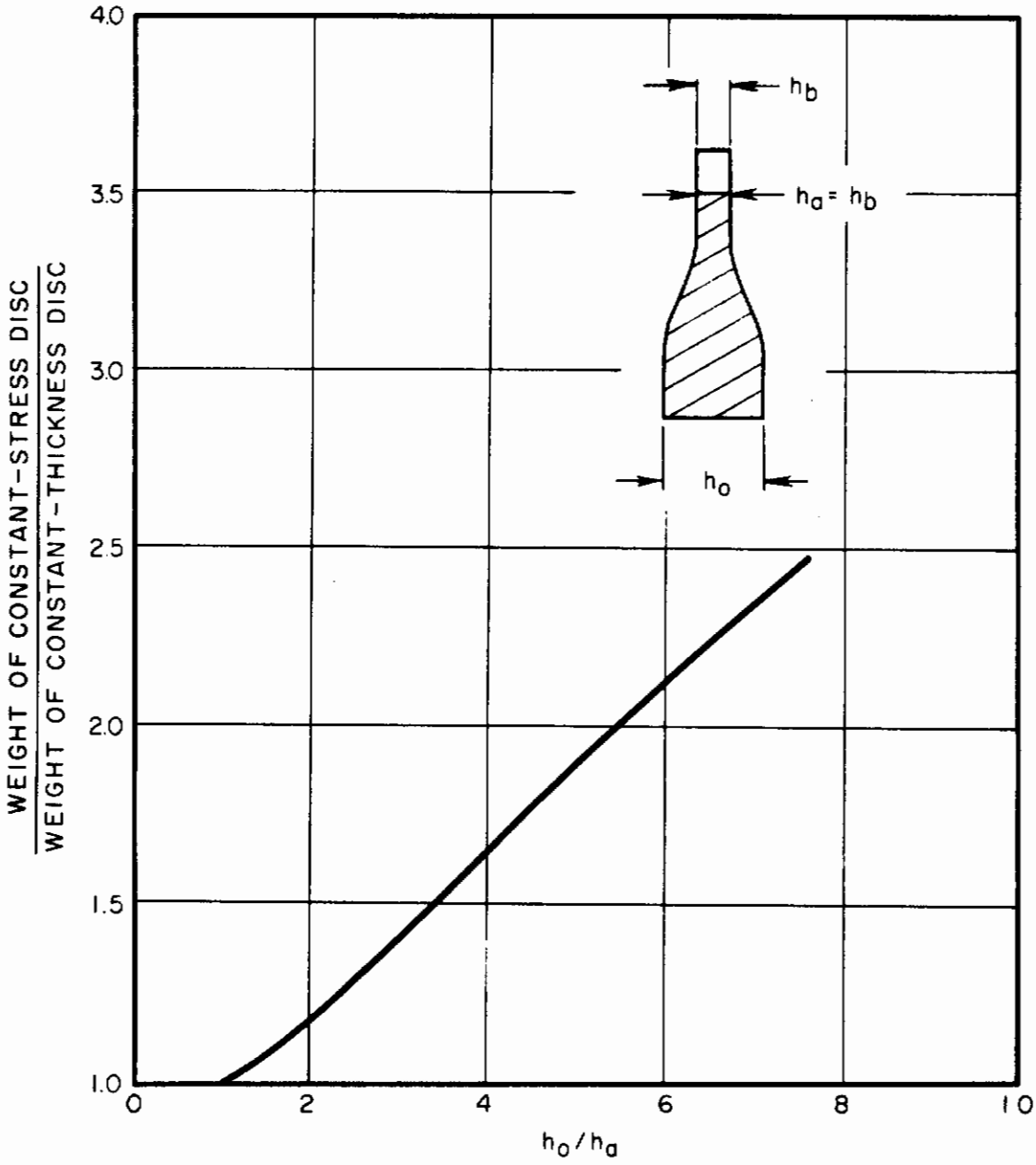

FIGURE III-B-22 WEIGHT PENALTY DUE TO PROFILING

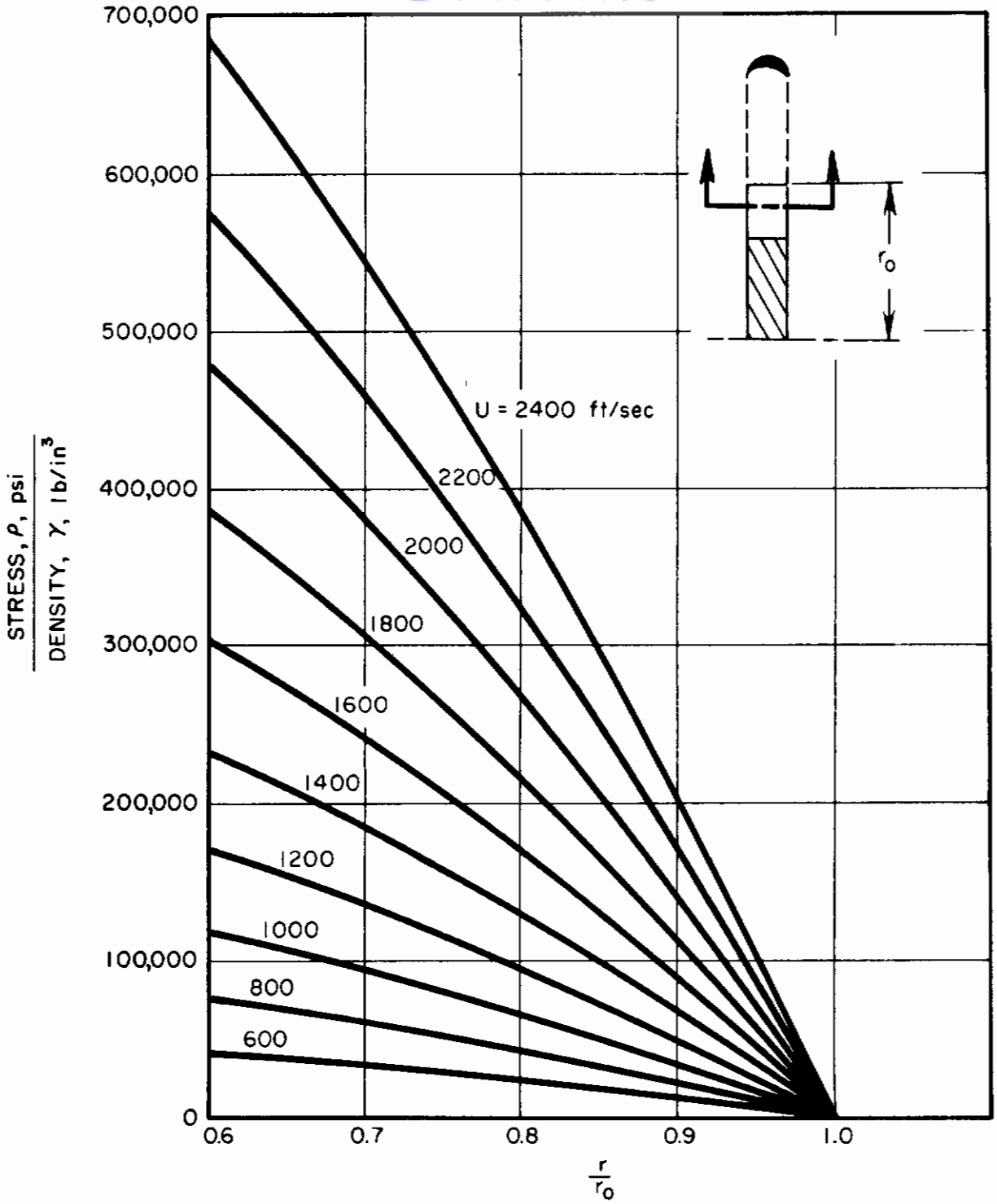

FIGURE III-B-23 DESIGN CURVES FOR CONSTANT CROSS SECTIONAL AREA, ROTATING TURBINE BUCKETS

approximately, to the stress level for the wheel at $h_o/h_a = 6.$)

The turbine design must not be limited to considerations of the steady-state stress. Frequently, transient conditions during start-up will induce stresses greater than those occurring while operating under steady load. Partial admission turbines often suffer from problems related to fatigue. Each time a blade enters the nozzle row, it is put under load and heated. As it leaves the row, the load is removed and cooling occurs. This cyclic application of stress may cause blade failure, but when the blade height is small, as it probably will be in space - power turbines, the time to failure will be more than adequate.

Sometimes the tips of the individual blades are connected by a shroud ring. This is done to reduce leakage (subsection 4.6) and vibration but induces additional stresses due to the added mass at the end of the blade. In space turbines, vibration should be minor since blade height is small.

Turbine housings are not subjected to the same high stresses which the wheel encounters. However, because the housing is not symmetrical, nor are the walls of uniform cross section, warpage occurs as the turbine is heated. Since clearances have to be maintained within close limits (see subsection 4.6), this warpage may be very detrimental. Careful design must, therefore, be applied to the housing also.

4.2 Materials

In the last decade, great advances have been made in the field of high-temperature, high-strength materials. Various new alloys have been developed. Most of them are developed for APU applications, and their use in space systems might be influenced by their compatibility with the liquid-metal vapors. Research to determine the corrosive properties of the metal

vapors is under way at various institutions and companies, but little has been published to date.

In Figure III-B-24 are shown the stress-rupture properties for some of these materials at elevated temperature. While the blade velocity which may be used depends on specific design constants, Figure III-B-25 shows typical velocities attainable with a particular design. Molybdenum with one-half percent of titanium added appears to be a material which can withstand the corrosive action of metal vapors. It also can be used at high temperature and high speed. Inconel 713C is also a possible material for space turbines.

As the state of the material art advances, more materials will become available. Detailed data can be obtained from the American Iron and Steel Institute and in Ref. III-B-26.

4.3 Fabrication

Since turbine wheels and turbine housing may be made from "exotic" materials, the fabrication may prove to be difficult. Usually the fabrication of the wheel, rather than the housing, presents the greater problem because of the higher stresses which must be combated and the close tolerances which must be kept.

Some of the materials which are used for turbine wheels are very difficult to machine by standard machining practice because of their hardness. Electric discharge machining is widely used in this case. New techniques in this field are constantly under development, leading to improvements in the technique and reduction cost.

Turbine wheels for space are also made by the investment casting process. Wax or plastic models are melted out of a plaster mold which

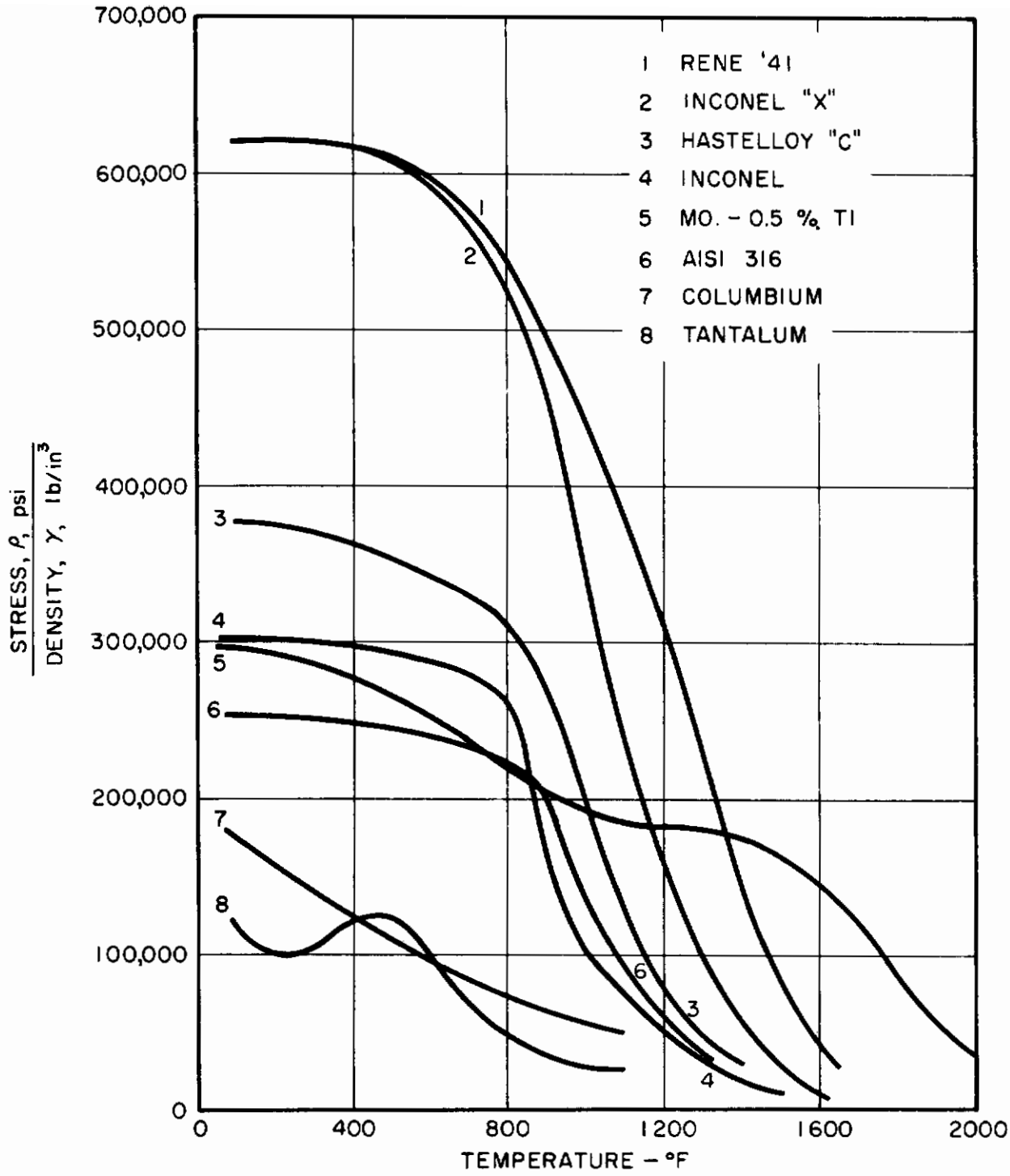

FIGURE III-B-24 10,000 HR. STRESS-RUPTURE PROPERTIES OF VARIOUS MATERIALS

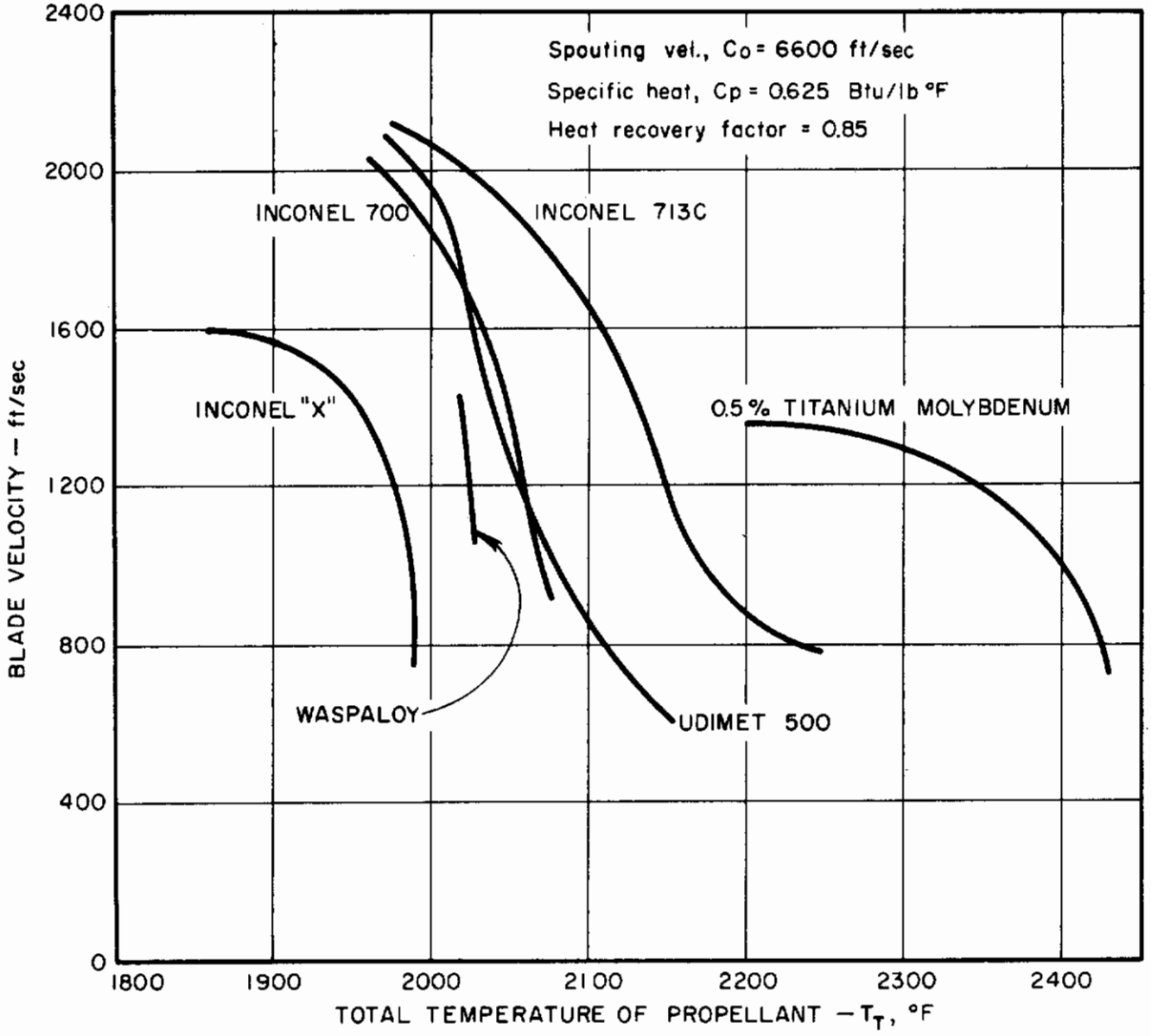

FIGURE III-B-25 ALLOWABLE BLADE SPEEDS FOR CONSTANT-STRESS TURBINE DISCS

is then filled with the refractory metal. This technique has been improved immensely in the past few years, so that relatively close tolerances can be kept. Some of the more sophisticated techniques involve the use of mercury instead of wax in the mold. The actual casting may be made in one piece, or individual blades may be positioned in a mold and the disc cast around them. Again the size, stress level, temperature, and blade shape will determine the best practice.

The advantage of the electric discharge process is an ability to hold much closer tolerances. It is highly desirable to maintain sharp edges on the turbine blade, especially on the trailing edge. If the jet issuing from the nozzle is supersonic, a sharp leading edge is also desirable. With castings, a radius of 0.005 in. seems to be a practical limit. Machining techniques make it possible to reduce this radius and to hold much closer tolerances in the blade spacing, i.e., the distance from blade to blade and the way the blades align axially. This is especially important in impulse designs where it is desired that no pressure drop exist across the blade row. Even a slight misalignment between blades will result in a very nonuniform area distribution along the blade channel (Figure III-B-26) which will result in pressure variation and losses.

It must be noted that many of the refractory metals being used for turbine applications are produced only as castings. If the blades are to be machined, a blank wheel must first be cast. Some techniques for the production of turbine wheels from powdered metals are also being developed. These do not appear to be far enough advanced to be commercially available for space turbines. Sheet metal turbines are also being produced but

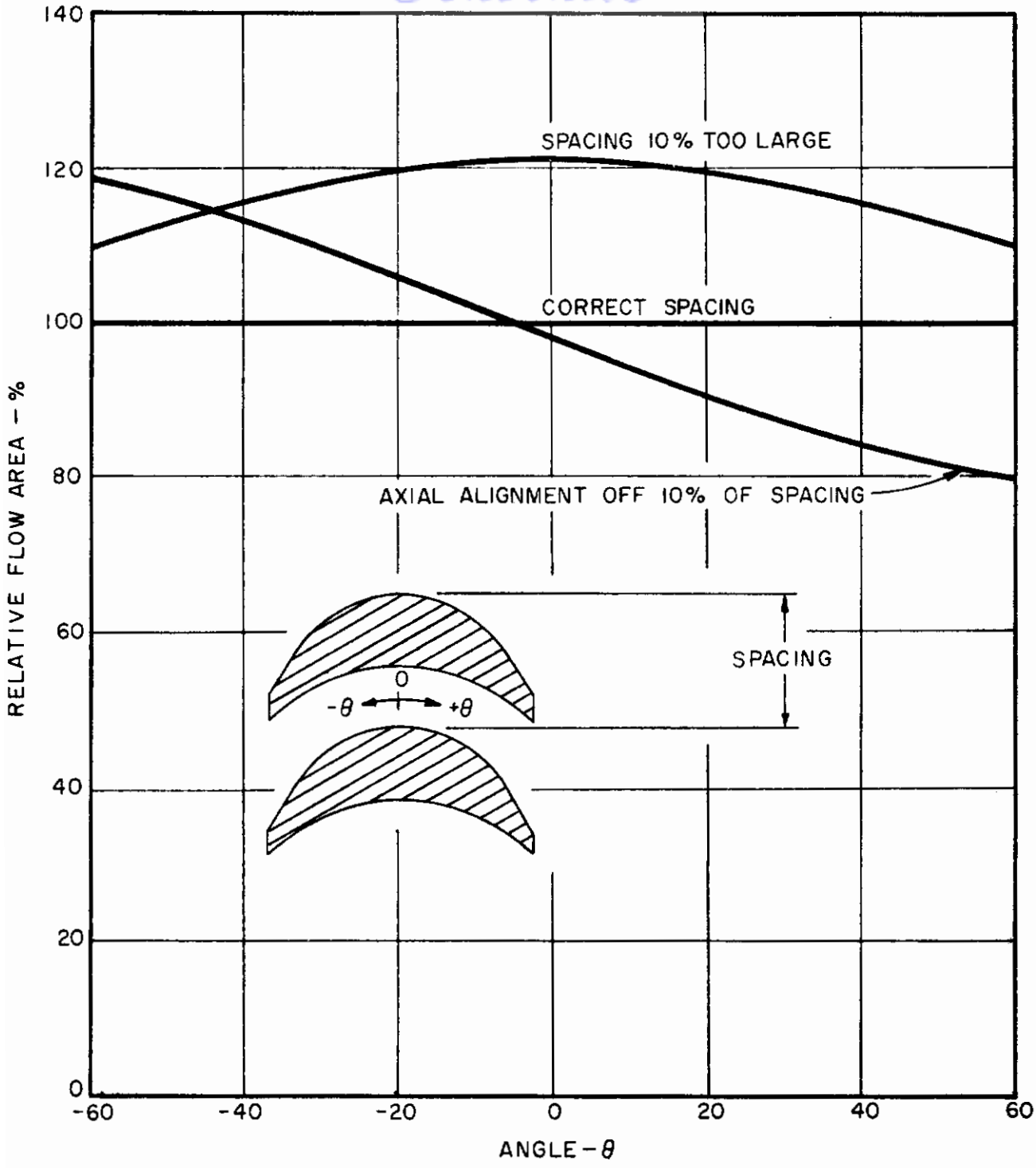

FIGURE III-B-26 CHANGE IN FLOW AREA DUE TO BLADE MISALIGNMENT

TYPICAL CONSTANT-AREA, CONSTANT-RADIUS IMPULSE BLADE

the need for expensive dies and the cooling of the wheel make this process unlikely for the production of space-power turbines in the near future, since the major attribute of sheet metal blades is their low cost in quantity - a factor which can be expected to be minor considering the limited production of space turbines.

Another fabrication problem encountered involves the joining of the turbine wheel to the high-speed shaft. Many of the refractory metals cannot be welded. Ordinary keying procedures cannot be used because of the centrifugal forces set up at the high speeds involved (greater than 20,000 rpm and up to 100,000 rpm). Splining is the most usual solution, but the difficulty of machining these metals makes this costly. This problem, too, is under study with various companies investigating the procedures for welding and brazing (e.g., Ref. III-B-27).

4.4 Seals

The problem of sealing a fluid on a high-speed shaft is one of long standing and one which has never been completely solved. In earth-bound power plants any leakage which exists will be detrimental because of the loss of energy of the leaving fluid and the loss of inventory from a closed system. However, the inventory can be made up and the losses tolerated. In space, the inventory loss is a critical problem, since there is no way of replenishing it, and the limitation on physical size of the package makes it difficult to keep the lost fluid from contaminating or interfering with the performance of other engine components. It is, therefore, usual to seal the rotating unit as a whole, allowing only the electric wires to pierce the sealing surface. Seals are provided to keep internal leakage low, but the whole rotating assembly is subjected to the working fluid vapor. This technique makes it impossible

to have two fluids within the sealed chamber so that the working fluid must now be used as the bearing lubricant (see subsection 4.5) and coolant for the alternator rotor.

Many specific types of seals are used. Labyrinth seals have been used in conventional application for many years and have been thoroughly investigated (e.g. Refs. III-B-28 and III-B-29). Face seals and shaft seals are also available and are discussed in Ref. III-B-30.

4.5 Bearings

In high-speed, auxiliary-power applications, it has been customary in the past to employ precision ball bearings. These bearings require some lubrication, not so much for the reduction of friction as for the cooling of the bearing. The heating is the result of deformation energy being converted to heat as each ball in the bearing picks up the load and releases it. Furthermore, it is impossible for all the balls to be precisely equal in diameter. This adds to the deformation loads. The reliability of the bearing is, then dependent on the care exercised in the selection and inspection of the bearings. Journal bearings are not subject to this type of fatigue.
If the bearing operates in the hydrodynamic regime, there is a thin film of lubricant separating the shaft and the journal so that no wear occurs. Journal bearings encounter trouble only on start-up and during the acceleration period as loads are changed. In space-power applications of the near future, there will be only one start and very little change in load for the life of the plant.

The trend in space-power packages has been to the use of journal bearings, and a body of technology is being built up on the use of journal bearings lubricated with working fluids such as liquid metals. Various companies

have already run bearings with liquid-metal lubrication, such as the mercury bearing used in the SNAP systems developed by the Tapco Group of Thompson-Ramo-Wooldridge, one set of which has run for over 2,500 hours on mercury.

Because of the criticality of the development of these bearings, the Air Force is sponsoring a study at Sunstrand Turbo. It will survey both hydrostatic and hydrodynamic bearings operating at up to 1500°F and up to 60,000 rpm. Five inorganic fluids will be used. They are rubidium, sulfur, mercury, potassium, and aluminum bromide.

From the experience of various contractors and the results of the study should come an understanding of which bearing materials can be used with the various working fluids. These must be chosen carefully to obtain long life and trouble-free operation.

4.6 Clearances

Since the pressures on the suction and pressure side of a turbine blade are not the same, some flow may be assumed to leak over the blade tip. The result is, of course, a reduction in work output. In Ref. III-B-20 it is shown that the leakage loss will be small if tip clearance-to-blade height ratio, $s/_h$, is less than 0.02. While this ratio is small, the blade height to be encountered in most space-turbine applications will also be small. Taking as a practical limit a clearance of 0.0005 in., the minimum blade height is 0.250 in.

The main problem is one of predicting and maintaining the clearance. In the first place, as the temperature of the wheel is raised during the start-up, the wheel expands. This expansion must be predicted accurately because it may be large, as is seen in Figure III-B-27, which shows the results for a typical turbine wheel. Second, the wheel is subject to creep which will

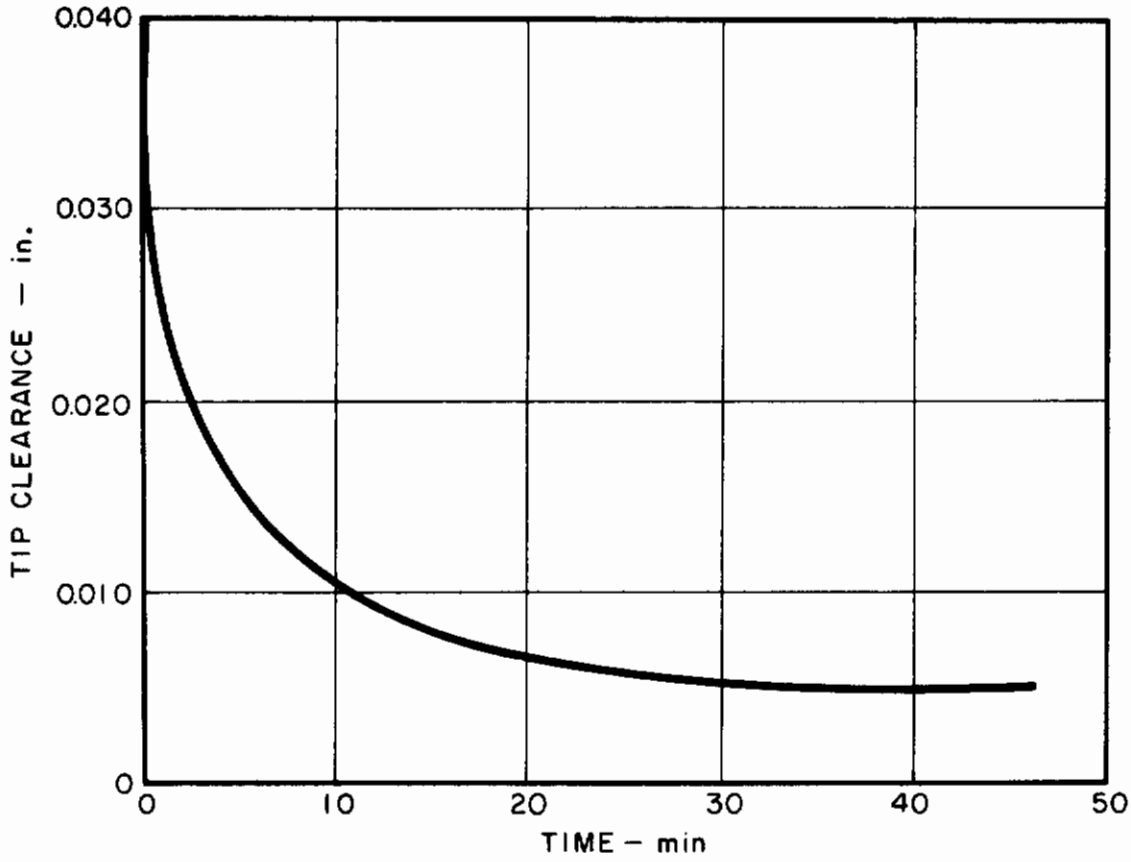

FIGURE III-B-27 TIP CLEARANCE FOR A TYPICAL TURBINE WHEEL

increase the wheel's diameter over a period of time. This must be anticipated to prevent the wheel from rubbing before its mission is complete.

The problems of tip clearance are sometimes solved by the placement of a shroud over the blade tips. This eliminates all tip leakage but increases the stresses due to the extra mass at the greatest radius. Another solution proposed is the inclusion of a band of honeycomb material around the periphery of the wheel (Figure III-B-28). As the wheel grows, it "mills" its own channel in the honeycomb keeping the clearance small. The difficulties associated with the elimination of the metal chips from a closed system present large problems, however.

Axial clearances are also a problem, but since wheel growth in that direction is much less, they are not as critical. An exception would be a multistaged, single-disc turbine such as the one described in Ref. III-B-9 where the axial clearance will determine the leakage between stages and, therefore, the total energy which can be utilized in the turbine.

FIGURE III-B-28 CLEARANCE CONTROL THROUGH THE USE OF HONEYCOMB MATERIAL

5.0 SPACE TURBINES - THE PRESENT AND THE FUTURE

5.1 The Present State-of-the-Art

At present, turboelectric power units which have been developed to an advanced state for space application include the 0.5 kw SNAP I system, the 3 kw SNAP II system, and the 1.0 kw SPUD unit. SNAP I is designed to operate with an isotope heat source, SNAP II with a nuclear heat source, and SPUD with a solar heat source. All three use mercury vapor. The SNAP II system -- which represents an extension of the basic design used in the SNAP I program -- is the most advanced of the units built and probably best represents the current state-of-the-art.

5.1.1 SNAP II Turboelectric Power Unit

According to Refs. III-B-31 and III-B-32, the turbine design-point operating conditions are as given in Table III-B-5.

TABLE III-B-5

SNAP II TURBINE DESIGN-POINT OPERATING CONDITIONS

Requirement	(a)	(b)	(c)
Rotational speed, rpm	40, 000	40, 000	40, 000
Outlet total pressure, psia	100	105	115
Inlet total temperature, ^{o}F	1150	1150	1150
Exit static pressure, psia	6.2	6.5	7.1
Required power output, kw	4.86	5.16	5.67

Requirement (a) is the original turbine requirement, and (b) represents a subsequent increase in output to achieve 3 kw of electrical power. Requirement (c) is an even later version. Figure III-B-29 is a block diagram of the system based on (c). Information in Ref. III-B-31 appears more complete than that in other references; therefore, this information will serve as the basis for

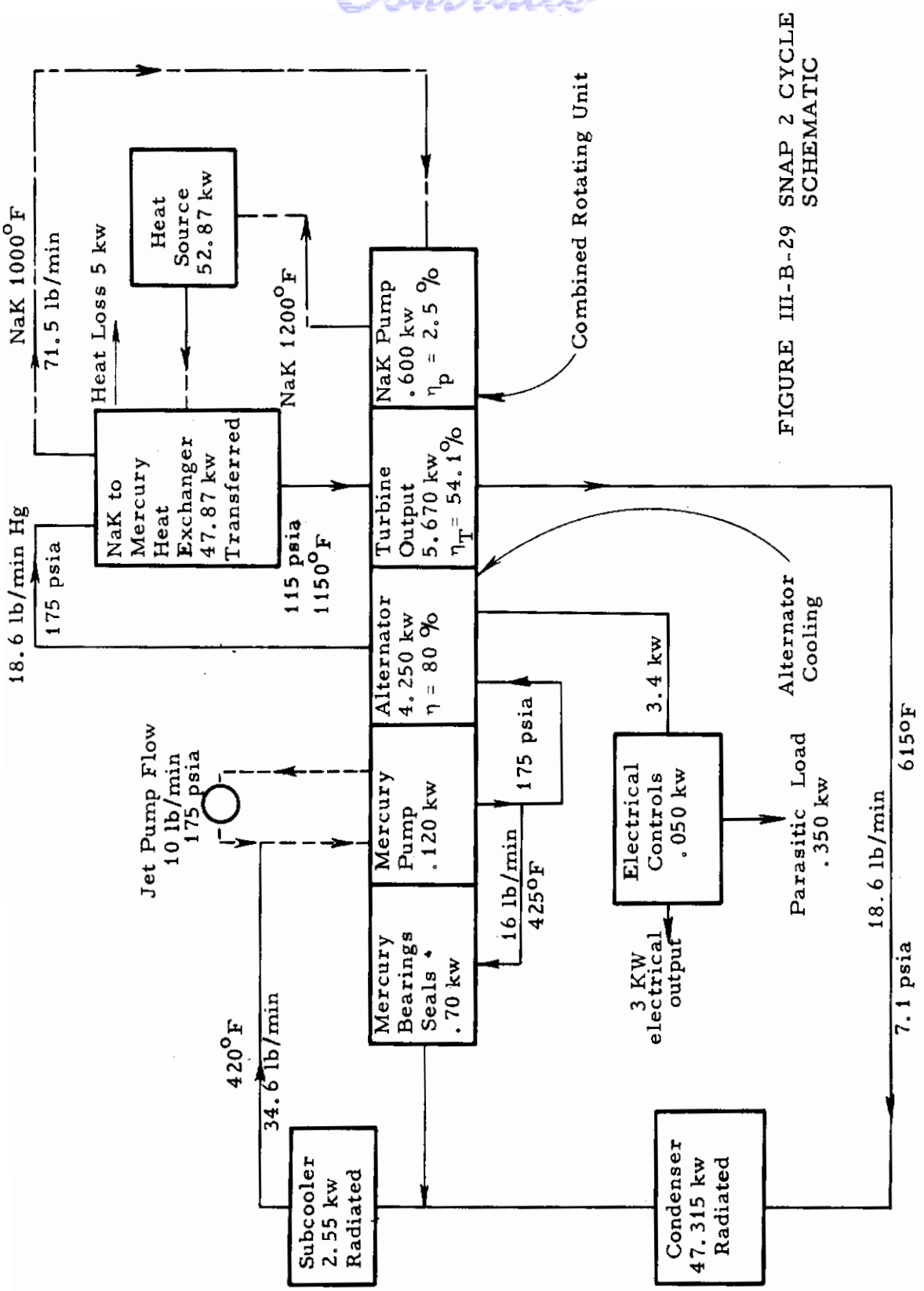

FIGURE III-B-29 SNAP 2 CYCLE SCHEMATIC

the following discussion. A comparison with the other systems is made to subsections that follow.

The expansion through the turbine results in a thermodynamic diagram such as Figure III-B-30. Tables III-B-6 and III-B-7, reproduced from Ref. III-B-31, show all the basic design data, A two-stage turbine is used, with each stage having full admission. From the description furnished, a shroud is provided at the tip of the blades. In Table III-B-8, the experimental results are compared with the anticipated performance. Ref. III-B-31 points out that three factors are the cause of discrepancies. They are as follows:

a. Insufficient pressure drop across turbine.

b. Reduction in flow rate.

c. Reduction in over-all efficiency.

Insufficient pressure drop seems to have been the major cause for low power output; it is caused by choking at the turbine exit and by failure to achieve as large a degree of supersaturation as had been expected. The choking effect is easily remedied by increasing exit area; it is no reflection on a lack of knowledge regarding the state-of-the-art of turbines. The anticipation of the correct degree of supersaturation will improve when more of the thermodynamic data for the liquid metals become available. The lower flow rate is a direct result of the choking effect, and the lower efficiency is due to the off-design operation resulting from the lower flow and wrong pressure ratio. In essence, then, all three factors are the same.

It might be of interest to compare the predicted performance of this turbine with the data discussed in section 3.0. The turbine and stage efficiencies listed in Table III-B-8 seem to be defined in some manner other than that commonly used.

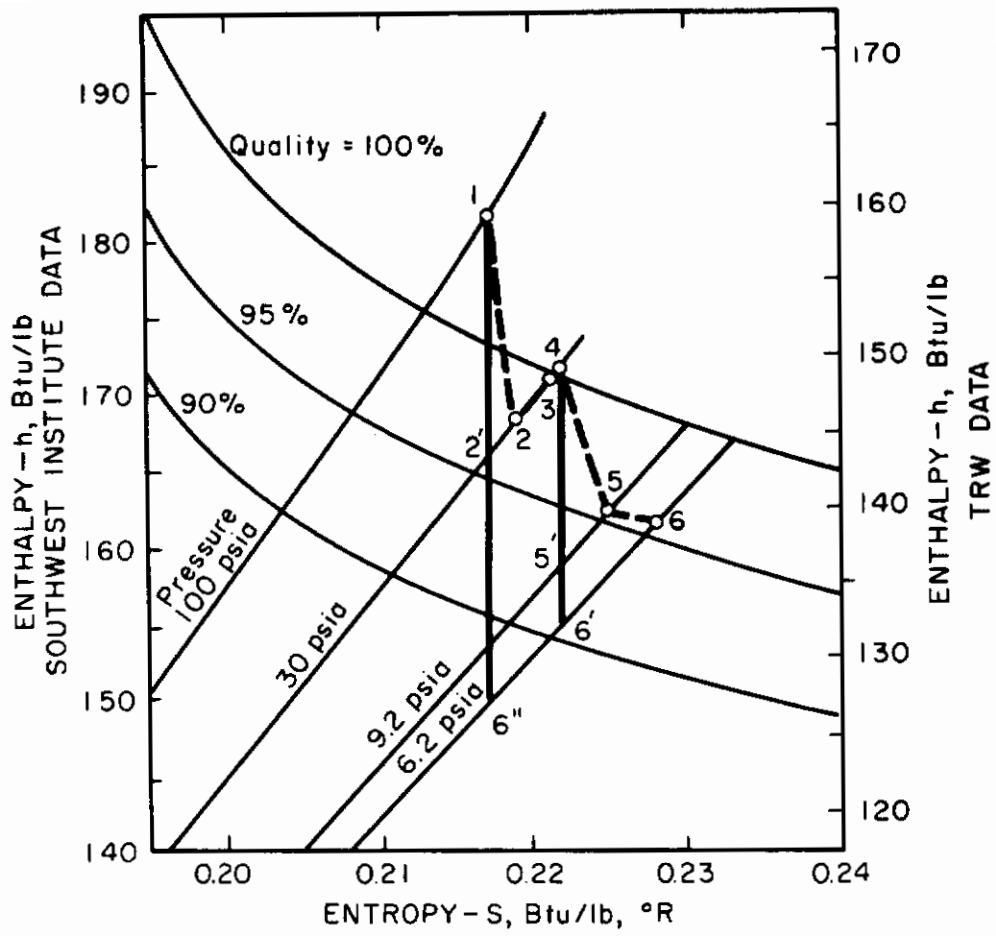

1 - First Stage Nozzle Inlet
2 - First Stage Nozzle Exhaust
3 - First Stage Rotor Exhaust
4 - Second Stage Nozzle Inlet
5 - Second Stage Nozzle Exhaust
6 - Second Stage Rotor Exhaust

FIGURE III-B-30 DESIGN TURBINE EXPANSION
SNAP II MERCURY TURBINE

TABLE III-B-6

TURBINE GEOMETRIC PARAMETERS

GEOMETRIC PARAMETERS		DESIGN DIMENSIONS	
		1st Stage	2nd Stage
Nozzle Pitch Diameter,	D_{m1}, in.	1.4	1.4
Rotor Pitch Diameter,	D_{m2}, in.	1.4	1.4
Nozzle Height,	ℓ_1, in.	.0883	.156
Rotor Blade Height,	ℓ_2, in.	.1155	.2160
Nozzle Axial Chord,	b_{x_1}, in.	.20	.28
Rotor Axial Chord,	b_{x_2}, kin.	.2	.2
Nozzle Inlet Angle,	α_o	138°	49°
Nozzle Exit Angle,	α_1	15°	20°
Rotor Inlet Angle,	β_1	27°	36°
Rotor Exit Angle	β_2	24°	32°
Number of Nozzles,	N_n	20	20
Nozzle Throat Width (gaging),	λ_1, in.	.05092	.07021
Rotor Exit Throat Width (gaging)	λ_2, in.	.04087	.04959
Nozzle Exit Actual Area	F_1, in^2	.08992	.21906
Rotor Exit Actual Area,	F_2, in^2	.1841	.50344
Labrinth Seal Clearance,	Δ_d, in.	.005	.005
Shroud Radial Clearance,	c, in.	.005	.005
Number of Blades,	N_b	39	47

TABLE III-B-7

TURBINE DESIGN-POINT AERO THERMODYNAMIC PARAMETERS

THERMODYNAMIC PARAMETERS			1st Stage	2nd Stage
Inlet Scroll Velocity	c_o	ft/sec	160	-----
Inlet Nozzle Velocity	c_o	ft/sec	160	243
Nozzle Exit Velocity	c_1	ft/sec	828	715.0
Turbine Flow	w_f	lb/min	16	16
Nozzle Inlet Total Pressure	poo	psia	100	33.33
Nozzle Static Exit Pressure	p_1	psia	30	9.2
Nozzle Exit Moisture	X_1	%	3	5.1
Rotor Inlet Velocity	w_1	ft/sec	596.5	494.53
Rotor Exit Velocity	w_2	ft/sec	458.8	554.60
Rotor Exit Static Pressure	p_2	psia	30	6.2
Rotor Tangential Velocity	u	ft/sec	244.3	244.3
Scroll Exit Velocity	c_4	ft/sec	----	450
Nozzle Inlet Total Enthalpy	hoo	Btu/lb	159.3	150.265
Nozzle Exit Static Enthalpy	h_1	Btu/lb	145.61	139.68
Rotor Inlet Total Enthalpy	h_{01}	Btu/lb	152.71	144.940
Rotor Inlet Total Pressure	p_{01}	Btu/lb	54	14.8
Rotor Exit Static Enthalpy	h_2	Btu/lb	148.50	139.19
Stage Power Output	HP	hp	3.408	3.199
Rotor Exit Moisture	X	%	.25	5

TABLE III-B-8

COMPARISON OF TURBINE PERFORMANCE AT THE DESIGN POINT

	Design Point	Experimental
First Stage		
Inlet Total Pressure poo, psia	100	102.7
Inlet Total Temperature Too, ^{o}F	1150	1163
Flow Rate W_f, lb /min	16	14.25
Stage Efficiency η_{ST}, %	57.2	46.60
Power Output HP, hp	3.408	2.663
Rotational Speed N, rpm	40,000	40,270
Interstage and Second Stage		
Total Temperature T_{02}, ^{o}F	780	848
Total Pressure p_{02}, psia	33.33	33.25
Static p_2, psia	30	27.90
Exit Static Pressure, p_4, psia	6.2	18.45
Exit Total Temperature T_{04}, ^{o}F	595	747
Stage Efficiency η_{ST}, %	45.3	34.20
Power Output HP, hp	3.199	.808
Turbine Over-All		
Isentropic Enthalpy Drop Δh_i, Btu/lb	31.630	21.72
Total Power Output HP_T, hp	6.607	3.471
Over-all Efficiency η_t, %	55.30	46.34

$$\eta_{1st} = \frac{h_1 - h_3}{h_1 - h_{2'}}$$

$$= \frac{159.3 - 148.5}{15.8}$$

$$= 68.3\%$$

$$\eta_{2st} = \frac{h_4 - h_6}{h_4 - h_{6'}}$$

$$= \frac{150.3 - 139.2}{18.8}$$

$$= 59.0\%$$

$$\eta_t = \frac{h_1 - h_6}{h_1 - h_{6''}}$$

$$= \frac{159.3 - 139.2}{31.6}$$

$$= 63.6\%$$

This compares with values of 57.2, 45.3, and 55.3 percent, respectively, listed in the table. The specific speed, specific diameters, and efficiencies can be determined and compared with values found from the N_s - D_s diagram, Figure III-B-31. The values are listed in Table III-B-9 for comparison.

TABLE III-B-9

DESIGN-POINT ANALYSIS -- SNAP II TURBINE

	N_s	D_s	η	η from N_s - D_s Diagram	D_s for opt.	η opt.	D for η opt.
First Stage	25.4	1.68	68.3%	65%	2.6	74%	2.3 in.
Second Stage	49.6	0.81	59.0%	55%	1.7	81%	2.9 in.

It is seen that the efficiencies compare favorably and that an increase in performance might be expected if the turbine diameter were increased. Full admission could probably be maintained in the first stage, and reaction could

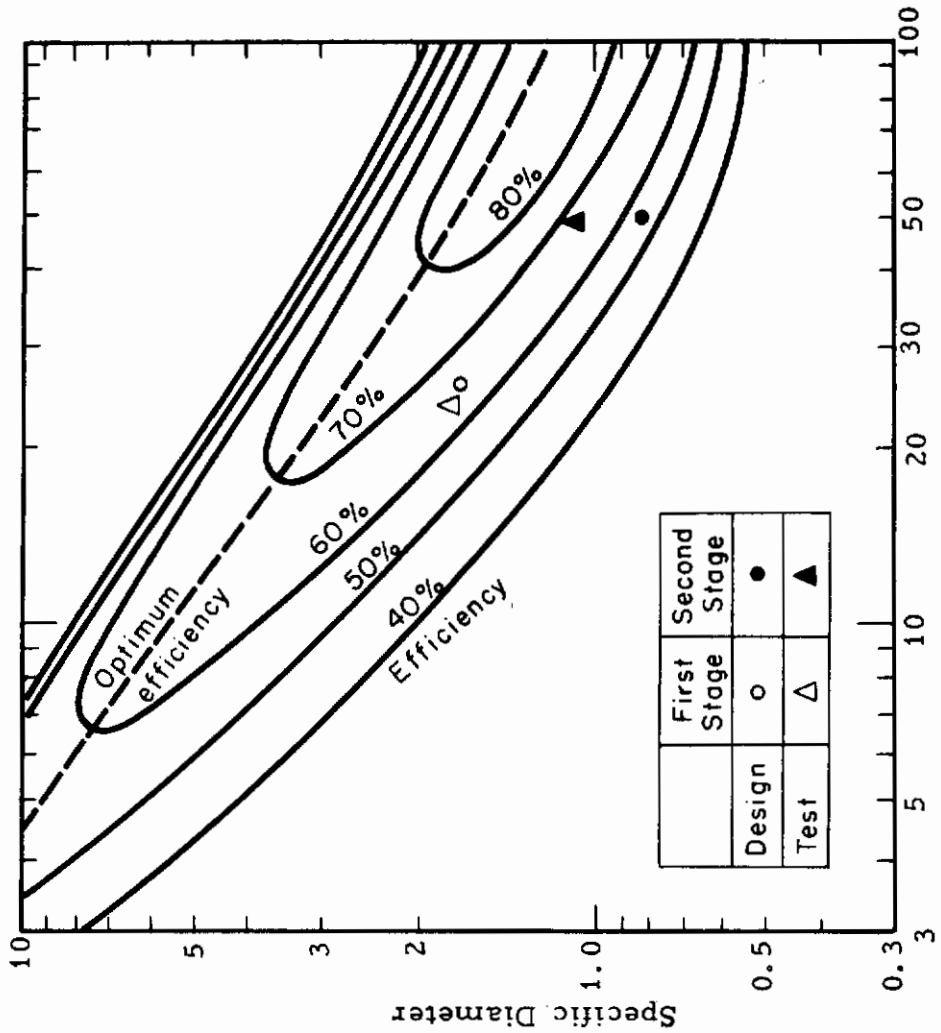

FIGURE III-B-31 OPERATING POINTS - SNAP II TURBINE

be kept in the second stage.

The reason a two-stage turbine was used in this design seems to be due to Mach-number considerations. In Ref. III-B-31, it is stated that absolute Mach number entering the blade row should be limited to 1.3 and the relative Mach number to 0.85. If all the expansion were taken in one stage, the velocity leaving the nozzle would be about 1,100 ft/sec. Since the sonic velocity is approximately 650 ft/sec, this means that the Mach number will be about 1.7 -- perhaps more than the design engineers were willing to use.

The efficiency for a single-stage turbine may be determined from the N_s - D_s diagram. The specific speed is 31.6, and the optimum efficiency is 76 percent. The relative Mach number is approximately 0.95. According to Ref. III-B-33, losses are not as high as they once were thought to be and are somewhat predictable. The correction should be about 0.96 - 0.98 for this Mach-number range. The efficiency for a single-stage turbine should then be about 74 percent. The corresponding specific diameter is 2.3, making the wheel diameter 3.5 in. and the tip speed 550 ft/sec at 40,000 rpm. This is low enough for long life at this temperature, according to the stress curves presented previously.

The actual performance figures can also be compared to the theoretical. In Figure III-B-32, the turbine expansion process as deduced from the data in Ref. III-B-31 is drawn for the test results. Again, the efficiencies must be recomputed to standard form. It is found that the results are as in Table III-B-10.

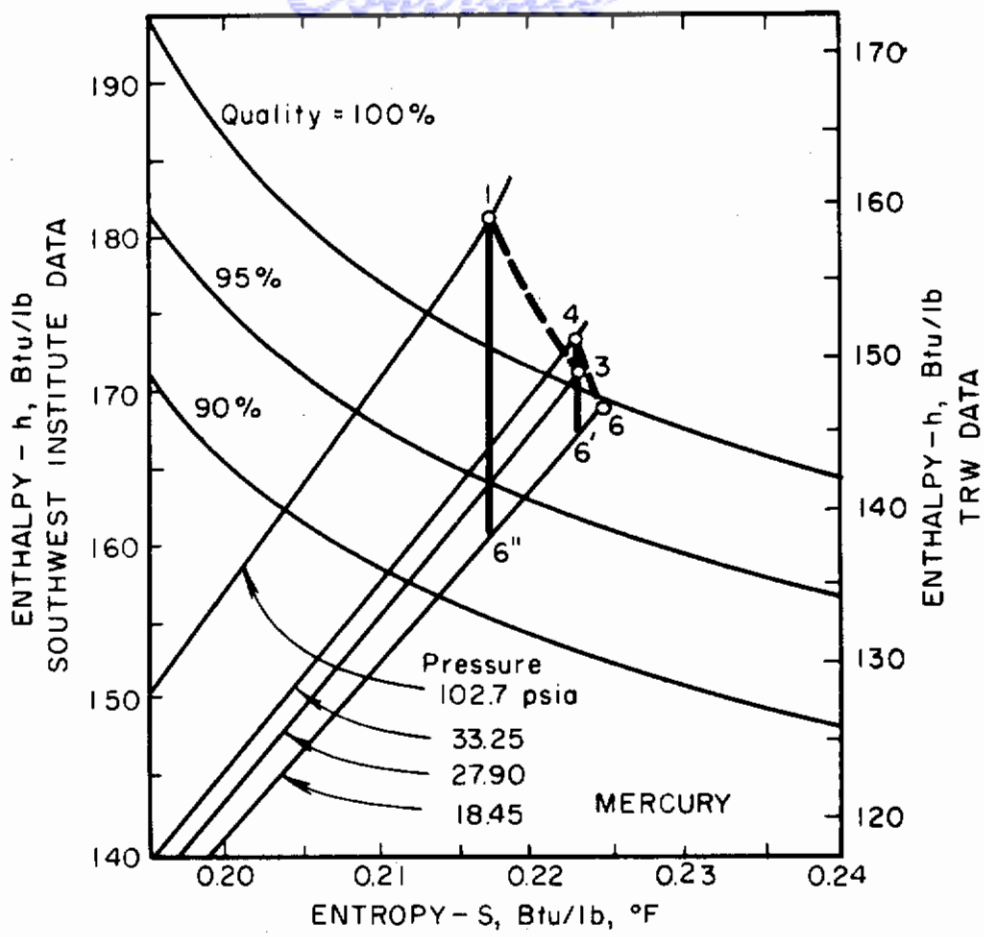

1 - First Stage Nozzle Inlet
3 - First Stage Rotor Exhaust
4 - Second Stage Nozzle Inlet
6 - Second Stage Rotor Exhaust

FIGURE III-B-32 TEST TURBINE EXPANSION
SNAP II MERCURY TURBINE

TABLE III-B-10

TEST-POINT ANALYSIS -- SNAP II TURBINE

	N_s	D_s	η	η from $N_s - D_s$ diagram	(D_s) opt.	η opt.	D for η opt.
First Stage	22.5	1.83	60%	63%	3.0	72%	2.3 in.
Second Stage	50.4	1.13	72%	70%	1.7	81%	2.1 in.

From the data found in Ref. III-B-32, it can be seen that the latest cycle parameters, shown as (c) in Table III-B-5, require 5.670 kw (design (a) required 4.86), and the flow rate and the inlet pressure have also been raised. The pressure ratio has been kept constant, but the pressure ratio per stage has been changed so that it is the same in each stage. (Ref. III-B-34). Basically, however, the cycle remains the same.

It can be concluded that the SNAP II power turbine is a fairly efficient unit and that its low net power output as reported in Ref. III-B-31 can be explained in terms of choking in the exhaust duct -- a problem which is easily remedied. It might well be desirable to increase the wheel size in both stages since, according to the $N_s - D_s$ diagrams, this should result in higher efficiency. It is also interesting to consider the substitution of a one-stage turbine, since based on the latest data the Mach number level to be encountered will be high but not excessive.

The SNAP II turbine is, without a doubt, the most advanced of the present space turbines. It is operational and in this the designers can take pride. Problems of designing bearings and seals, as well as those connected with wet-vapor operation, had to be solved. The mechanical design of this power unit is rugged but straightforward. From the data in Ref. III-B-32, the whole rotating unit is mounted on two mercury lubricated bearings, with the alternator and turbine straddle mounted and the various pumps located outboard.

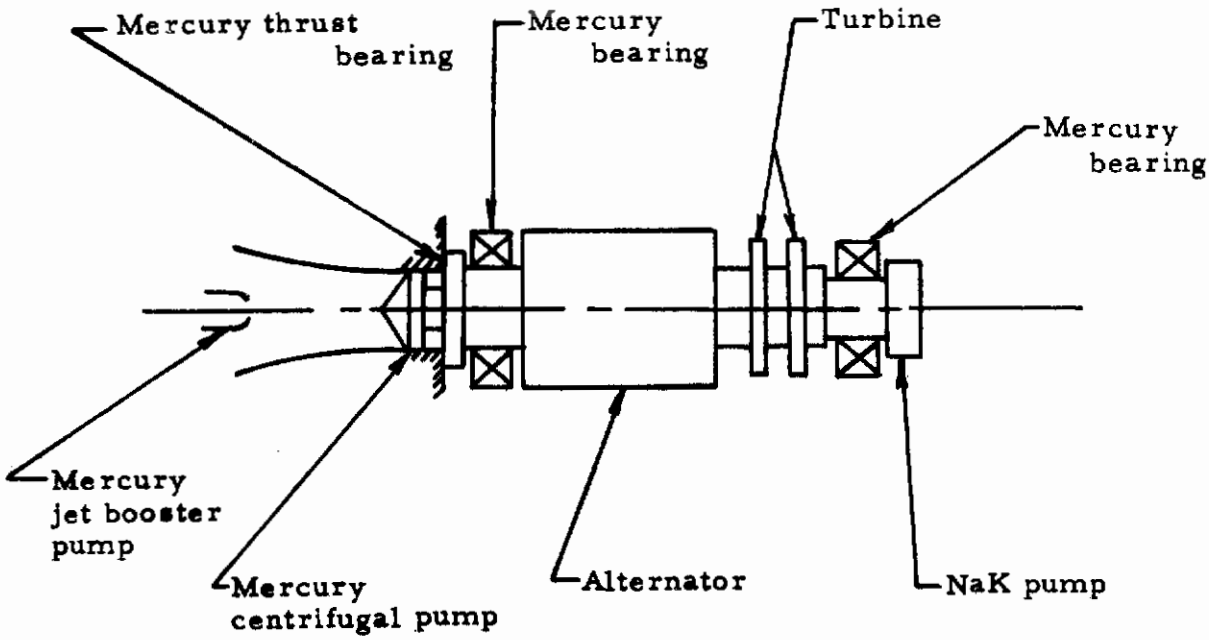

The combined rotating assembly has accumulated 870 hours of test time, including a 20-day endurance run. Mean conditions during the endurance run were as follows:

Unit Speed	35,000 rpm
Inlet Temperature	1145.8°F
Inlet Pressure	94.7 psia
Exhaust Temperature	643.7°F
Condenser Pressure	9.1 psia
Flow Rate	15.03 lb/min.

5.1.2 SNAP I Systems

The SNAP I turbine consists of a three-stage assembly. Design-point specifications are

Fluid	Mercury
Inlet pressure	210 psia
Inlet temperature	1300°F

Rotational speed	40,000 rpm
Exhaust pressure	2.06 psia
Weight-flow rate	0.0311 lb/sec
Power	0.875 hp
Design efficiency	40 percent

During test all these conditions were met with an average efficiency of 42 percent at the design point.

The turbine assembly consists of partial-admission first and second stages and a full-admission third stage. Mercury hydrosphere bearings are used. The configuration is as indicated with the whole unit straddle

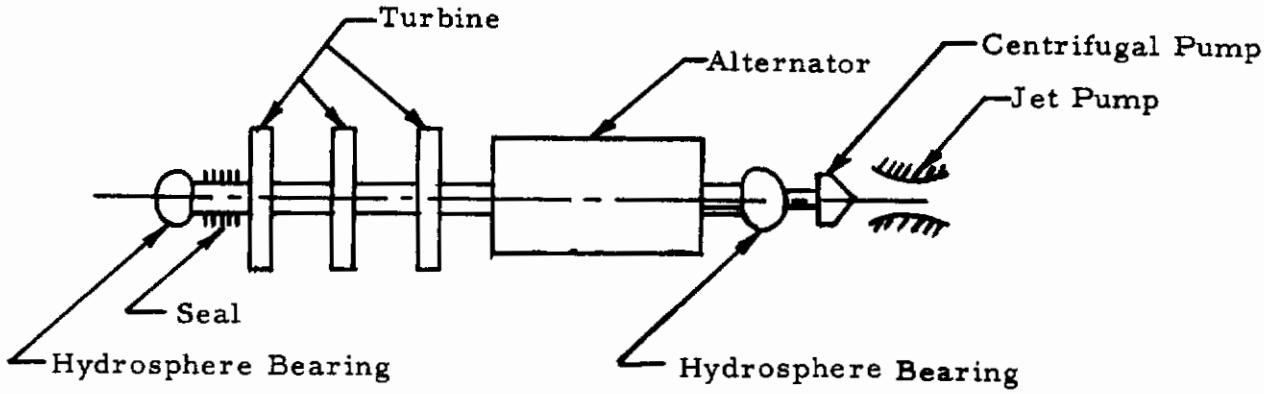

mounted between the bearings except for the pump which is overhung.

Perhaps the most remarkable achievement of this unit is the duration of 2510 hours of remaining time with no deterioration of performance.

5.1.3. Developments at AiResearch

AiResearch Corporation of Phoenix has been active for sometime in the development of closed cycle space turbines. A turbine rated at 3 kw using mercury vapor was built and tested during 1957-58. The specifications as given in Ref. III-B-36 are listed in Table III-B-11.

TABLE III-B-11

SPECIFICATIONS OF AIRESEARCH 3 KW TURBINE

Working Fluid - Mercury
Flow Rate - 16 lb/min.
Power level - 3 kw
Duration - 400 hr

	Inlet Press.	Exhaust Press.	Inlet Temp.	Dia.	RPM
First Stage	125 psia	14.2 psia	1100°F	2.86 in.	36,000
Second Stage	14.5 psia	6.3 psia	1100°F	2.86 in.	36,000

There is a marked similarity between this system and the SNAP II turbine discussed previously. Significantly, the turbine diameter is much larger (twice that of SNAP II) and much closer to that found by using the N_s - D_s diagram. In fact, the specific speed and specific diameter of the first stage cross at the optimum efficiency line. The results are shown in Table III-B-12.

TABLE III-B-12

DESIGN-POINT ANALYSIS -- AIRESEARCH 3 KW TURBINE

	N_s	D_s	Efficiency	
			from N_s - D_s diagram	optimum
First Stage	20	3	71 percent	71 percent
Second Stage	149	.71	70 percent	82 percent

Measured efficiencies are not given, but from the thermodynamic data the available energy should have been 18.5 and 6 Btu/lb for the two stages. The power should be 6.9 kw and, since the unit is rated at 3 kw, this seems to indicate that maximum efficiency was not attained.

Some of the results are of particular interest in considering the wet-vapor operation. It was found that the second stage exhibited significant erosion after 37 hours of operation. The erosion seems to have occurred in the last 15 hours. Subsequently, the turbine blades were refinished and restored to their original surface finish and rerun for 150 hours at half speed. From the pictures available, the blade angle seems to have been slightly changed also. Much less erosion occurred.

A look at the velocity diagram (Figure III-B-33) is significant. The blade angle is -12° at the design condition. Suppose that the liquid velocity is 50 percent of the vapor velocity. The relative liquid velocity is then 266 ft/sec, and the angle between two relative vectors is 54°. Erosion is exactly in the region indicated in the diagram. Now when the tip velocity was reduced, the relative vapor-velocity vector hits on the pressure side and the relative liquid velocity is reduced to 107 ft/sec, impinging at almost the correct angle of -12°. The test results confirm the area of impingement, and the lower velocity means less erosion, since the damage caused by droplet impingement must be a function of this velocity.

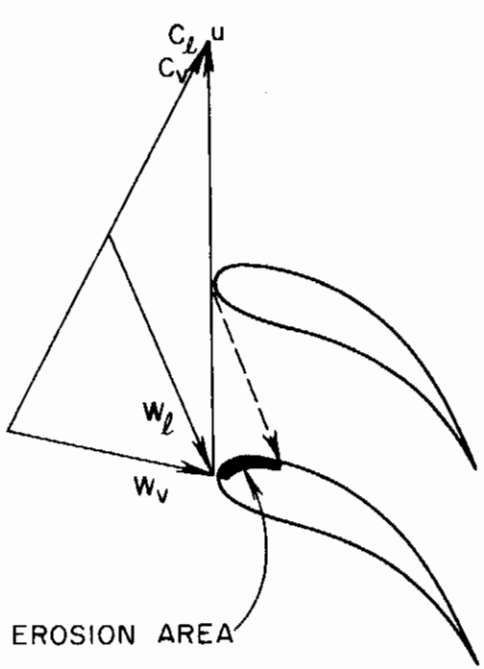

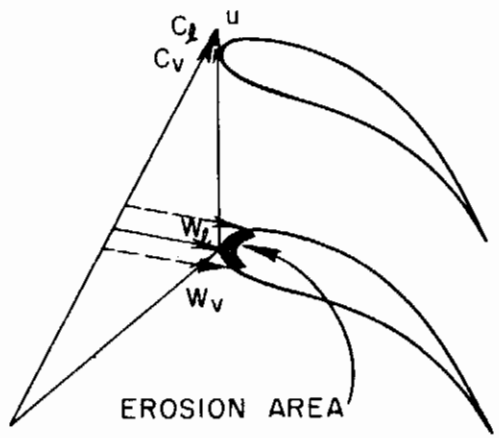

FIGURE III-B-33 VELOCITY DIAGRAMS - AIRESEARCH 3 KW TURBINE - SECOND STAGE

5.2 The Immediate Future

During the fiscal year 1960, four major space-power systems involving turboelectric power conversion were initiated. They are as follows:

a. 15 kw Solar Power Unit -- Sundstrand Turbo

b. 3 kw Sunflower -- Tapco Group, Thompson Ramo-Wooldridge

c. 30 kw SNAP VIII -- Aerojet-General Corp.

d. 300 kw Nuclear Power -- AiResearch Corp.

Each will have unique problems for its turbomachinery. The working fluids for these units will be mercury for the SNAP VIII and the Sunflower system, rubidium for the 15 kw Solar Power Unit, and potassium for the 300 kw Nuclear Power Unit. Pertinent data on the SNAP VIII program are classified and not included in this section. The choice of working fluids represents an important trend. When temperatures are low enough, mercury (which has a high vapor pressure) is used. At high temperature, the pressures for mercury are excessive, and rubidium or potassium with lower vapor pressure are used (Figure III-B-34). High pressure requires thick walls in the tubes to contain the fluid, thereby adding to the system weight.

System considerations significantly effect the choice between potassium and rubidium. Rubidium has a greater density (Figure III-B-35 shows about four times that of potassium). The required mass-flow rate is about 2-1/2 times that of potassium, as is shown below, making the volume-flow rate somewhat smaller for rubidium. Since the weight needed for meteorite protection is a function of the exposed area, smaller tubes (i.e., smaller volume-flow rates) are to be preferred. On the other hand, system weight is also influenced by the weight of the working fluid which must be carried. Here the less dense liquid has an advantage. Pump work will also be greater for the denser fluid. All in all, the decision is not simple, and each application must be considered separately.

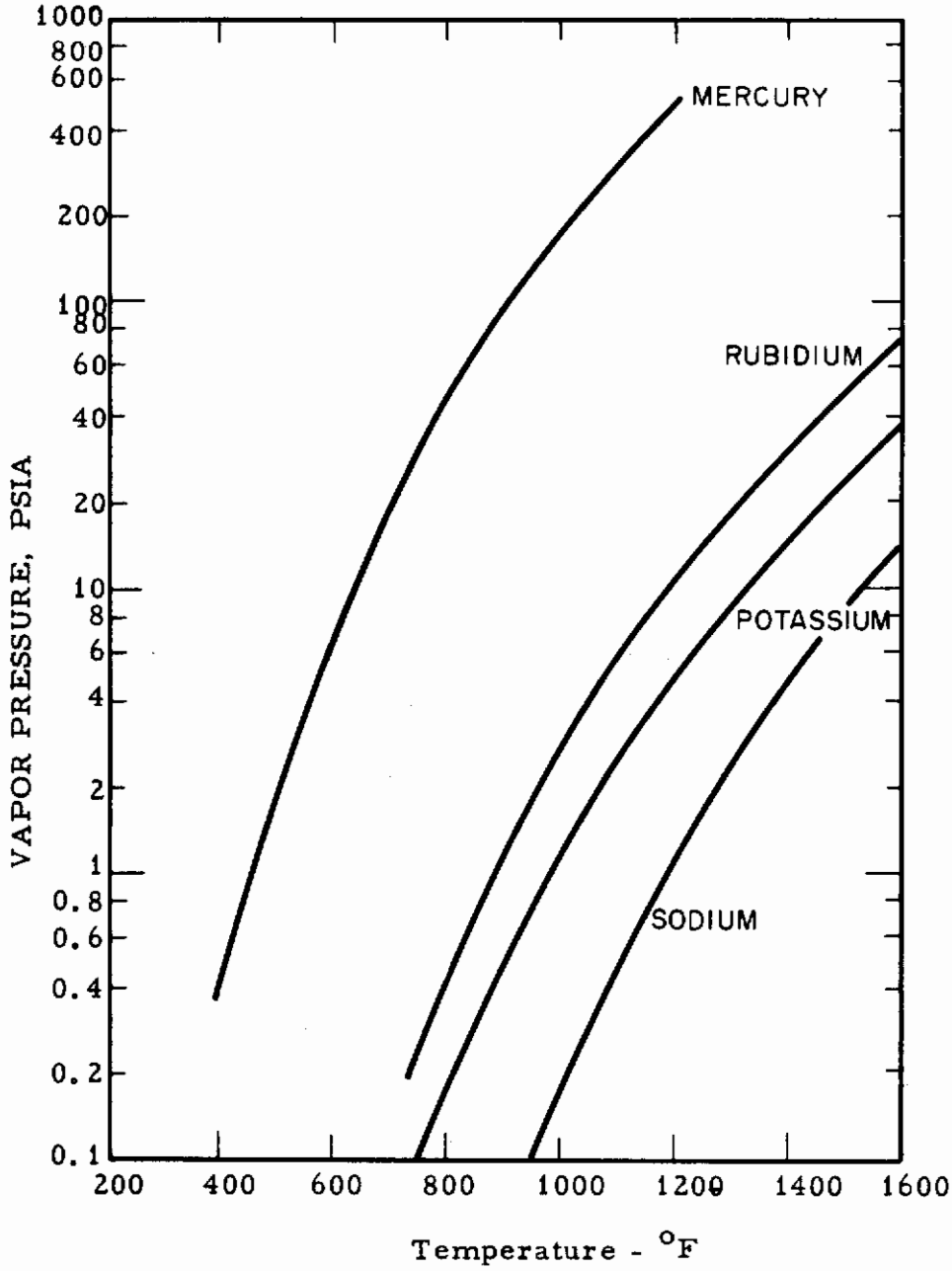

FIGURE III-B-34 VAPOR PRESSURE OF VARIOUS WORKING FLUIDS

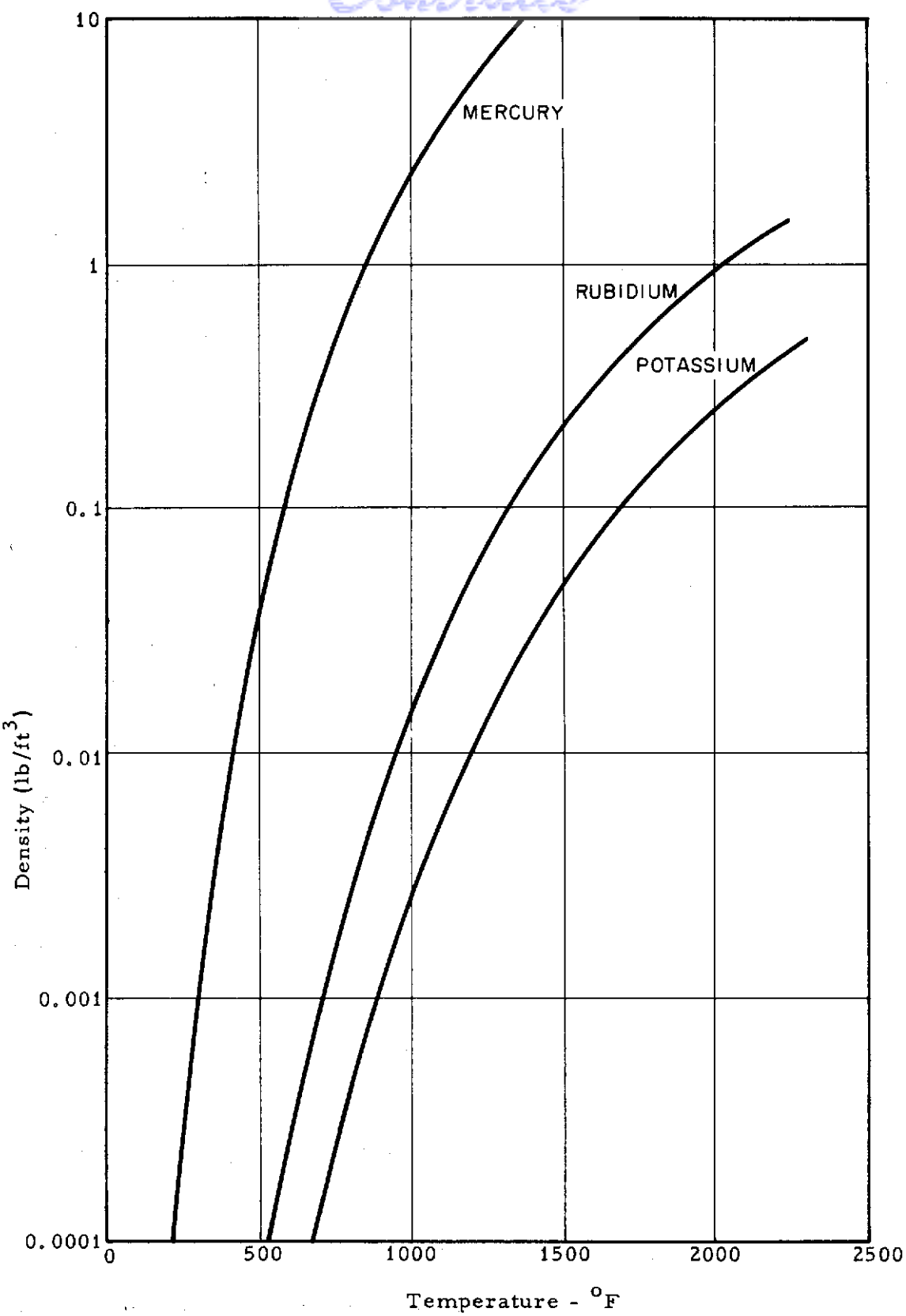

FIGURE III-B-35 DENSITY OF THE SATURATED VAPOR OF VARIOUS WORKING FLUIDS

Considering the turbine apart from the system, the choice between potassium and rubidium is much clearer. The enthalpy change occurring across a turbine stage determines the spouting velocity which, in an impulse turbine, is approximately the absolute velocity entering the blade row. Since efficiency has been shown to be a function of the ratio of wheel tip speed to spouting velocity, $^{u}/c_{o}$, higher values of c_{o} imply higher tip speeds. Since they are limited by the stresses, there exists a limit to the head drop which may be taken in each stage.

In Figure III-B-36, it is shown that, for an equal temperature range (2300°R to 1700°R), potassium has 2.6 times the isentropic enthalpy change which is, of course, indicative of the actual enthalpy change. At the same tip speed, the number of stages must therefore be increased by this factor, or the tip speed and stage number must both be raised. It must again be pointed out that rpm is not an independent parameter because of the synchronous frequencies required by the alternator, so diameter may have to be increased. Increased stage number and increased wheel diameter both contribute to greater turbine weight and lower reliability. Rubidium, therefore, enables simpler turbine design. Potassium, however, has an advantage in that the need for many turbine stages should make it easier to prevent the formation of very wet vapor.

Sodium is to be considered for future systems, according to some authorities. In fact, the AiResearch 300-kw power unit uses sodium as a back-up program. The major problem associated with this material is its extremely low vapor pressure (Figure III-B-34). On the same basis of comparison as used in Figure III-B-36, sodium has an enthalpy change of 440 Btu/lb, about twice that of potassium, but the density is approximately

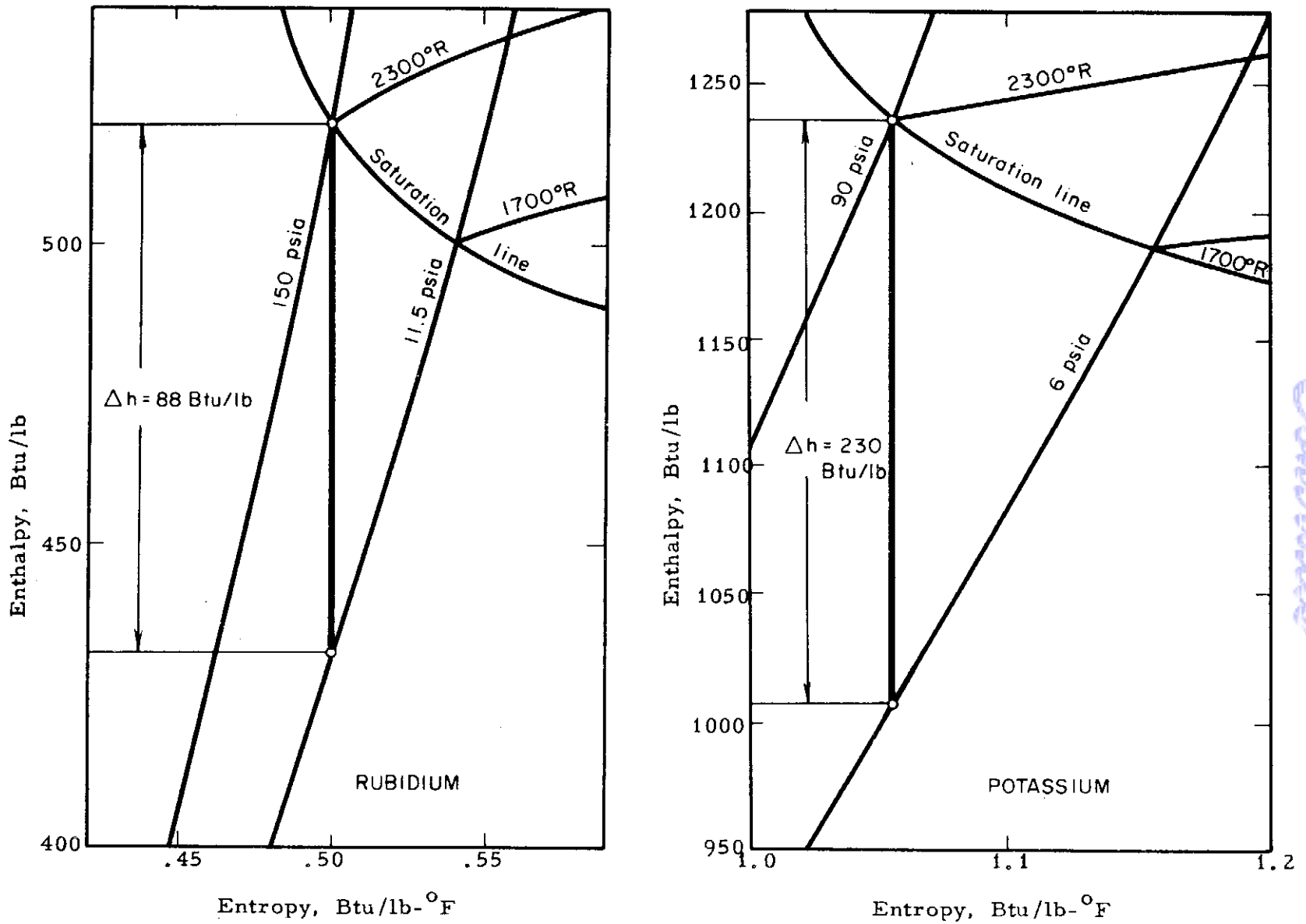

FIGURE III-B-36 COMPARISON OF THE ADIABATIC HEAD FOR RUBIDIUM AND POTASSIUM

10 percent that of potassium. The volume-flow would then be about five times that of potassium, and the pressure-level ratio is about one-half.

Another major problem for operation with sodium is the extremely flat vapor dome. Isentropic expansion would result in a quality of 76 percent, so that many stages are needed in a sodium turbine. Nevertheless, at very high-temperature operation, sodium might be expected to become the dominant working fluid, because the pressure level will then be reasonable; According to Ref. III-B-35, sodium cycles will be operating in 1970 with peak temperatures of 2,400° F and power levels up to 20 megawatts.

5.2.1 15 kw Solar Power Unit

Sundstrand Turbo has undertaken the design of a complete solar-power plant delivering 15 kw of electrical energy. Since the contract was awarded only recently and much of the information contained in the Sundstrand proposal is classified, only fairly sketchy design data are available.

A brief description of the system can be found in Ref. III-B-37. The turbine is composed of three stages, and it appears that the first is of the impulse type and that the second and third have reaction. The working fluid is rubidium boiling at 1,200°F (10 psia) and superheated to 1,750°F. Condensation delivers fluid subcooled to 675°F.

It is of some interest that Sundstrand expects to superheat by about 550° and then reheat to 1,600° and 1,450°F. If the amount of superheat in the reheaters is assumed to be 550° also, interstage pressures may be expected to be 3.3 psia and 1.0 psia. The pressure ratio in the first two stages is then 3.3.

Since it is likely that condensation does not occur at 675°F (as stated in Ref. III-B-37) and that 675°F represents the subcooled state, a pressure ratio of 3.3 might be assumed for the third stage also. This makes the exhaust pressure 0.33 psia and the condensing temperature 775°F. One hundred degrees of subcooling are therefore provided, as shown in Figure III-B-37. The specific speeds for the stages (based on a reasonable guess for the flow rate) and the efficiencies based on Sundstrand's own curves are as follows:

	N_s	η
1st Stage	25	73 percent
2nd Stage	40	80 percent
3rd Stage	80	82 percent

The analysis is based on reasonable assumptions but not on published information. It can be safely stated that the specific speeds are approximately correct and that the first stage is of the impulse type, the second has some reaction, and the third is at least 50 percent reaction.

The mechanical design published in Ref. III-B-37 shows the first and second stages overhung on one end and the third stage overhung on the other end of the alternator rotor. All are combined with the pump on one shaft. The bearings are between the turbines and the alternator making the fluid machinery overhung. It is claimed that pump location at the third-stage end will keep the pump cooler. The journal bearings are lubricated with rubidium and are placed to equalize the loads.

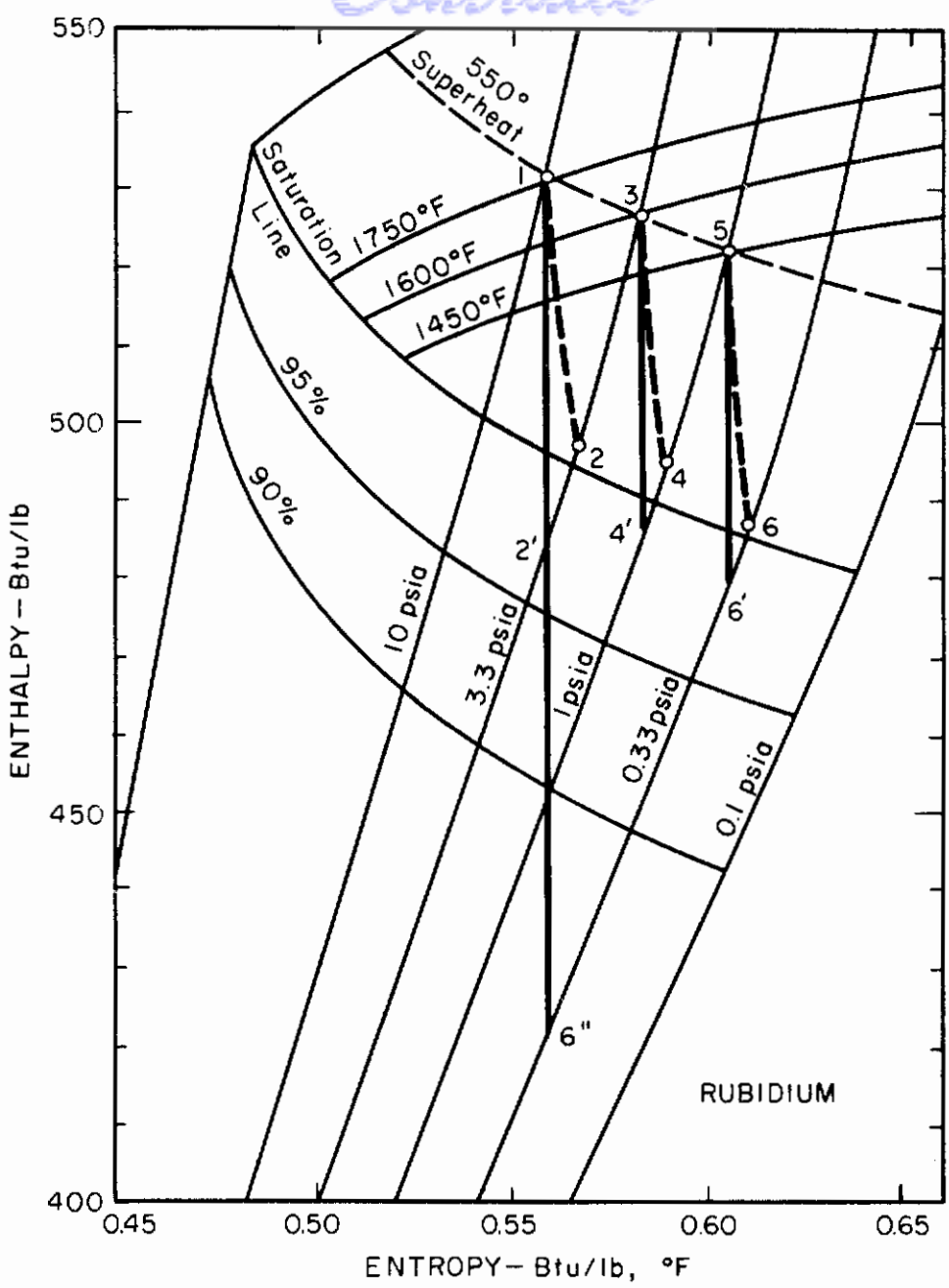

FIGURE III-B-37 PROBABLE CYCLE - 15 KW SOLAR POWER UNIT SUNDSTRAND TURBO

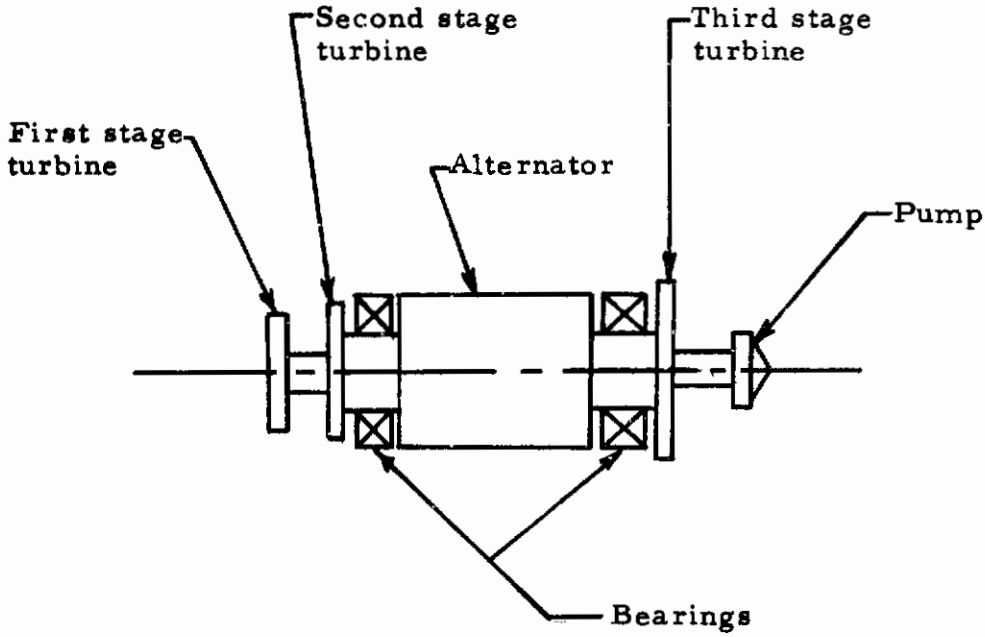

The major development problems for this turbine unit will be in the development of the rubidium bearings. The turbomachinery is fairly straight forward because each stage has a high enough specific speed, and expansion does not carry far into the wet region, i. e., vapor quality is nearly 100 percent. Successful completion of the turbine unit may be expected within a year.

5.2.2 Sunflower I

Sunflower I is a 3 kw solar auxiliary space-power system being developed by the Tapco Group of Thompson Ramo-Wooldridge. The power level is the same as that of the SNAP II system and the turbogenerator part of the system will be a modified version of the SNAP II unit using mercury. Duration is expected to be one year.

5.2.3 300 kw Nuclear Power Unit

Most details regarding the 300 kw Nuclear Power Unit (being developed by the AiResearch Manufacturing Company of Arizona) are classified. It can be established that this cycle will use potassium as the working fluid. The choice was based on the advantages of low pressure and the growth potential of a potassium power plant. The turbine design is not firm, because the contract is fairly new, but between 5 to 8 stages are expected. With rubidium, fewer stages would have been needed, but AiResearch does not expect major problems with the extra stages. Velocities in each stage will be low, and impulse designs will be used wherever possible. The last few stages will have fairly long blades requiring some reaction, at least at the tips. At present, the design does not include superheat or reheat, but these may be added in the future.

No details of the mechanical design are available, except that potassium is to be used to lubricate the bearings.

5.2.4 Other Projects

The Los Angeles Division of AiResearch has been developing turbines for space applications. According to Ref. III-B-38, they are developing a hydrogen engine operating with a triple re-entry single-disc turbine. The inlet condition is 1, 000 psia and 1, 240°F, and the pressure ratio per stage is 10:1. The tabulation below summarizes the information obtained.

	Turbine type	Press. ratio	Inlet press.	Inlet temp.	Dia.	RPM
1st Stage	Impulse	10	100 psia	1340°F	7.5 in.	48, 000
2nd Stage	Impulse	10	10 psia	939°F	7.5 in.	48, 000
3rd Stage	Impulse	10	1 psia	604°F	7.5 in.	48, 000

Working Fluid - Hydrogen

Flow Rate - 56 lb/hr

Power Level - 40 hp

Duration - 4.5 hr

No test results are available, but the expected efficiency based on these data is approximately 36 percent.

5.3 The Future of Turbines in Space

In the compilation of this report, various experts in the field of turbomachinery were asked for their opinion regarding (1) the future of turbines for space-power plants and (2) what would contribute most to an advance in the state-of-the-art. The answers were almost unanimous in the view that the perfection of turbines to handle supersonic flow would assure the future of turbines and would do most to advance knowledge. Second to be mentioned was the development of materials capable of higher temperature operation.

5.3.1 The Supersonic Turbine

It was pointed out previously that turbines must use more than one stage to keep the enthalpy drop per stage low enough to limit fluid velocities in the turbine. The limiting condition is, of course, the Mach number. At the present time, every effort is made to keep the absolute Mach number at a value less than 1.4 or 1.5, although values up to 1.8 or 1.9 are often encountered. Some losses are engendered, but up to this range they are tolerable. If a turbine could be perfected to handle flow of higher Mach number, the number of stages could be decreased, thereby saving weight, volume, and the added losses of the extra stages.

This problem is under study at present, especially by NASA. As early as 1952, Boxer, et al. developed a theory regarding supersonic turbine construction and published it with limited test data in Ref. III-B-39. The theory holds that uniform parallel supersonic flow can be transformed into a flow with vortex distribution and then turned in a shock free manner. After sufficient turning has occurred, the flow is reconverted to a uniform parallel flow field. Figure III-B-38 describes the process. Cascade tests of this process were made, and the problem of starting the flow was investigated. Everything indicated that a successful design could be developed. When the design was applied to a rotating rig, however, the performance did not meet expectations. Repeated tests have shown that the effects of the third dimension, absent in cascade tests, is of great influence and must be accounted for.

Work has continued in the field. According to Ref. III-B-40, the shock waves produced by supersonic flow past impulse blades were investigated and photographed. The question of eliminating the losses due to the shock remains.

5.3.2 The Materials Problem

Over the past decade, great strides have been made in developing materials for high-temperature, high-stress service. These materials have made it possible to design turbines with tip velocities exceeding 2,000 ft/sec when high-energy (i.e., high-combustion temperature) fuels are used.

The development of the new materials can only be the result of extensive, and expensive, metallurgical research. The most promising areas seem to be in the field of ceramics or ceramic-coated metals. Although these materials can withstand the temperatures involved, their brittleness is a cause of concern.

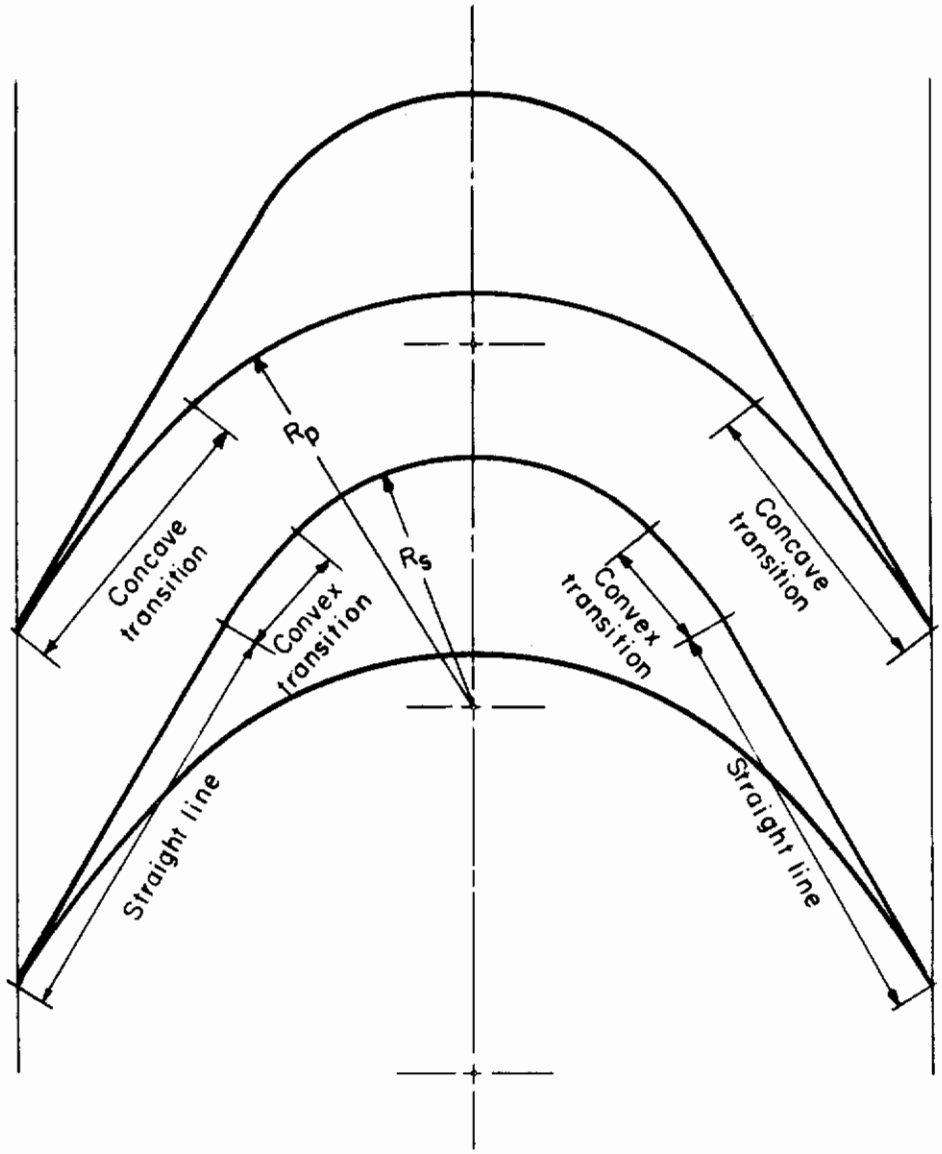

FIGURE III-B-38 SUPERSONIC BLADE PASSAGE VORTEX-FLOW THEORY

At the present time, many companies are working to perfect better materials. It must be of some concern to the turbine engineer, however, that the economic incentive for their development is very limited in many cases and that the development costs will not be borne by private concerns completely. The unique feature required for turbine wheels is high strength at high temperature. Most other applications may require one but not both simultaneously. The number of space turbines which will be built will always be limited, and conventional turbine power plants will not require such high strength. Development, therefore, will occur through government-sponsored research in the field of metallurgy. This is being done and will undoubtedly continue.

5.3.3 The Fabrication Problem

Associated with the material problem is the problem of fabricating the turbine wheel to the exacting standards set by the turbine designer. This will be especially true when supersonic turbines are built. It is always desirable, from a flow standpoint, to have sharp trailing edges in the blades; and in supersonic flow, sharp leading edges will also be required. As long as most of the refractory metals must be cast, this will not be possible. Even the best casting techniques cannot produce radii smaller than 0.005 in. Electric discharge methods of machining can be rather costly. In the over-all cost of space-power systems, this cost is minor, but the desire for cheaper, faster, machining methods is certainly well founded.

REFERENCE LIST

III-B-1. Zwick, E. B., and Zimmerman, R. L. "Space Vehicle Power Systems," ARS Journal, Vol. 29, No. 8 (August 1959), pp. 553 ff.

III-B-2. Fisher, J. H., et al. An Analysis of Solar Energy Utilization, WADC TR 59-17, Vol. III, Part III (Feb. 28, 1959), p. 105.

III-B-3. Martin, C. G., et al. Dynamic Heat Engines -- Fundamental Concepts for Lightweight Compact Application. Proceedings of a Seminar on Advanced Energy Sources and Conversion Techniques, Pasadena, California (November 3-7, 1958), p. 109.

III-B-4. Weatherford, W. D. Jr., et al. Properties of Inorganic Working Fluids and Coolants for Space Applications, Southwest Research Institute, WADC TR 59-598, December 1959.

III-B-5. Stenning, A. H. Design of Turbines for High-Energy Fuel, Low-Power-Output Applications, Massachusetts Institute of Technology, DACL Report No. 79, September 30, 1953.

III-B-6. Ohlsson, G. Partial Admission, Low Aspect Ratios and Supersonic Speeds on Small Turbines, Massachusetts Institute of Technology, ScD Thesis, January 1956.

III-B-7. Heen, H. K. Nonsteady, Two Dimensional Flow in a Partial Admission Turbine - The Hydraulic Analogy, Massachusetts Institute of Technology, ScD Thesis, September 1958.

III-B-8. Mann, R. W. Fuels and Prime Movers for Rotating Auxiliary Power Units, Massachusetts Institute of Technology, DACL Report No. 121, September 30, 1958.

III-B-9. Linhardt, H. D., and Silvern, D. H. Analysis of Partial Admission Axial Impulse Turbines, ARS Paper 1202-60, May 9, 1960.

III-B-10. Von derNuell, W. T. "Single-Stage Radial Turbines for Gaseous Substances with High Rotative and Low Specific Speed," Trans ASME, Vol. 74 (May1952), p. 499.

III-B-11. Balje, O. E. "Accessory Drive Turbines for Aircraft and Missiles," Aeronautical Engineering Review, Vol. 15, No. 3 (March 1956), p. 60.

III-B-12. Martinuzzi, P. M. "Multistage Radial Turbines," Trans ASME, Vol. 74 (July 1952), p. 663.

III-B-13. Wosika, L. R. "Radial-Flow Compressors and Turbines for the Simple Small Gas Turbine," Trans. ASME, Vol. 74, November 1952.

III-B-14. Balje, O. E. Untersuchungen an Radial Turbinen für Nichtraumbestä ndiges Arbeitmittel, Dr. Ing. Thesis, Munich, Germany. February 1945.

III-B-15. Naumann, E. O. A., and Balje, O. E. Design and Performance Study of Small Gas Turbines up to 1000 shp, WADC TR 53-342, August 1953.

III-B-16. Balje, O. E. Radial Inflow Turbine Design, Gas Turbine Lectures, Lecture No. 8, Department of Mechanical and Industrial Engineering, University of Michigan, Ann Arbor, 1953.

III-B-17. Balje, O. E. "Drag Turbine Performance," Trans ASME, August 1957, p. 1291.

III-B-18. Spies, R. A Study of High Pressure Drag Turbines Using Compressible Fluids, Sundstrand Turbo Report S/TD No. 1735, Vol. II, January 30, 1960.

III-B-19. Jackson, E. A. "Experiments to Determine the Best Shape and Number of Vanes for a G. G. G. Pump Runner," Institute of Mechanical Engineering Proceedings, 1956, p. 415 ff.

III-B-20. Balje, O. E., and Silvern, D. H. A Study of High Energy Level, Low Power Output Turbines, Sundstrand Turbo Report S/TD No. 1196, April 9, 1958.

III-B-21. Wood, H. Discussion of "Drag Turbine Performance," Trans ASME, August 1957, p. 1302.

III-B-22. Dubey, M. Low Specific Speed Turbines Based on Tangential-Flow Theory, Sundstrand Turbo Report S/TD No. 1735, Vol. III, January 30, 1960.

III-B-23. Spies, R. Test of a Low Speed Tangential-Flow Turbine With Wet Vapor, Sundstrand Turbo Report S/TD No. 1847, July 15, 1960.

III-B-24. Spies, R. "Losses in Wet-Steam Turbines," Paper in preparation at Electro-Optical Systems, Inc.

III-B-25. Biezens and Grammal. Engineering Dynamics, Vol. III, p. 31.

III-B-26. Lyman, T., ed. Metals Handbook, The American Society of Metals, 1948.

III-B-27. Brazing Inconel 713C, The International Nickel Company, Inc., Bayonne, Works, Bayonne, New Jersey.

III-B-28. Trutnovsky, K. "Untersuchungen An Berührungsfreien Dichtungen," Konstruktion, Vol. 6, 1954, p. 389.

III-B-29. Gruenagel, E. "Resistance of Blade Edges in Blade Rows," Forschung, Vol. 9, No. 4.

III-B-30. Trutnovsky, K. Berührungsdichtung, Springer Verlag, 1958.

III-B-31. Poulus, E. N., and Furman, E. R. The SNAP II Power Conversion System, Topical Report No. 4 - Turbine Design and Testing, Thompson Ramo-Wooldridge, Inc., Cleveland, Ohio, Report No. ER-3896, January 18, 1960.

III-B-32. Anderson, G. M. SNAP II - A Reactor Powered Turboelectric Generator for Space Vehicles, SAE Paper No. 154B, April 5, 1960.

III-B-33. Balje, O. E., Verbal communication with the author, August, 1960.

III-B-34. Kovacik, V. P. Reply to EOS Questionnaire August 19, 1960.

III-B-35. Ray, E., and Ross, D. P. Trends in Turboelectric Power Generation for Space Vehicles, Western Regional Meeting of the ASME, May 20, 1960.

III-B-36. Chadbourne, L. E. Reply to EOS Questionnaire, August 19, 1960.

III-B-37. LaFond, C. D. "Solar Mechanical Engine to Give 15 KW," Missiles and Rockets, Vol. 7, No. 7 (August 15, 1960), p. 24.

III-B-38. Coppage, J. E. Reply to EOS Questionnaire, August 13, 1960.

III-B-39. Boxer, E., et al. Application of Supersonic Vortex - Flow Theory to the Design of Supersonic Impulse Compressor - or Turbine Blade Sections, NACA RM. L52 BO 6, April 24, 1952.

III-B-40. Deich, M. E. Flow of Gas Through Turbine Lattices, NACA TM 1393, May 1956.

NOMENCLATURE

Turbines

A	=	area			
D	=	diameter	D_s	=	specific diameter
H	=	head			
J	=	Joule's equivalent			
K	=	loss coefficients			
N	=	turbine rpm	N_s	=	specific speed
P	=	power			
Q	=	volume flow rate	Ma	=	Mach number
R	=	gas constant	Re	=	Reynolds number
T	=	temperature	HP	=	horsepower level
W	=	work			
N_b	=	number of turbine blades			

v	=	absolute velocity
c_o	=	spouting velocity
g	=	gravitational constant
h	=	enthalpy
p	=	pressure
u	=	blade velocity, wheel tip velocity
w	=	relative velocity
$\dot{w}$	=	weight flow rate

	nozzle angle, corrected temperature
	blade angle
ρ	density
	efficiency
γ	ratio of specific heat
	viscosity
σ	Thoma parameter
ϕ	flow coefficient
	head coefficient
	correct pressure
α	nozzle angle

ENERGY CONVERSION SYSTEMS REFERENCE HANDBOOK

Volume III - Dynamic Thermal Converters

Section C

ELECTROMAGNETIC GENERATORS

W. R. Menetrey
Energy Research Division
ELECTRO-OPTICAL SYSTEMS, INC.

Manuscript released by the author
September 1960 for publication in this
Energy Conversion Systems Reference Handbook

WADD Technical Report 60-699

III-C ELECTROMAGNETIC GENERATORS

C O N T E N T S

I L L U S T R A T I O N S

T A B L E S

C. ELECTROMAGNETIC GENERATORS

In contrast to the fabrication of electrostatic generators, electromagnetic generator design is based on extensive development carried on for a number of years. Many "off-the-shelf" designs are available for a variety of applications. Generator development has generally kept pace with the environmental and performance demands presented by modern aircraft, the transition to static control systems, the change to environment-free and air cooled brushless AC generators, and other such problems.

The problem of space-power systems presents a new challenge which is actively being investigated at many companies throughout the United States. Some general design principles and anticipated performance characteristics of electromagnetic generators suitable for space application are presented here. The optimum generator has yet to be built and will require still further advances in basic and applied research. Generator selection and design will depend heavily on the specific system and its transient and steady-state characteristics.

Of the many types of electromagnetic generators that can convert rotational into electrical energy, the homopolar inductor alternator has been almost universally selected as the best configuration at power levels above a few kilowatts. This design eliminates rotating windings, as well as all sliprings and brushes, and utilizes a solid steel rotating structure which is capable of withstanding maximum mechanical and thermal stresses. At present, it is felt this machine can be designed to operate reliably with coolant temperatures ranging up to about 1000°F and at speeds up to about 24,000 rpm. The selection of optimum speed and coolant temperatures combination depends on a parametric analysis as discussed in later paragraphs.

The heat engine cycle will probably utilize an alkaline metal as a working fluid. A perfect rotating seal between the turbine and the generator does not appear possible with present techniques or knowledge. Other couplings are inefficient. Therefore, generator materials must be used which are not affected by the corrosive vapor, and/or protective "cans" designed such that eddy current losses are minimized. In the inductor alternator design, all the conductors are located at the stator, and this problem is decreased.

1.0 SELECTION OF GENERATOR TYPE

In advanced systems the surfaces of the generator will be at high temperatures (1200°F or more) in order to prevent condensation of metallic vapors. To obtain the optimum machine, the generator will be operated at high speeds. The severe high temperature-high speed operation presents problems and influences the choice of generator type.

Even 500-hour life, in modern high speed generators which use brushes, requires a special atmosphere. Long life requirements and the severe space environment indicates that the generator must be brushless.

One type of brushless generator uses rotating rectifiers and windings and uses the salient pole synchronous generator concept with its inherent high efficiency, quick response, and low weight. Two severe disadvantages of this design are as follows:

a. A 600°F rotating rectifier is not available at this time.

b. The design requires rotating windings which will produce severe problems in creep of the metallic conductor, cracking of the insulating ceramic coating, the creation of imbalances due to winding shifts, and winding end containment problems.

The asynchronous (squirrel cage) generator (sometimes called induction generator) is inherently lightweight and is brushless. The machine is made self-exciting by using capacitors on the line. It is necessary to change the slip with load changes. Voltage and frequency regulation are accomplished by changing the capacitor loading. The chief adisadvantages are:

a. The weight penalty of the capacitors.

b. The difficulty of voltage regulation.

Cascade generators consisting of two generators on the sarne shaft have been constructed. The rotor output of one DC excited generator is supplied to the rotor of the main generator. Excitation is applied to the main alternator winding in such a manner that a rotating flux is generated which rotates at frequency f_1 relative to the rotor and in the same direction as the rotor rotates. The rotating flux then generates voltage on the stator of the main generator at frequency $f_1 + f_s$ where f_s is the shaft frequency. The machine is brushless. One disadvantage is that the rotating flux of the main alternator cuts the rotor winding at frequency f_1 and generates a large back voltage which the exciter must overcome. The auxiliary generator must overcome the back voltage of the main r otor and must also supply a magnetization trap and other voltage losses in the system.

The cascade generator tends to be long because of the two machines in tandum. The long rotor then increases the critical shaft frequency problems. Another important disadvantage is the requirement of rotating windings and relative high voltages on the rotor. It does not appear that this cascade generator offers any advantage over the inductor generator.

A broad class of generators which is acceptable for space systems uses stationary field coils. General types include the Lundell, the homopolar inductor, the heteropolar inductor, the inductor-Lundell, the "Secsyn", and the flux switch generators.

The Lundell design operates with a complete reversal of flux in the stator coils, as in conventional generators. The Lundell generator is the lightest of the fixed field coil generators because of the full utilization of stator iron. The maximum speeds of operation, however, are limited by the overhanging poles. Also, the flux paths are long and the pole spacing small, resulting in excessive leakage. Furthermore, there is a problem in supporting a stationary field coil.

The inductor-Lundell has an advantage in reducing the leakage flux over that of an inductor or a Lundell generator. A small saving in weight may be realized over an inductor generator, but the generator is longer between bearings, limiting the critical speed. The same overhanging pole construction as a plain Lundell generator also limits high-speed capabilities.

The homopolar inductor generator offers many outstanding features, although being heavier in weight than the Lundell or the normal salient pole generator. A weight penalty results from the stator flux varying between a maximum and a minimum without reversing. The rotor is a simple piece of electromagnetic material which is simple in construction and highly reliable at high speeds. A disadvantage of this generator is that the armature leakage reactance is about twice that of a conventional generator.

The heteropolar inductor alternator has the advantage of a shorter span between bearings than the homopolar inductor, thus raising the critical speed. However, this design is somewhat heavier than the homopolar type

since the field coils are integral with the stator and run parallel to the armature winding, requiring larger slots and more volume of surrounding iron.

A flux switch generator is perhaps the simplest of all stationary field generators. It is also the most efficient. A real limitation is the high flux leakage and the fact that it is a single phase generator. Polyphase generation of power by use of a flux switch tenchique requires one generator per phase on the same shaft, displaced by the proper phase angles. Three phase power is commonly required for most electrical equipment. Consideration should be given to single phase power in future applications because of the simplicity, lightweight, and high efficiency of the flux switch generator. It only has two armature coils and two field coils, and the frequency is determined by the number of rotor teeth.

The "Secsyn" generator is an unconventional Lundell type generator where a complete reversal of flux occurs. The mechanical problems generally increase with high speeds and high temperatures, and poor reliability generally rules this type out.

The advantages of permanent magnet generators as a class are several. The fact that positive excitation is used results in higher reliability. This means that if the voltage regulator fails or the control winding circuit opens, the machine still will generate power. It also means that the voltage will build up positively on start-up without external "field flashing" circuitry. Permanent magnet alternators are inherently efficient machines, having no excitation losses. Also, the iron losses in a radial gap machine are usually small, since it is common design practice to run the magnet circuit at low flux densities. Another advantage is good thermal characteristics; the low core losses and lack of excitation losses tend to make these machines run quite cool. Also,

in the case of a radial gap machine with a saturating winding, the copper losses tend to balance with load variations. That is, at heavy loads, when the load winding losses are highest, the saturating winding losses are lowest; and at light loads, when the saturating winding losses are highest, the load winding losses are lowest.

The disadvantages of permanent magnet alternators also are several. If the magnets are stabilized against short circuits or removal from the stator, they are relatively heavy. This is not a serious disadvantage in some applications, particularly at low power levels, since the higher efficiency which is associated with high magnetic circuit weight may result in an over-all saving in system weight. However, at power levels above about 5 kw, the weight penalty associated with a permanent magnet generator is high enough to eliminate it from serious competition for a main power unit. A permanent magnet alternator might be used to advantage as an auxiliary machine to supply control or accessory power.

A general summary of conclusions based on the discussion above, was prepared by AiResearch and is presented in the following table. The table is based on present state-of-the-art knowledge. The homopolar inductor generator offers the best compromise of desirable features for most applications.

TABLE C-1
AIRESEARCH SUMMARY OF GENERATOR CHARACTERISTICS

Generator Type	Polyphase	Operating Speed	Efficiency	Weight	Reliability
Lundell	Yes	Low	Fair	Low	Fair
Homopolar Inductor	Yes	High	Fair	Low	High
Heterpolar Inductor	No	High	Fair	Low	High
Inductor Lundell	Yes	Low	Fair	Low	Fair
Flux Switch	No	High	High	Low	High
Secsyn	Yes	Low	Fair	Low	Fair
Synchronous	Yes	High	Fair	Low	High

Further improvements in generator weight and size could be achieved by advances in materials state-of-the-art, It has been estimated, for example, that a conventional salient pole synchronous generator would provide weights on the order of 1/2 lb/kw-a and efficiencies on the order of 95 percent at temperatures of 600°F for the provision of 3200 cps, 400 kw-a power. This is less than half the weight required of an inductor generator.

The following developments beyond the present state-of-the-art would require a re-examination of generator parameters to determine the optimum configuration:

a. Development of a magnetic material with magnetic characteristics as good or better than present materials and with a strength as good or better than present high strength alloy steels.

b. Development of high-temperature wire insulation that would have essentially no flow when subjected to the centrifugal forces encountered on the rotor.

c. Development of rectifiers the same size as present day silicon rectifiers which would operate continuously at a temperature range from 600°F to 1100°F and in a corrosive liquid atmosphere.

The selection of the electrical control system is based on the need for long life and high reliability. A constant load will result in a system that tends to be self-regulating, and controls required for regulation of frequency and control can be of a simple minimum type. Also, since the generator load will be essentially constant, the field excitation power will be constant. The bulk of the field excitation power, therefore, can be obtained directly by rectifying

a portion of the generator AC output and supplying the resultant DC power to the primary field winding of the generator, with a small amount of trim power supplied from the voltage regulator. Systems wherein inherent voltage regulation exists are currently being designed.

The three types of voltage regulators considered for this application include the carbon pile regulator, the magnetic amplifier regulator, and the transistorized regulator. The carbon pile is light in weight and utilizes a small number of components; however, it contains moving parts with a consequent decrease in reliability. A magnetic amplifier is highly reliable but is also heavy with a large volume; this may become of less significance as the frequency at which the magnetic amplifiers operate is increased. The transistorized regulators are limited by their maximum temperature ratings. Good design, however, can take advantage of the small volume and lightweight, extremely low heat rejection, high power handling capabilities, high reliability, and completely static operation. The transistorized type of regulator is generally favored for this application.

A means must be provided for assuring electrical system voltage buildup during the start-up of the power system. Three possible means include field flashing of the generator field, a permanent magnet within the generator, and residual characteristics within the generator. The simplicity of the latter method and the minimum weight penalty involved indicate this to be the most favorable method.

2.0 INDUCTOR GENERATOR DESIGN

The inductor generator incorporates two stator stacks, north poles at one end of the machine and south poles at the other. The three phase AC winding is wound into the stator as in a synchronous generator except the iron

stack of punchings is effectively separated into two sections. The sketch in Figure III-C-1, shows a cross section of a typical inductor generator. As the rotor turns, the AC winding seeks alternate north and south flux. Figure III-C-2 depicts sketches of a conventional salient pole design and a homopolar inductor machine.

One difficulty in this generator is the fact that the total stack lengths must be twice the length of the conventional salient pole machine. Stator leakage reactance and machine weight are therefore greater than in a conventional generator. The important advantages are: (1) brushless operation (2) no rotating windings (3) relatively small leakage flux (4) a simple solid rotor construction (5) the excitement of all poles by one stator coil, and (6) coil losses approximately the same as any conventional generator.

Over-all system optimization usually indicates that the lightest weight over-all system can be achieved by using a generator operating at high speeds and at high temperatures. The generator, however, is limited by materials parameters. The weight of the inductor type machine will vary with speed and temperature, as will the efficiency. For example, ranges of operation appear to be three quarters to two pounds per KVA and 70 to 94 percent efficiency for a 400 KVA (.75 Pf) generator. Over-all system weight will not necessarily coincide with either minimum generator weight or maximum generator efficiency, but an optimization analysis must be performed.

The generator speed must be selected on the basis of desired frequency and the number of poles in order to satisfy the equation:

$$\text{Speed in RPM} = 120 \frac{(\text{Frequency in CPS})}{\text{Poles}}$$

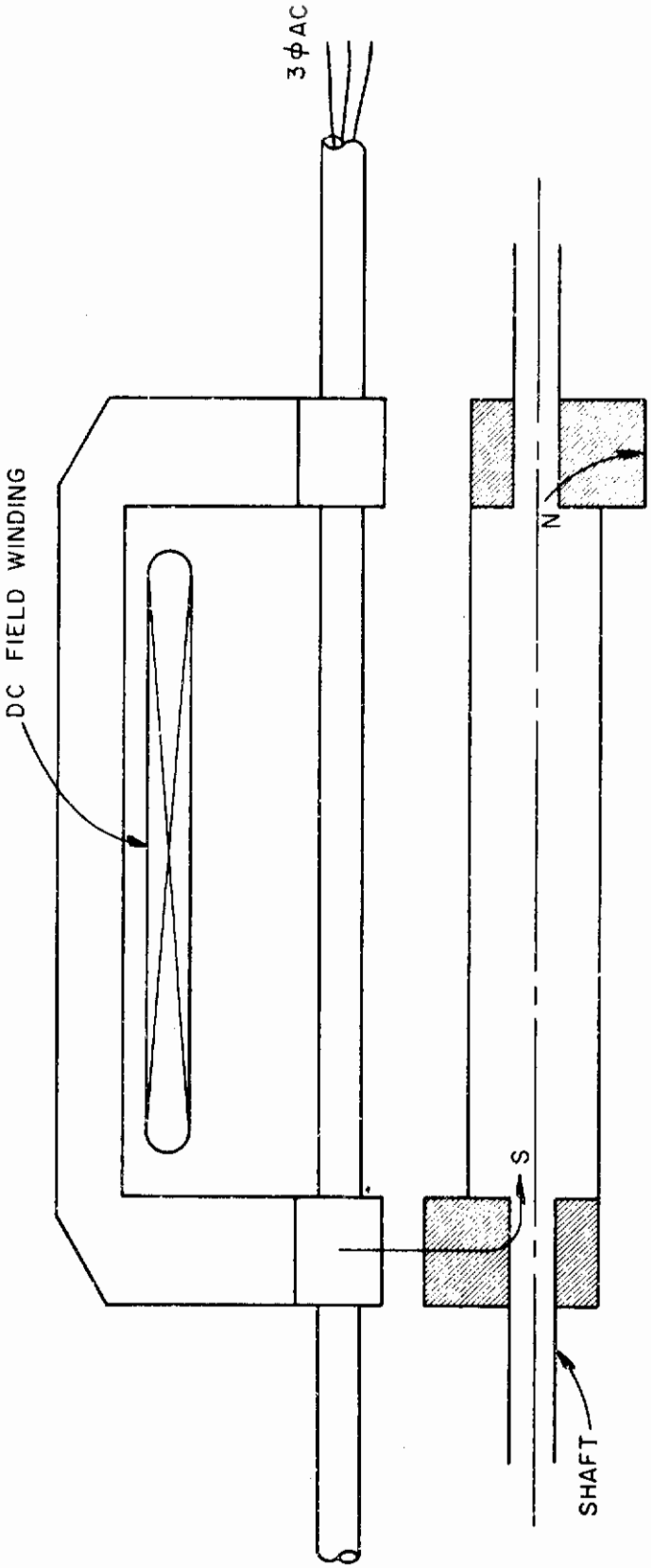

FIGURE III-C-1 TYPICAL INDUCTOR GENERATOR

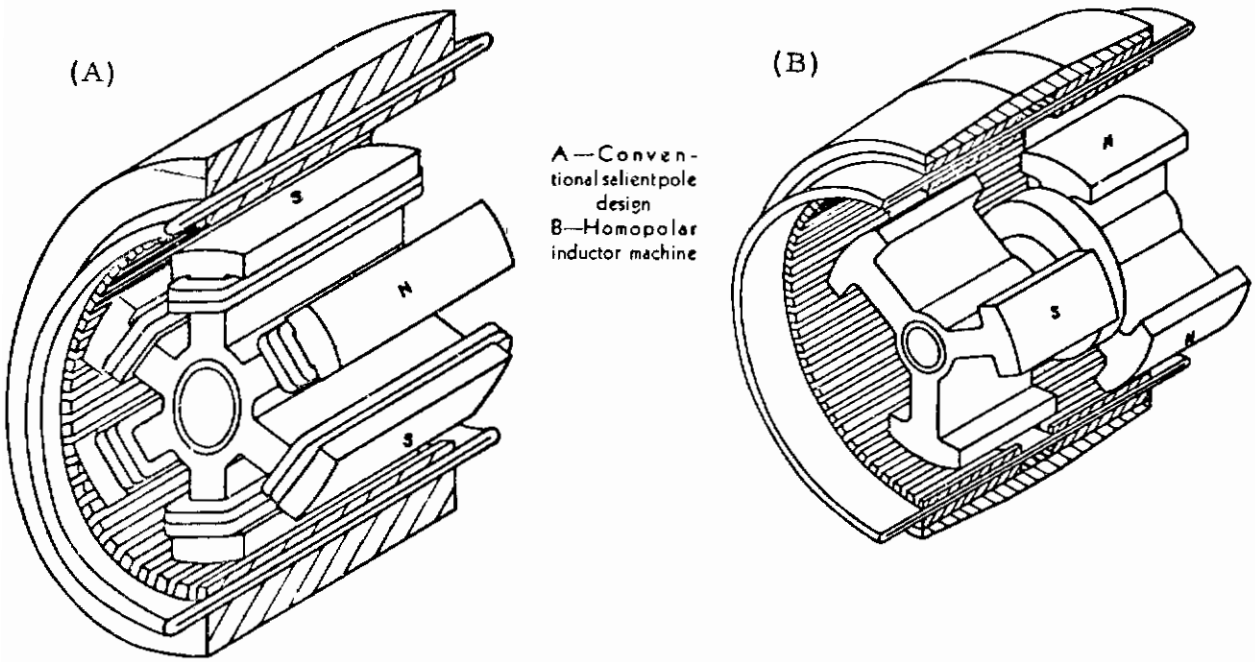

FIGURE III-C-2 COMPARISON OF SALIENT POLE AND HOMOPOLAR INDUCTOR ALTERNATORS

The selection of optimum frequency depends significantly on the load characteristics. The relative weight of the generator does change significantly with the number of poles required at a given rotational speed. For example, for a typical salient pole AC generator operating at 6,000 rpm, the relative weight was 1 using 6-8 poles, 1-15 using 2 poles, and 1.2 using 14 poles. Therefore, for loads requiring several frequencies or a frequency far removed from the optimum generator design point, consideration must be given to the use of transformers.

A study by Westinghouse indicated that the optimum operating speed for 3200 CPS is contained within a relatively narrow band between roughly 19,000 and 24,000 rpm for minimum generator weight. The reasons for a weight increase at high rotational velocities is due to a far from optimum length to diameter ratio. At 24,000 rpm, the allowable rotor diameter is much less than at lower velocities, and, therefore, the generator length must be increased. This increase in length increases the leakage reactance voltage drop. This in turn requires that more voltage be generated which requires more magnetic iron and, therefore, more weight. The optimum electrical length to diameter ratio is considerably less than it is possible to obtain for any design because the mechanical strength of the rotor limits its diameter. Because the allowable rotor diameter goes down with an increase in speed, the actual L/d ratio becomes more removed from the optimum ratio as speed is increased. At speeds above 24,000 rpm, the rotor diameter must be decreased to a point where the design becomes impractical.

At high temperatures of operation on the order of 1000°F, the normal magnetic steels used for the rotor must be replaced by other types which require approximately twice the area for a given amount of flux. Since the flux

flows actually through the rotor, an increase in rotor diameter is required. At speeds above roughly 18,000 rpm, the required electrical area results in a rotor diameter which is above a maximum diameter allowed by available mechanical strength.

Based on the above discussion and the fact that turbine efficiency generally goes up and turbine weight goes down with an increase in speed, it appears that the operating speed of the inductor generator for this case should be in the range of 17,000 rpm for temperatures of 1000°F, and in the range of 20,000 rpm to obtain the lightest over-all system. These speeds will probably increase as new and better materials are developed.

Previous discussion indicated the effect of choice of frequency on generator weight. Optimization studies by Westinghouse, Inc. have indicated an optimum frequency of 1,600 cycles per second, for minimum generator weight. 1600 CPS permits the best number of stator slots per hole per phase which results in the best diameter to length ratio. The optimum frequency also occurs in this area, due to the rotor diameter being limited for mechanical reasons. At higher frequencies, the leakage reactance becomes high. The largest losses of an AC generator above 1,600 cycles per second are in iron losses. These iron losses are proportional to the 1.5 power of the frequency times the volume of the magnetic iron. The losses below 1,600 cycles per second are mainly iron losses and I^2R losses of the copper.

The optimum design of a generator will depend on a wide variety of parameters applicable to the specific system. These include voltage, frequency, power level, coolant temperatures available, and others. No general over-all parametric study of this type has yet been performed.

Several alternator characteristics affect the design of the overall power system. The most significant are shaft speed, efficiency, and operating temperature. These variables are interrelated and also related to the weight of the alternator and to the design and weight of other parts of the system. The alternator efficiency is related to system weight through its effect on the design of heat transmitting and heat rejecting elements - the boiler, condenser-radiator, and alternator coolant radiator. It is also related to alternator weight in that reducing core losses means using more iron to operate at lower flux densities, and reducing winding losses means larger conductor area--both of which are achieved by increasing the electromagnetic weight of the alternator. The shaft speed affects the alternator weight in that, for a given geometry and rating, the electromagnetic weight varies inversely with the speed. The operating temperature of the alternator affects both alternator weight and the weight of the alternator coolant radiator.

To illustrate the design optimization procedure, Sundstrand Turbo Inc., performed a system design study to determine the optimum design point for a 300 kw alternator to be used in a reactor system. The study considered only those components affected by the pertinent variables of shaft speed, efficiency, and operating temperature. Values for the base weights of components are approximate but are considered accurate enough to establish relative system weight. The optimization consisted of minimizing the sum of component weights sensitive to alternator efficiency, i.e.,

$$\Sigma W = W_A + W_{AR} + W_{SR} + W_B$$

where

W_A = alternator weight in pounds

W_{AR} = alternator radiator weight in pounds

W_{SR} = system radiator weight in pounds

W_B = boiler weight in pounds

ΣW = summation of W_A, W_{AR}, W_{SR}, and W_B, called "relative system weight".

The effect of turbine weight was omitted. The alternator weight was taken directly from Westinghouse parametric data. The alternator radiator weight was computed assuming a specific weight of one pound per square foot of radiating surface, the area varying directly with the alternator losses and inversely as the fourth power of the absolute coolant temperature. The system radiator rejected heat at 1150°F and had a specific weight of 1 lb/ft^2, the area varying directly with the total system heat rejected. The boiler weight was assumed to vary directly with the alternator losses, the base weight being 90 lb at an alternator efficiency of 85 percent. The cycle efficiency was assumed to be .2165.

The individual weights then could be expressed as follows:

W_A: from curves VI-11-10, VI-I-11, VI-I-12, showing weight vs. efficiency at 400, 600, and 1000°F coolant temperature taken from the Westinghouse Proposal (Reference III-C-1).

$$W_{AR} = \frac{2.4\, Q_{LA}}{\left(\frac{T_A}{1000}\right)^4}, \quad \text{where} \quad Q_{LA} = 284 \left(\frac{1 - \eta_A}{\eta_A}\right) = \text{alternator heat rejection, Btu/sec.}$$

T_A = alternator coolant temperature in degrees Rankine

η_A = alternator efficiency, per unit

$$W_{SR} = 102 \left(\frac{1}{\eta_{cyc}\, \eta_A} - I\right)$$

where

η_{cyc} = cycle efficiency, per unit = .2165

$W_B = \frac{.85}{\eta_A} \times 90$

"Relative System Weight", W, was tabulated in Table III-C-2 for rpm's of 14770, 17480, and 24,000 at alternator coolant temperatures of 400, 600, and 1000°F. This table indicates that the lowest relative system weight can be achieved with a 600°F coolant inlet temperature and a shaft speed of approximately 17,480 rpm. The trend shown is toward lower system weight at lower alternator efficiencies. Operating at this shaft speed, rather than a higher one, also offers the advantage of a relatively conservative mechanical design; the lower stresses should give better reliability here than at 24,000 rpm.

TABLE III-C-2

RPM	T_A °F	η_A %	Q_{LA} Btu/sec	W_A lbs	W_{AR} lbs	W_{SR} lbs	W_B lbs	ΣW, lbs.
17480	400	92	24.7	515	108.2	409	83	1115.2
		90	31.6	453	138.5	421	85	1097.5
		86	46.3	352	203.0	446	89	1090.0
	600	92	24.7	575	46.8	409	83	1113.8
		90	31.6	500	59.8	421	85	1065.8
		86	46.3	380	87.7	446	89	1002.7
		84.7	51.3	350	97.1	454	90.2	991.3
14770	1000	86	46.3	690	24.5	446	89	1249.5
		83	58.7	600	31.05	464	92.2	1187.25
		80	71.0	531	37.6	487	95.5	1151.1
	600	90	31.6	565	59.8	421	85	1130.8
		86	46.3	437	87.7	446	89	1059.7
		83	58.7	360	111.3	464	92.2	1027.5
	400	92	24.7	600	108.2	409	83	1200.2
		88	38.7	450	169.8	431	87	1137.8
		86	46.3	400	203.0	446	89	1138.0

TABLE III -C- 2 (cont.)

RPM	T_A °F	η_A %	Q_{LA} Btu/sec	W_A lbs	W_{AR} lbs	W_{SR} lbs	W_B lbs	ΣW, lbs
24000	400	92	24.7	550	108.2	409	83	1150.2
		90	31.6	480	138.5	421	85	1124.5
		86	46.3	376	203.0	446	89	1114.0
	600	92	24.7	615	46.8	409	83	1153.8
		90	31.6	526	59.8	421	85	1091.8
		86	46.3	408	87.7	446	89	1030.7

A = Alternator
AR = Alternator Radiator
B = Boiler
SR = System Radiator
T = Temperature
W = Weight
ΣW = Relative System Weight
η = Efficiency

Thompson Ramo-Wooldridge recently completed a conceptual design study of a high temperature electromagnetic inductor alternator (Ref. III-C-4). The ground rules for the study were based on assumed advances in the state-of-the-art for the next five years.

The power ratings considered varied from 80 to 1000 kilowatts with the following detail specifications:

a. Voltage - 3,000 volt

b. Frequency - from 260 to 870 cps

c. Speed - maximum allowable

d. Power Factor - unity

e. Environment

Outside - space

Inside - high temperature mercury vapor

Regarding this last specification, if the mercury vapor environment could be eliminated from the inside of the alternator, slightly lighter weights would have resulted. The weights presented are based on the assumption that a seal can be developed which will be effective in preventing the mercury vapor from reaching the armature gap. The alternator studied was a brushless Lundell-inductor type. The heat generated due to losses in the alternator will be radiated to space at a maximum frame temperature of 800°F.

Four different ratings were investigated with results shown on the following table:

TABLE III-C-3
CHARACTERISTICS OF LUNDELL-INDUCTION GENERATOR

Ratings KW	Shaft Speed RPM	Length Inches	Diameter Inches	Weight Lbs.	lb. /KW	Eff. %
80	30,000	11	11.25	120	1.5	94
125	26,000	12	12.5	193	1.55	95
275	19,000	15.5	17	468	1.7	96
1000	8,000	28	29	2750	2.75	96.5

The above efficiencies do not include excitation losses which amount to about 5 percent. Therefore, the alternator over-all efficiencies for the above range will be approximately 90 percent.

Critical speed calculations were also conducted in the design study and indicate that the speed range of the above alternators are satisfactory. Advancements in materials and in detail design techniques should improve the above performance results.

The design study indicated that at the present time there are severe mechanical limitations as regards constructing this type of alternator at

larger L/d ratios than in the preceding table. However, even at the present L/d ratios the alternator is operating near the turbine limiting speed which is a considerable advancement over current state-of-the-art. The alternator specific weights are slightly higher than anticipated from the parametric study. This is to be expected for all components and will result in a more realistic overall propulsion system.

Figure III-C-3 summarizes the specific weight resulting from the design of electromagnetic generators at various power levels. The TRW and Westinghouse designs have already been discussed. Also shown are data points for the SNAP II and SNAP VIII nuclear power systems. SNAP II utilizes a permanent magnet machine. The rotor is constructed of Alnico V permanent magnets -- unaffected by the high temperature mercury environment. The stator wound field coil is sealed from the mercury environment with a glass seal. The generator is a two-phase unit connected externally to produce a single-phase output.

The SNAP VIII unit is designed by Aerojet and is a homopolar inductor machine. AiResearch designed a 15 KW generator for use in a solar power system of the homopolar inductor type. Each of these units operates in a mercury vapor environment.

As shown, expected specific weight will increase with a decrease in power level. The TRW analysis showed a steadily increasing weight with an increase in power level due to the limitation of a 800°F frame temperature and direct radiation cooling. Depending upon radiator characteristics, the generator weight at high power levels might be lowered through use of an auxiliary cooling radiator.

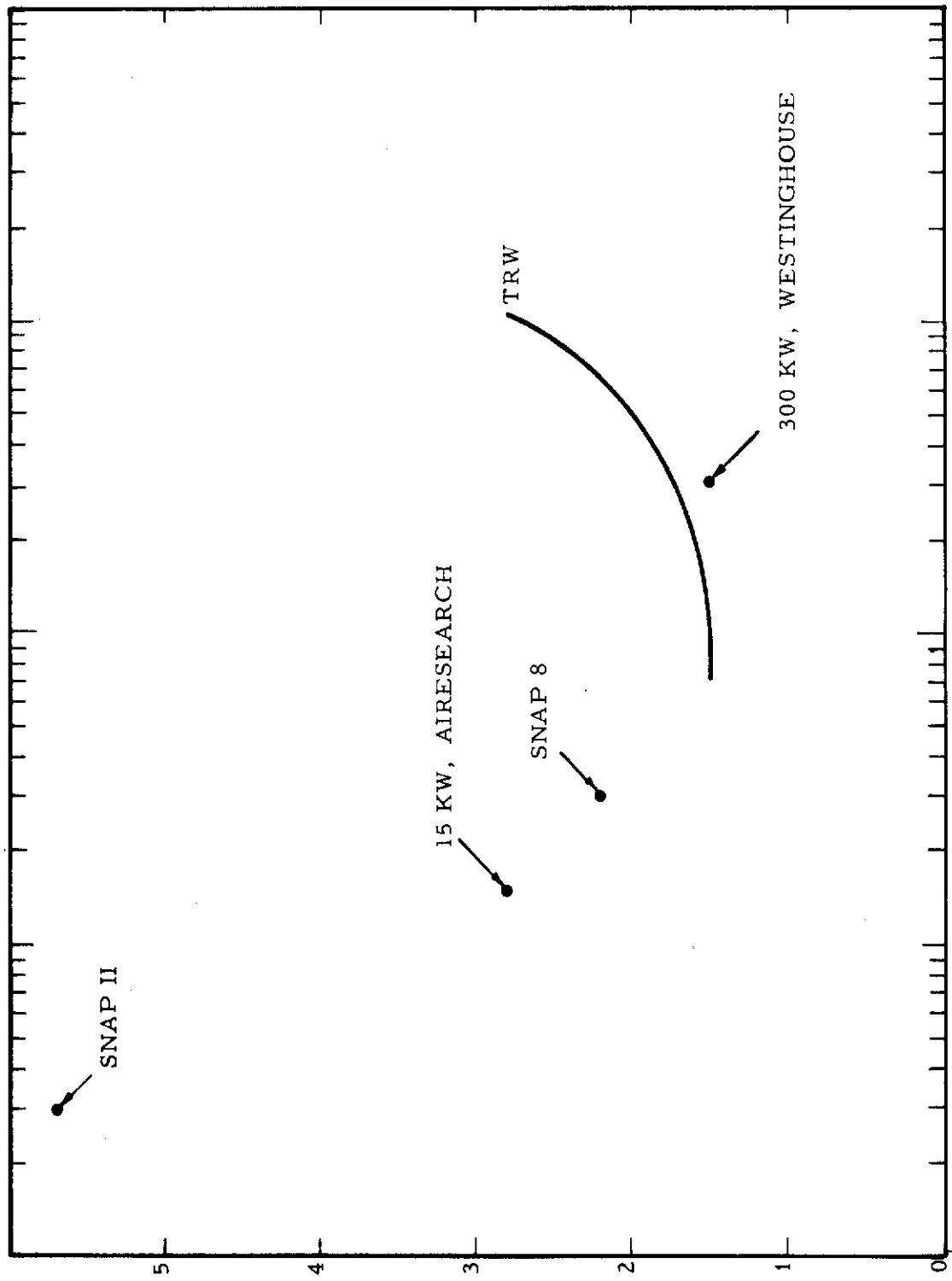

FIGURE III-C-3 PREDICTED WEIGHT OF ELECTROMAGNETIC GENERATORS

REFERENCES

III-C-1. Westinghouse Electric Corporation, Aircraft Equipment Department, Lima, Ohio. "Design Study and Development of a 300 KW Electrical Power System," Proposal 2036, January 1960.

III-C-2. AiResearch Manufacturing Division. "Supplementary Data on Electrical Power System Design for 15 KW Solar-Mechanical Power System." Report No. SY - 5166 - R- Supplement 1, January 26, 1960.

III-C-3. Allison Division of General Motors Corporation. "Design and Development of a 3 KW Stirling Cycle Solar Power Plant," First Semiannual Technical Summary Report, Engineering Department Report No. 1628, January 22, 1960.

III-C-4. Thompson Ramo-Wooldridge, Thompson Products Division, " Electrical Generating Equipment for Space Systems," November, 1958.

III-C-5. Bateman, J. T. "A Solid Rotor AC Generator for High Temperature Electrical Systems," AIEE Proceedings, Applications in Industry, January 1960.

III-C-6. Duane, J. T., and Yeager, L. J. "Reliability and Analysis for Aircraft Generators," AIEE Proceedings, Applications in Industry, January 1960.

III-C-7. Sutton, J. P. (Rocketdyne) "Ion Rocket Study Program - Final Report," January 31, 1958. Contract AF 46(638)-16, AFOSRTR-58-81.

III-C-8. Toffole, D. S., and Hanrahan, D. J. "Permanent Magnet Generators, Part II' Design Considerations," Naval Research Laboratory Report 4931, May 1957.

III-C-9. Kober, W. "Basic Performance Characteristics of Modern PM Generator," Symposium on Auxiliary Power For Guided Missiles, Volume II, February 1957.

III-C-10. Anderson, G. M. "SNAP II - A Reactor Power Turboelectric Generator for Space Vehicles," SAE Paper 154B, presented 8, 1960.

III-C-11. Wetch, J. R., et al. (Atomics International) "The Practical Application of Space Nuclear Power in the 1960's". Presented at the Internation Astronautical Congress, April 15, 1960.

ENERGY CONVERSION SYSTEMS REFERENCE HANDBOOK

Volume III - Dynamic Thermal Converters

Section D

ELECTROSTATIC GENERATORS

W. R. Menetrey
Energy Research Division
ELECTRO-OPTICAL SYSTEMS, INC.

Manuscript released by the author
September 1960 for publication in this
Energy Conversion Systems Reference Handbook

WADD Technical Report 60-699

III-D ELECTROSTATIC GENERATORS

C O N T E N T S

III-D ELECTROSTATIC GENERATORS

I L L U S T R A T I O N S

D. ELECTROSTATIC GENERATORS

The developing need for a DC high voltage generator and other apparent advantages of an electrostatic generator in space applications have given an impetus to their development. Analysis has indicated that the electrostatic generator, operating in vacuum, can be comparable in specific size and weight to the electromagnetic generator and will be considerably more efficient. In space applications, the expected higher efficiency of the electrostatic machine is quite important in decreasing total package weight.

The industrial electrostatic generator has already been highly developed: in America, under the auspices of R. J. Van de Graaff and J. G. Trump with their belt type generator, and in Europe with the rotating type of electrostatic generator developed by Joffe and Hochberg (Russia), Neal and Felici (France), and Neuberg, Cossel, and Herchenbach (Germany). These terrestrial machines operate under high-pressure gas insulation and are somewhat bulky, due to the need for a heavy high-pressure container. Also, lower efficiency results from the aerodynamic friction on the moving parts. Consequently, they cannot be applied to space applications directly; however, the principles evolved in the development of these machines can be applied to the space generator.

The following sections offer a brief review of the principles and limitations of several types of electrostatic generators. As discussed later, the Trump - Van de Graaff generator is most suitable for space application due to the elimination of commutation mechanisms (e.g., brushes), light weight, and greater adaptability to lower voltages. Analysis by Thompson-Ramo-Wooldridge has indicated weights of 1.8 lbs/kw at 50 kilovolts and

0.9 lbs/kw at 100 kilovolts are obtainable within the near future after the solution of developmental problems discussed in later paragraphs. Analysis by Goodrich-High Voltage Engineering and Cosmic Inc. predict specific weights of 2 16/kw. These analyses are based on extrapolations from data obtained from low power experimental machines with relatively poor characteristics for space application. No electrostatic generator suitable for space operation has as yet been constructed. Current developmental programs are discussed in section 3. 0.

1.0 GENERAL PRINCIPLES

All electrostatic generators operate under essentially the same physical limitations. These result from the fact that the power output is proportional to the charge on a moving surface times the velocity of the moving surface.

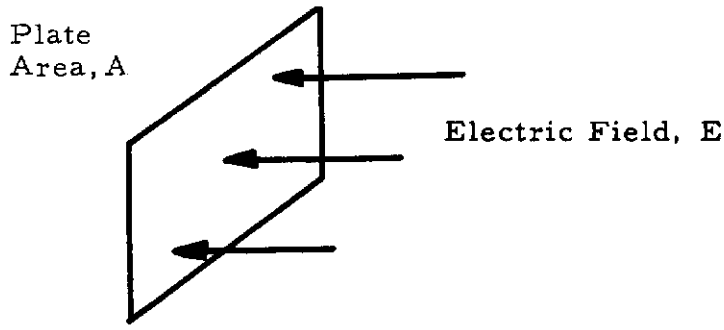

Current to Plate

$$I = \frac{dQ}{dt} = \frac{d(EXA)}{dt}$$

Referring to the above figure, a plate of area A connected to a ground in an electric field E will acquire a charge. If the area is changed at a constant rate, the charge will also change and a constant current

will flow, When a second parallel load is added to the first, the original current is shared and both the emf and the current through the first load will fall. Thus, in a commercial situation some feedback means is required for automatically stabilizing the emf. The maximum charge density and voltage are established by the breakdown voltage gradient of the surrounding medium, and the maximum velocity of the charge-carrying surface (either a belt, a disk, or a drum) is established by the stress and wear on essential parts and, if the machine is operating in high pressure gas, by the aerodynamic losses.

As in all generators, optimum operation occurs for a matched load. The voltage output is sufficiently variable that if a constant voltage within close tolerances is desired, some regulation must be used. In addition, a change in load results in a change of output voltage, as illustrated by Fig. III-D-1, which is the current-voltage curve reported by Joffe and Hochberg for their machine. Similar curves occur for all machines tested so far. No load characteristics have been presented for the Trump - Van de Graaff machine, but it is apparent from the description of its operation (see subsection 2.5) that a similar variation of voltage with current output is to be expected.

Commutation poses a difficulty with generators operating in a vacuum, due to rapid deterioration of devices such as brushes and combs, lack of an ionization medium, etc. This difficulty can be removed, as in the Trump - Van de Graaff machine, but at the price of constructing the charging surfaces from conducting materials. Since a conductor cannot support a tangential voltage gradient, it is apparent that the forces against which the driving mechanisms must work will be applied only

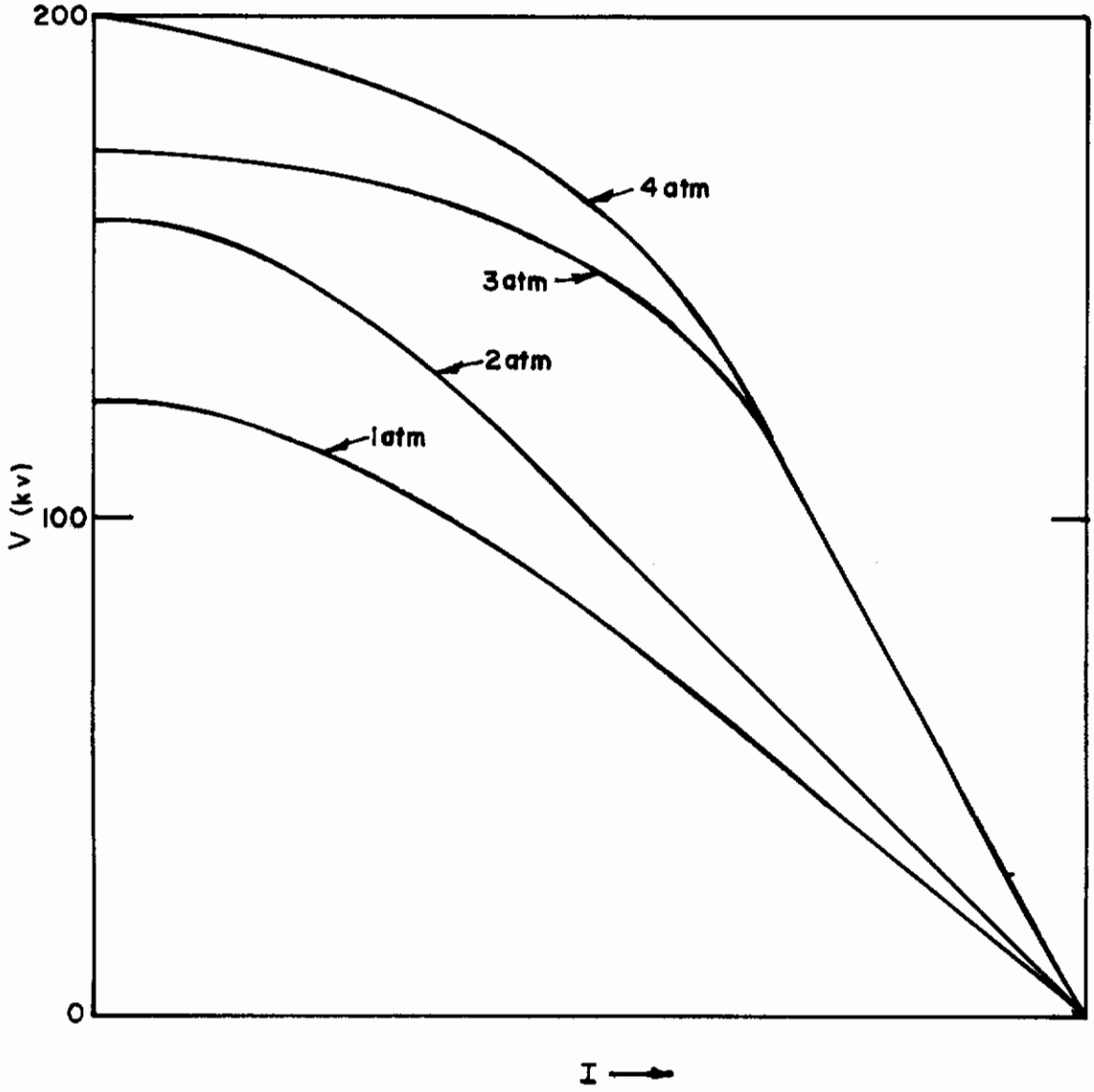

FIGURE III-D-1 VOLTAGE CURRENT CURVE OF JOFFE-HOCHBERG GENERATOR

at the edges of a conducting sector, with consequent localization of material stresses and accompanying fabrication difficulties. For example, the force between two parallel metallic plates of one square inch area would be about 5×10^{-3} lb for an electric field of 30,000 volts per cm. Maximum pressures on a typical machine might be on the order of 7×70^{-4} lb/in^2 exerted on the edge of the rotor. A first approximation of the maximum power output of the Trump machine can be obtained from estimating the electrostatic pressure: Power = electrostatic pressure x area x speed.

In addition to minimizing the ratio of the maximum to average tangential gradient, the ideal machine will have nearly equal tangential and normal voltage gradients between stator and rotor, so as to maximize the product, $F\sigma$ (where F is the force and σ, the charge density on the plate) subject to a maximum allowable voltage gradient. Since the maximum voltage gradient is on the order of a half megavolt percentimeter for both high-pressure gas and vacuum operation, a structurally reasonable electrode or stator plate separation of a centimeter or more would result in output voltages of 500 kilovolts or higher. This is higher than is anticipated for ion propulsion purposes.

The dielectric strength of the vacuum gap is illustrated by the curves of Fig. III-D-2 and Fig. III-D-3, which depict experimental data points for breakdown voltage between two spheres of 4-in. radius (Reference III-D-15). Figure III-D-2 refers to maximum breakdown voltage obtained with direct, alternating, and impulse voltage applied across a steel electrode gap. Figure III-D-3 gives the mean insulation strengths for using a direct voltage with steel copper and bright aluminum. In practice, breakdown strength will vary with surface finish, surface history, material, and other physical factors. The difficulty of maintaining a vacuum in ground

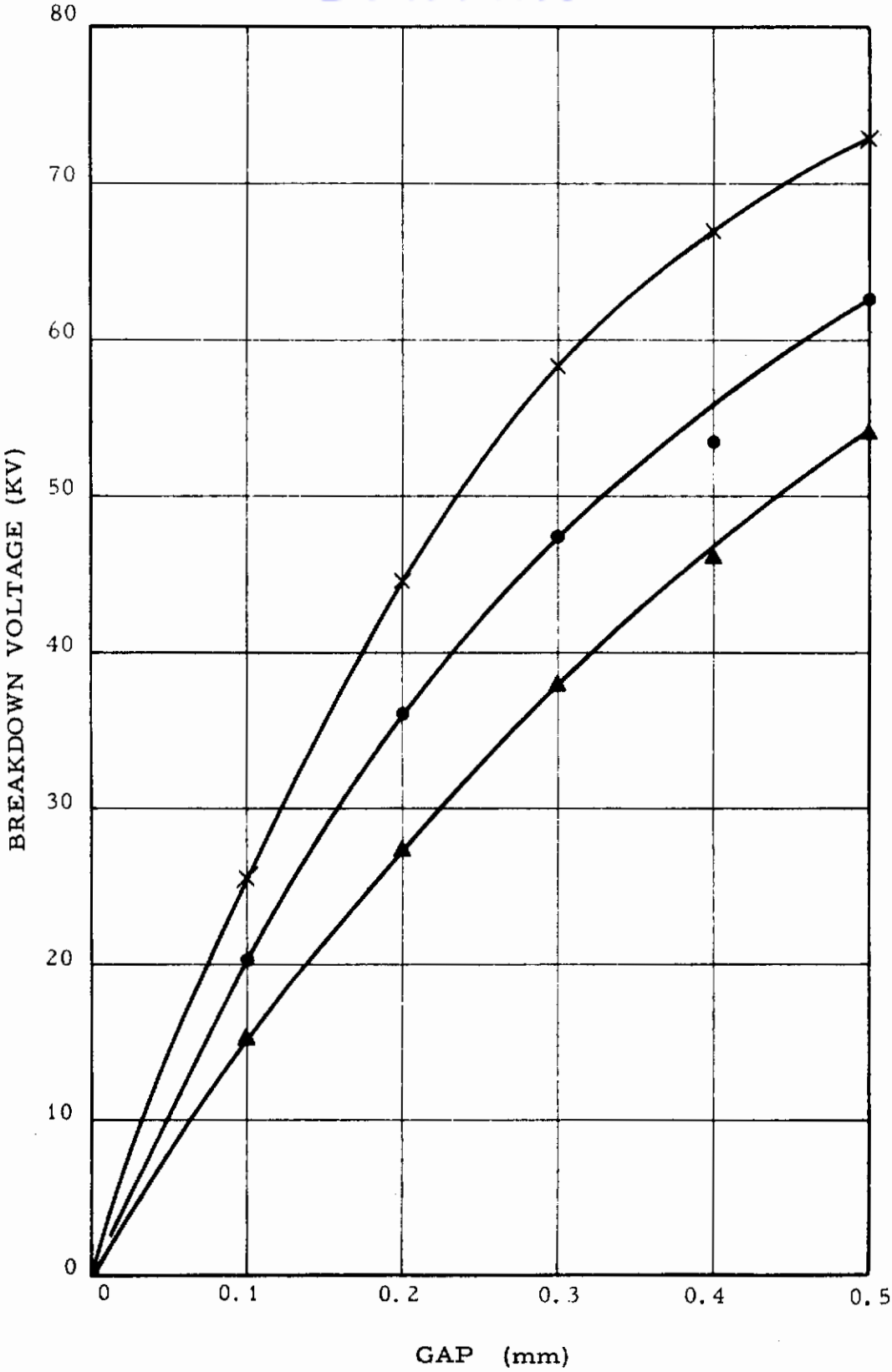

FIGURE III-D-2 IMPULSE, ALTERNATING, AND DIRECT BREAKDOWN VOLTAGE, STEEL ELECTRODES. X, IMPULSE (12/50); ●, ALTERNATING (50 C.P.S.); ▲, DIRECT (6 KV./SECOND)

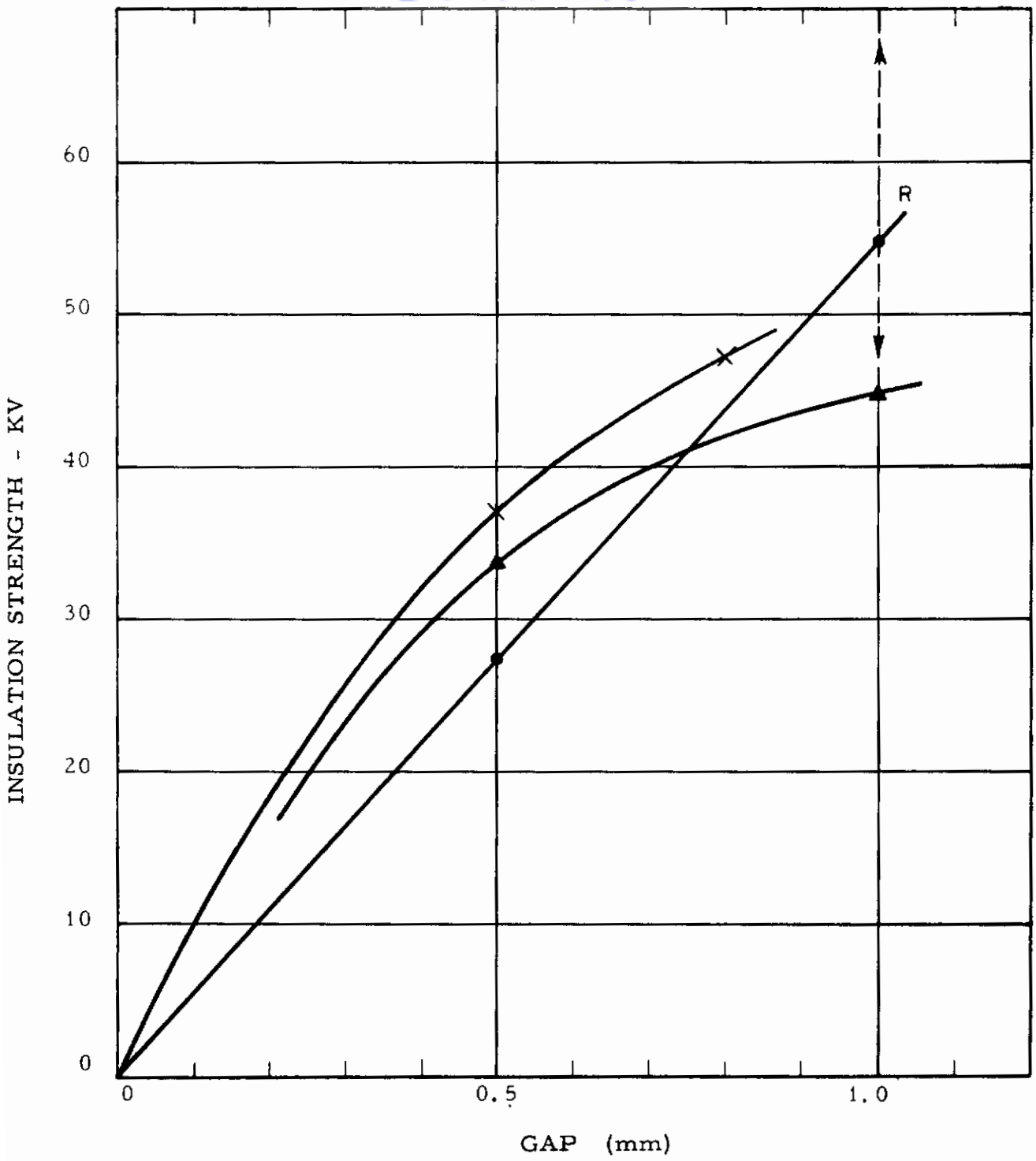

FIGURE III-D-3 INSULATION STRENGTH, X, STEEL; O, COPPER; Δ, BRIGHT ALUMINUM; R, RANGE FOR DULL ALUMINUM

application has led to the gas encapsulation of the generators within chambers filled with inert gas under high pressure, with insulating qualities roughly the same as high vacuum. High-pressure insulation using bulky containers is too heavy for space application.

In spite of the handicap of designing for a voltage that is considerably less than ideal, good specific weights are predicted in theoretical analyses conducted by Thompson Ramo-Wooldridge (Ref. III-D-2, 3), Goodrich-High Voltage Engineering Corporation (Ref. III-D-1), and Cosmic Inc. (Ref. III-D-16). Analyses are based on the use of the Trump-Van de Graaff type of machine, and weights compare favorably with those obtainable with DC electromagnetic machines.

Development efforts to date have been on increasing the charge density, on utilizing a more compact geometric configuration, and reliability. Further improvements will probably come about through the use of lighter materials, faster rotation speeds, and vacuum insulation. Several developmental problems are discussed in Subsection 2.3.

The various types of electrostatic machines which have been proposed are described in Subsection 2.0. Except for the Trump-Van de Graaff machine, all of these machines have been designed to operate in a high-pressure gas. However, they all can, with some modification, be made to operate in vacuum.

2.0 CURRENT OPERATIONAL ELECTROSTATIC MACHINES

This section presents a brief review of several machines which have been developed for industrial and laboratory utilization. The Trump - Van de Graaff influence generator appears most favorable for development for space application, and the developmental problems remaining for the machine are discussed in Subsection 3.0.

2. 1 Van de Graaff Generator

The development of the belt-insulated type Van de Graaff generator (Fig. III-D-4) was initiated by Van de Graaf in 1932 and has been extremely successful as a laboratory instrument. Extremely high voltages on the order of well over a megavolt can be obtained. While the power output is small compared to the size and cost of the machine, it performs its function (the output of high voltages for the acceleration of particles) quite well. These machines operate at high gas pressure, and the two methods of reducing the tangential voltage gradient due to rotor charge-counter-moving surfaces and/or a conducting charge compensating surface neighboring the charged moving surface have been utilized.

2. 2 The Cossel Machine

The Cossel machine (Ref. No. III-D-4) is depicted in Fig. III-D-5. It consists of two counter-rotating disks made of insulated material which carry charges up to the high voltage electrodes. This configuration has the advantage of compactness, since no stator is required. Thus, the weight and size can be half the weight and size of the best of the other machines. In addition, since the charges on the two rotors are equal and of opposite sign, there is little tangential voltage gradient due to the charges, as would be the case for a single rotor. This is illustrated in Fig. III-D-5, which shows the voltage gradient as a function of the distance between the low and high voltage terminals for the double and single rotor machines. Thus, greater charge density can be placed on the counter-rotating machine without causing a breakdown voltage gradient. This is an important principle, and all subsequent workers have effected means of applying it to their machines without the difficulties of the counter-rotating disc construction.

4. The high-voltage is insulated from the shell of the accelerator by an atmosphere of compressed nitrogen which prevents arc-over.

3. At the terminal, the charge is automatically transferred from the belt to the terminal, thereby establishing a high potential or voltage difference with respect to the lower end of the accelerator.

2. The belt mechanically carries the charge to an insulated hemispherical, high-voltage terminal.

1. Electric Charge is sprayed on a rapidly moving insulating belt.

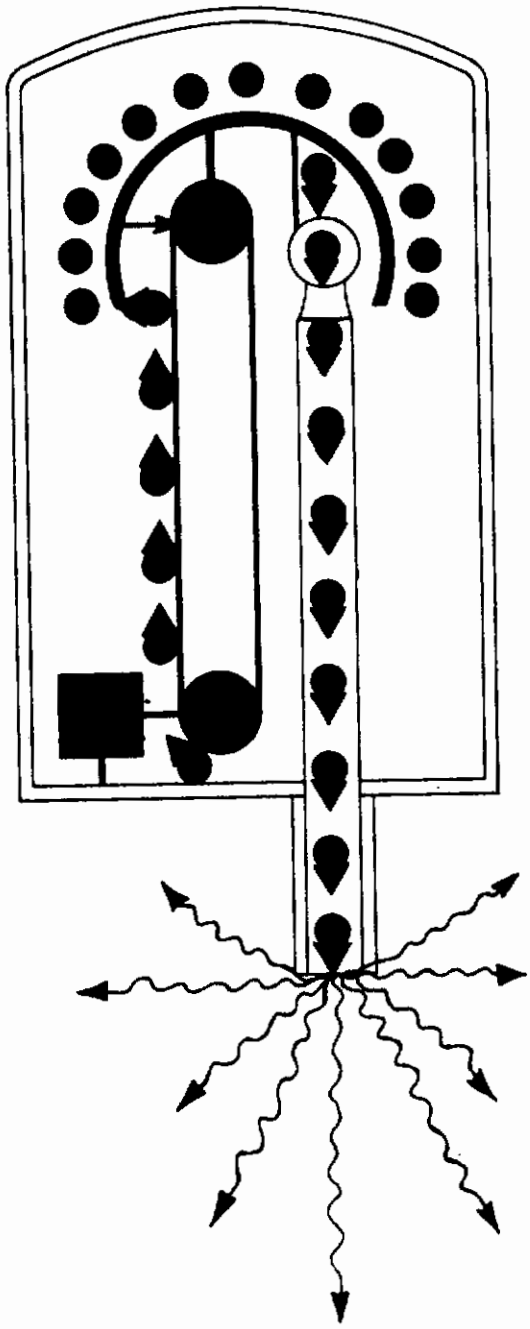

5. Electrically charged particles are made available for acceleration from a heated cathode (for electric

6. A glass and metal tube maintained at a very high vacuum, provides the only path for charged particles to escape from the high-voltage terminal.

7. The particles forming the high-energy beam are accelerated to extremely high velocities by the potential difference between the terminal and the lower end of the accelerator.

8. The accelerated high-energy particles are contained within a tightly collimated beam bombarding special targets, to produce X-rays.

FIGURE III-D - 4 VAN deGRAAFF PARTICLE ACCELERATOR

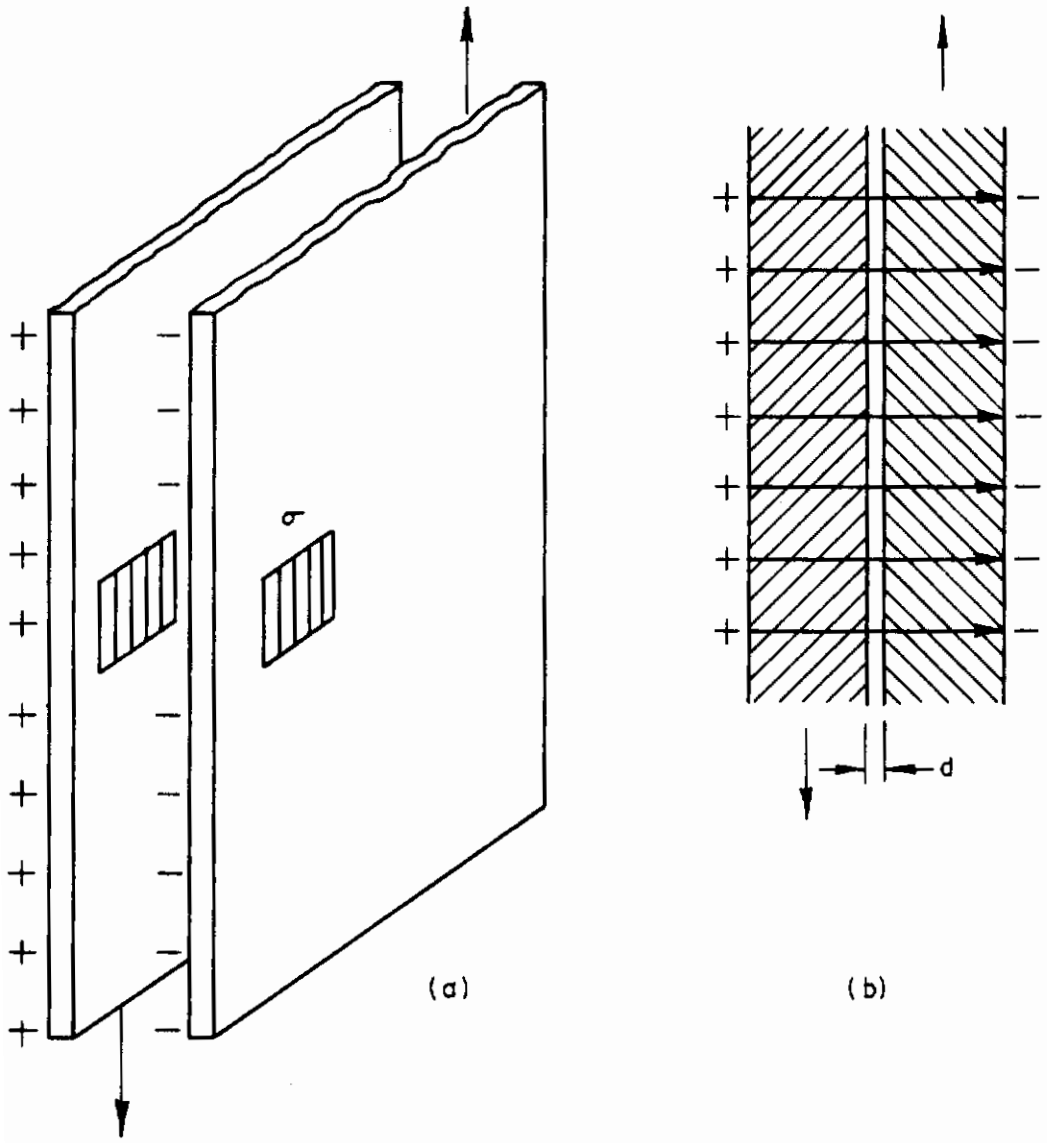

FIGURE III-D-5 COSSEL MACHINE

2.3 Joffe and Hochberg Machines

In the late 1930's, Joffe and Hochberg in Russia developed the cylindrical and rotor disk machines, using high-pressure gas insulation and the principle of the weakly conducting stator as it is found in the commercial machines of today. The final form of this cylindrical rotor machine, Fig. III-D-6, consisted of four rotors inside a cylindrical high pressure gas filled tank. As will be discussed later, Joffe and Hochberg did not feel the cylindrical form had the potentialities of the disk type but had advantages in the production of high voltages.

Their method of solving the space charge (the voltage gradient due to the charges on the rotor) problem is illustrated in Fig. III-D-6, which shows the four rotors used in the machine with a weakly conducting stator space charge shield. The stator is connected to the high voltage electrode at its high voltage end and to the low voltage electrode at the low voltage end of the machine. Due to the weakly conducting layer, the constant voltage gradient is maintained from the low voltage electrode to the high voltage electrode. This is due to the fact that in a conductor $\Delta . j = \Delta . E\sigma = 0$. Therefore, the physical effect of the weakly conducting layer is to distribute the charges along its surface. This will minimize the high field which would be found midway between the low voltage electrode and the high voltage electrode due to the charge on the rotor. By this method, they solved the problem which was solved previously by Cossel with the counter-revolving disk. Felici (Ref. III-D-6) states that for this purpose a resistivity of 10^{11} ohm centimeter is the best.

This principle is used in their disk machine (shown in Fig. III-D-7). The figure shows, instead of a continuous

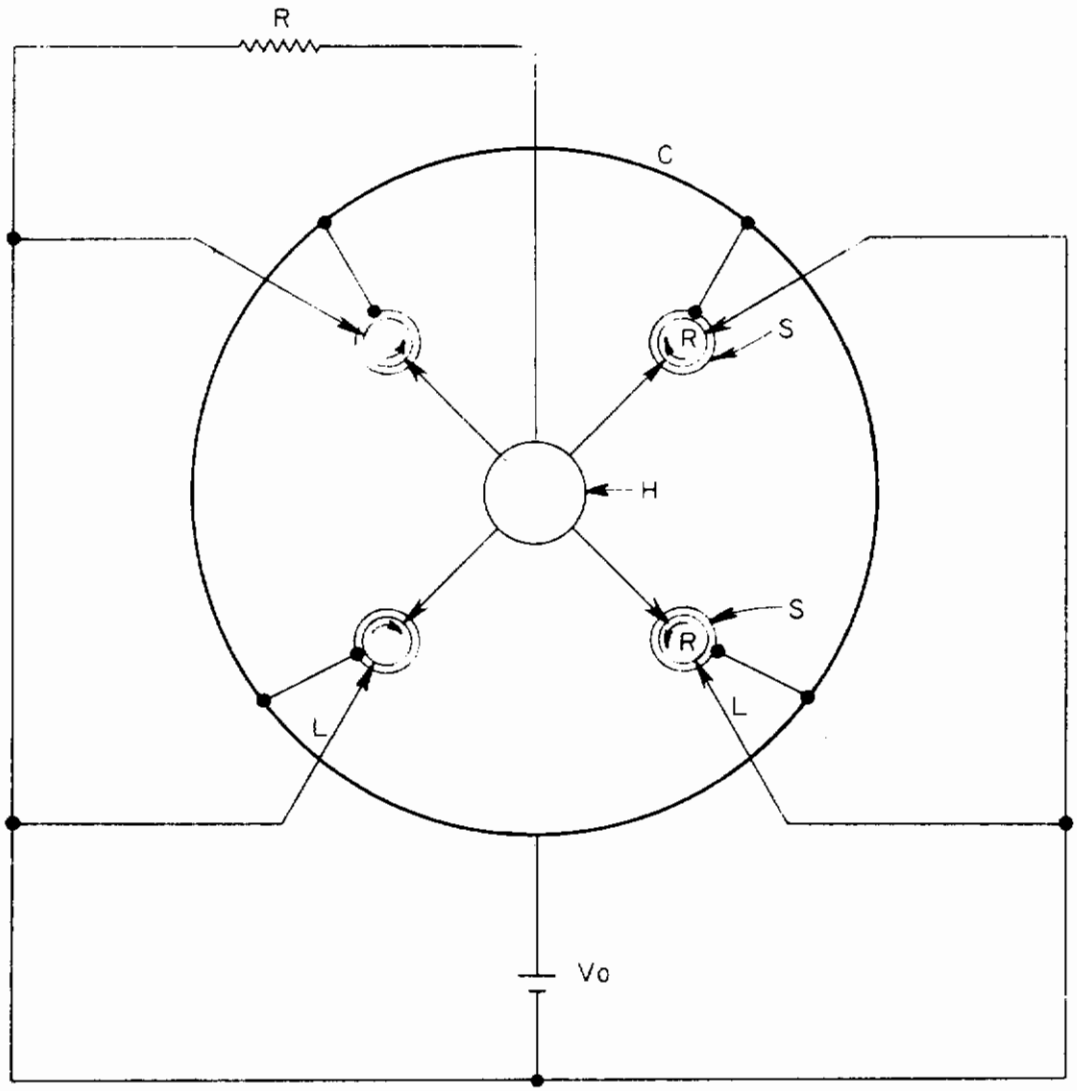

C = Conducting cylindrical shell
H = High voltage electrode
L = Low voltage electrode
R = Non conducting rotor
S = Weakly conducting stator
Vo = Excitation voltage

FIGURE III-D-6 SCHEMATIC OF JOFFE-HOCHBERG GENERATOR

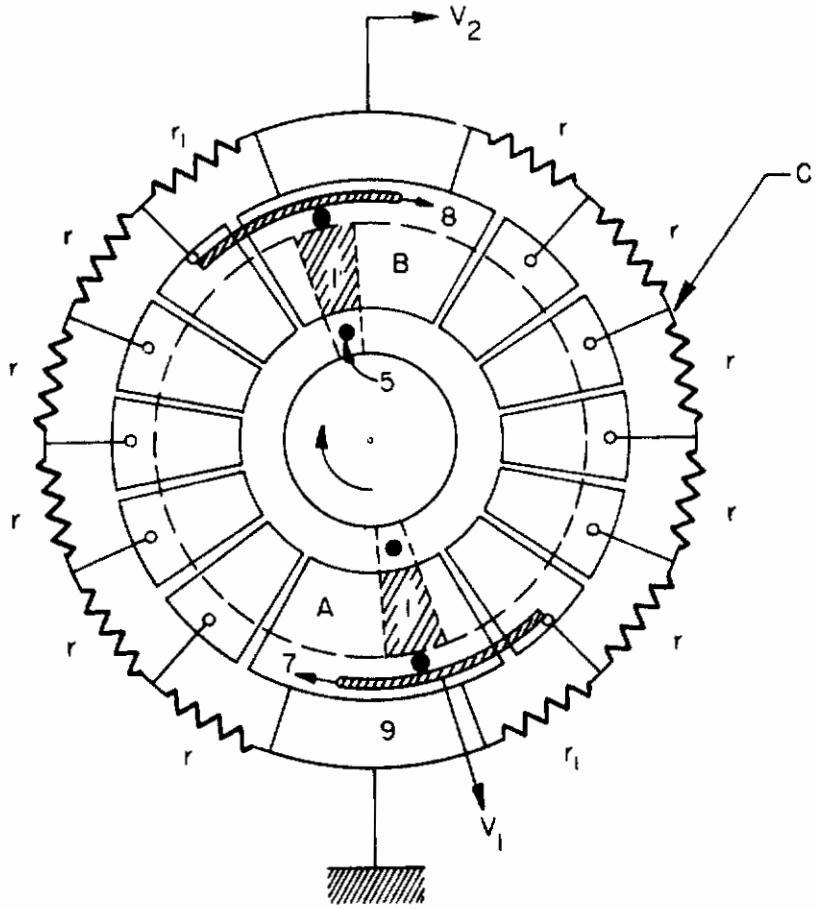

FIGURE III-D-7 DISK MACHINE

resistivity, a step-wise finite jump in resistivity from sector to sector. However, a semiconductor coating on the sector could be used for this purpose rather than a set of resistance elements. The primary advantage in the sector method, of course, is its application in a high vacuum. One of the advantages of the high-pressure system is that brushes can be used with little wear on material and with a uniform charge deposit due to the fact that ionization of the gas aids in the distribution of charges on the moving surface. Where this ionization does not aid (i.e., a high-vacuum situation), using a nonconducting disk is difficult due to the fact that the whole area of the disk must be sprayed with charge, rather than just a small segment of it, or a contact made in the case of using a segmented type of disk.

Joffe and Hochberg were somewhat influenced in the disk design by communications with Van de Graaff in America, and it is apparent that they hoped this could be utilized in a vacuum design at some time. However, their development work was done under high pressure. They did not feel that, from the standpoint of economy, the cylindrical rotor design was satisfactory due to the fact that only the surfaces of the cylinder acted as working surfaces and the remaining volume being useless. They decided then to go to a disk type.

The disk type does not differ in general principles from the cylindrical multirotor model, except that the available space is used to better advantage. The single condenser of the multirotor model is here replaced by a number of condensers placed at right angles to the axis of the rotor with the field parallel to this axis. A multidisk generator consists of a multidisk stator (Fig. III-D-7) whose disks enter in between the disks of a rotor. Each disk is divided into a great number of

of conducting sectors separated by nonconducting layers. Sector 19 of the stator is connected to earth. Sector 8 represents the high-voltage collector. The intermediate sectors charge up to intermediate potentials supplied by the distribution system, C. The rotor sectors receive a charge from the low voltage source when they are inside the stator sectors. This charge is then transferred to the collector at the time when the disk enters sector 8 of the stator. In the further part of the same sector 8, they recharge, receiving a charge q of opposite sign. In other respects, performance of the multidisk generator is very much like that of the multirotor design from which it differs in constructional details.

In calculating the current delivered by the generator, it must be taken into consideration that both surfaces of the disk charge up and that, in the high voltage sector, recharging takes place so that during one revolution the charge q is transferred by this sector twice.

The charge does not spread over the whole disk but only to the conducting sectors which have an area constituting a fraction a of the whole area. In the Joffe-Hochberg model, a was .6 to .75.

The electric scheme of a disk generator is given in Fig. III-D-7. Here r represents the distributing resistances of the stator, A is the low-voltage collector, B - the high-voltage collector, 1 - one of the sectors of the rotor disk, r - the resistance recharging the sector when it passes through the high-voltage collector B.

In choosing the number of sectors on the stator and on the rotor disks, it must be borne in mind that when the stator sector passes from one rotor sector to the next, part of sector 1 faces the section with potential V_n, while the remaining part already enters the next

section having the potential $V_n + \Delta V$. If the potential difference between sector 1 and the stator is equal to V_1 volts, then in that part which has entered the rotor section V_{n+1} this difference will amount to $V_1 + \Delta V$. It is obvious that the breakdown potential will be determined by the value $V_1 + \Delta V$ while the maximum charge q depends on V_1. If ΔV is large compared to V_1, then, at a given clearance between the rotor and stator disks, the primary potential V_1 must be lowered. This leads to a decrease in both the current and the obtainable potential V_2. Thus, in the case of a multidisk generator, the condition for normal operation is

$$\Delta V \ll V_1.$$

The calculation of the voltage V_2 is based on the allowable field intensity E' along the surface of the rotor disk between two successive conducting sectors.

The intensity E' is

$$E' = \frac{V_{2^n}}{2\pi r \beta}$$

where n = number of sectors.

r = inner radius of sector.

This was confirmed by the experiment of Joffe and Hochberg. Based on their experiments and on communications with Van de Graaff, the authors state: A multidisk, multirotor generator operating in vacuum would not prove inferior to any electromagnetic device as regards efficiency in output per unit volume and could be further converted into an electric motor of equal output. The authors computed that the output of a multirotor generator would be two kilowatts per m^3 for a cylindrical type multirotor generator and that for a multidisk generator it would be on the

order of several hundred kilowatts per cu meter. This estimate is similar to the estimate given by A. John Gale (Ref. III-D-1) of 100 kilowatts per cu ft, if we allow for modern rotation speeds of 40,000 - 50,000 rpm which is a factor of over 10 higher than assumed by Joffe and Hochberg. Gale proposes a very similar machine for space application.

2.4 Neuberg and Felici Machines

Neuberg in Germany and Felici in France (Refs. III-D-4, 5, and 6) applied the principles developed by Cossell and Joffe and Hochberg to produce commercial electrostatic machines, very similar both in size configuration and output. Felici's machine is shown schematically in Fig. III-D-8. The rotor is made of a nonconducting material, usually resin. The stator is made of a slightly conducting material, bakelite or glass. The charge is put on a comb running along the length of the cylinder. Due to the fact that the generator is surrounded by a high pressure, the placing of the charges on the rotor is facilitated by the ionization process.

The plates on the inside have varying purposes. The plate A at the low voltage terminal acts as an attractive surface to the charge being placed on the rotor and also makes contact with the stator so as to maintain the low voltage potential at the portion of the stator. In addition, the plate gives an attractive force to the charge which is being pulled away from it in the direction of the high voltage terminal by the rotor. In this manner, work occurs on the generator. The terminal B has the purpose of keeping the end of the stator near the high voltage potential. Voltage regulation is accomplished by varying the voltage of plate A in relation to the low voltage comb which in turn is maintained at ground

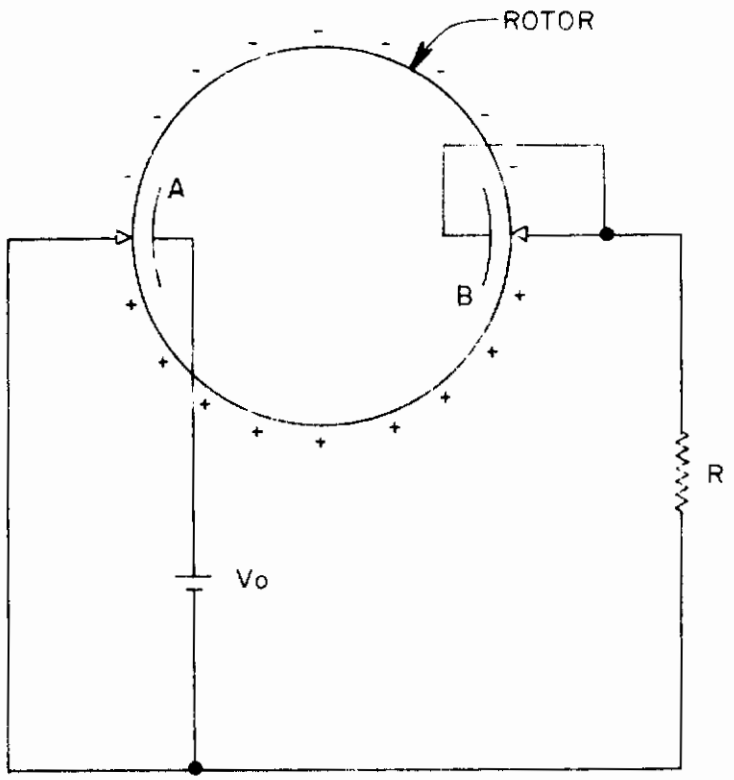

FIGURE III-D-8 NEUBERG-FELICI GENERATOR

potential. The series coupling of several generators can be accomplished to give higher voltage than can be obtained from a single generator. These can also be coupled in parallel to get high currents at the same voltage.

The efficiencies of these machines are given in Ref. III-D-5 as over 90 percent and in Ref. III-D-4, over 80 percent. The losses are due almost entirely to friction in the high gas. The generators themselves are not heavy since plastics, and light metals are used throughout. However, the accessory apparatus is heavy, requiring a pressure tank, heat dissipation mechanism (usually a fan), voltage control apparatus, and, of course, the driving motor.

Felici, prior to developing this type of machine, did a considerable amount of work over a period of 8 years on the disk machine, trying numerous methods. He derived one rule, a separation rule, which he calls " theoretical profile for constant dielectric stress". For a disk machine, the rule states that the separation between a disk and the neighboring plate should be 1/2 the thickness of the disk itself, in the case where the disk is between two plates.

Felici states that the primary reason for using the cylinder type of machine is the fact that the tolerances are not as close and oscillation is reduced, which he indicates is an important cause of voltage breakdown. Fabrication difficulties have been experienced with the disk machines. Although the results obtained from his machines were satisfactory, considerable difficulty was encountered in keeping sectors and disks in proper alignment, even though parts were machined from metal and were of considerable bulk. The use of a carefully machined monoblock construction, where disk separation was fixed, offered no improvement, due to the additive effects of small errors on each separate disk. Another

difficulty arose due to the random nature of sparks between metal surfaces depending on the presence of accidental impurities. The risk of sparking, therefore, becomes greater as generator surface area increases. Hence, for a disk machine with large surface area using a conducting surface, the certainty of maintaining a large electric field is less than for other machines.

The characteristics of several commercially available cylindrical-rotor generators produced by the SAMES Company under the direction of Felici are given below. All of these machines use a high-pressure dielectric gas and are contained by a heavy steel cylinder.

Rotor Diameter in m.m.	No. of Poles	Voltage kv	Current m.a.	Power kva
240	8	150	18	2.7
240	6	220	12	2.64
240	4	300	7	2.1
300	2	600	5	3.0

2.5 The Trump- Van de Graaff Influence Machine

The Trump - Van de Graaff type of machine is a true influence machine in that the revolving part carries no charge to be deposited on the high voltage terminal. Instead, it creates an oscillating charge between the ground and the stator, with the advantage that there is no commutation mechanism in the machine. A disadvantage is that for a given charge density and size of machine, the voltage is somewhat more limited than the brush type machine. This occurs because, in order for work to be performed on the machine, a force on the stator in the direction that the rotor travels must be applied. However, the stator must be made of a conducting material which cannot support a tangential voltage gradient. It is apparent that since the desired voltage gradient is found at the edges of the

stator, the forces must necessarily be much smaller than would be obtained if the elements were nonconducting, as in the case with the brush type machine.

This machine is best used for loads which require lower voltages on the order of 10 to 100 kilovolts. These voltages are nonoptimum for maximum power generation per unit volume. Fig. III-D-9 depicts a schematic of the machine discussed in Trump's thesis and also patented by Trump and Van de Graaff. The machine depicted in Fig. III-D-9 is a modification in that the Trump - Van de Graaff machine does not have a complete stator plate, and oscillates the charge between the stator plate and ground rather than between two stator plates. In addition, the Trump - Van de Graaff machine uses a bypass condenser in place of the series inductor. However, the results are essentially the same.

A DC electrostatic generator of the interleaving metallic plate type can be arranged so that the rotor-stator capacitance varies cyclically between a minimum value C_o and a maximum value C_m. The rotor is maintained at a voltage V_o relative to the ground by an auxiliary supply. The stator is connected to the junction of two electronic tubes connected in series across the load. The average output power is

$$P_a = \frac{4.63 \times 10^{-15} \, KNsp \, (r_1^2 - r_2^2) \, VE \text{ watts}}{d}$$

where

$$K = \frac{1 - C_o (E+V) + (C_s + C_v) E}{C_m V} = 0.75 \text{ in a practical machine design}$$

where

N = RPM
s = no. of rotor plates
p = no. of poles

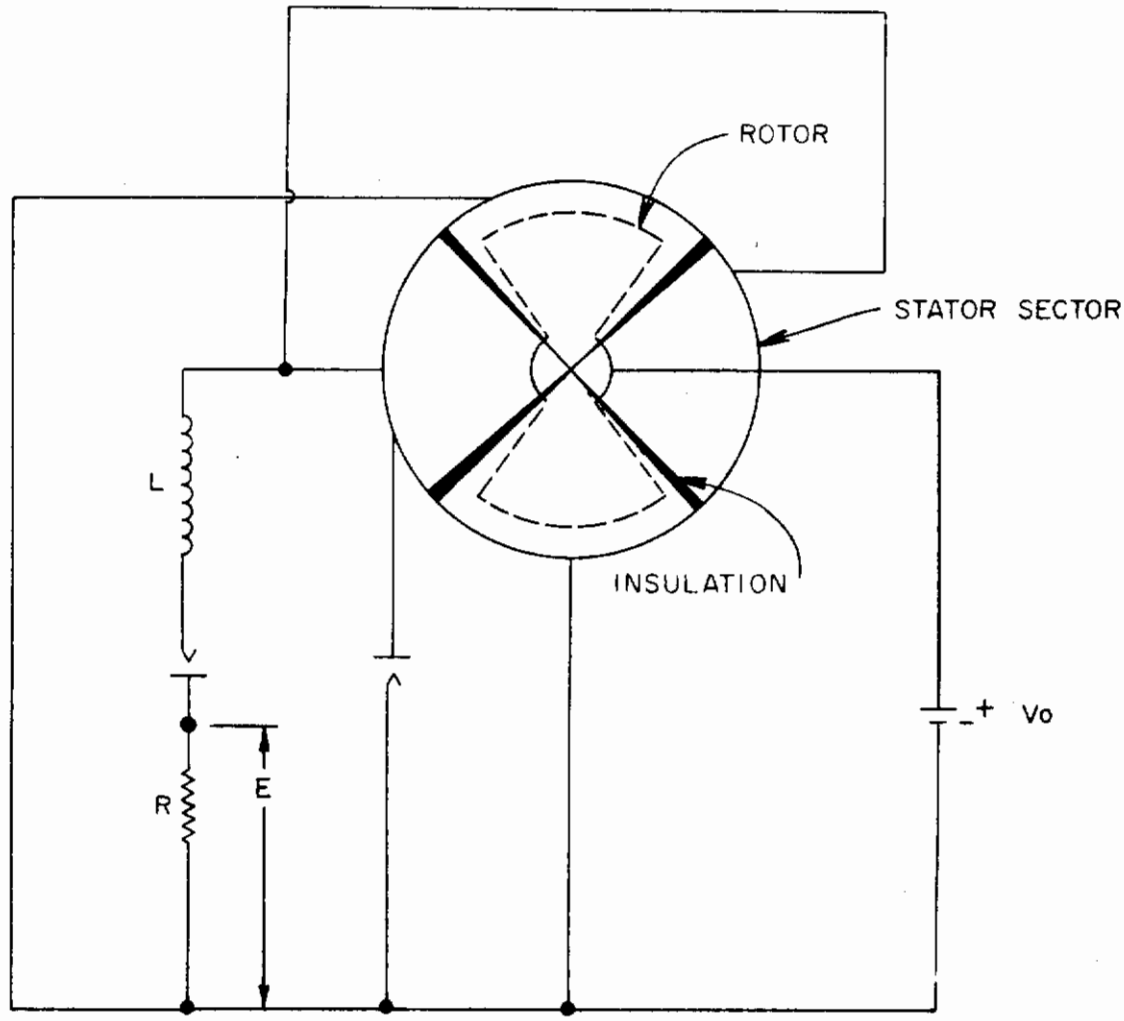

FIGURE III-D-9 TRUMP-VAN DE GRAAFF INFLUENCE (VARIABLE CAPACITANCE) MACHINE D. C. OUTPUT

d = separation between rotor and stator in cm

r_1, r_2 = rotor radii in cm

C_s = capacitance of stator to ground

C_v = capacitance of tube to ground

Trumps experimental machine operated in an ac mode in high vacuum with an output of 60 watts and with a measured efficiency of slightly higher than 99%. This machine was recently rehabilitated at Goodrich-High Voltage Engineering and provided 100 watts at 3,600 rpm.

The time rate of capacitance variation of ac electrostatic machines at constant synchronous speed must be of double line frequency and may be of any wave form from rectangular to sinusoidal. The latter is preferable because of the relative absence of harmonics. The average output power of such a machine is given by

$$P_a = \frac{E^2 w C_m}{4} \sin 2\theta$$

where E is the maximum line voltage, w is the angular velocity, C_m is the maximum capacitance during the cycle, and θ is the phase angle between the start of the voltage cycle and the start of the capacitance variation cycle. The practical formula for the average power developed by this synchronous electrostatic machine with sinusoidal capacitance variation in terms of its dimensions can be shown to be

$$P_a = \frac{139 \times 10^{-15} E^2 fs(r_1^2 - r_2^2)}{d} \sin 2\theta \quad \text{watts}$$

where E is the maximum value of line voltage of frequency f, s is the number of rotor disks, r_1 and r_2 are the inner and outer radii of the rotor, and d is the rotor and stator separation in centimeters.

Gale (Ref. III-D-8) has postulated a specific weight of between 0.2 and 0.4 lb/kw; however, this estimate seems somewhat optimistic when the dimensions of the machine, 15 inches in diameter and 10 inches in length, are considered along with the power output of 100 kw. Assuming that the machine is composed of 1/2 metal, a weight more near that given by the TRW estimate is obtained. Using anticipated material improvements and the techniques discussed in Subsection 3.0 TRW predicts weights on the order of .9 to 1.8 lb/kw as potentially possible in the near future, operating at 100 kv and 50 kv respectively, and 40,000 rpm. Goodrich-High Voltage predicts 2 lb/kw for a machine providing 50 kv at 30,000 rpm.

3.0 CURRENT DEVELOPMENT PROGRAMS

Laboratory development as well as theoretical analyses on the electrostatic generator for space are now being conducted by the Thompson Ramo-Wooldridge Corporation, Cleveland, Ohio; the Goodrich-High Voltage Engineering Corporation, Burlington, Massachusetts; NRL; and Cosmic Inc. Theoretical studies have also been conducted by many organizations including General Electric, Philadelphia, Pennsylvania; Rocketdyne Division of the North American Aircraft Company, Los Angeles, California; and Lockheed Missiles and Space Division, Palo Alto, California.

The laboratory development work includes the testing of several types of electrostatic generators and various materials in a vacuum tank. Much work must be done before the electrostatic generator will be fully developed.

The objective of the Goodrich-High Voltage Engineering program (funded by WADD) is to fabricate a 5 kw, 50 kv, 10,000 rpm electrostatic generator to demonstrate feasibility. The model will not be designed for

minimum weight. The contract calls for the investigation of new materials, new techniques of fabrication and is of a basic as well as applied research nature. The plates will be constructed of steel, and 1 mm spacing is anticipated. Current testing difficulties include organic contaminates in the test chamber which enhance a secondary emission.

Low specific weights can be obtained only by having very thin plates, close plate separation, and high rotation speeds. These specifications create fabrication problems in addition to those inherent in the electrostatic generator operating in a vacuum.

A survey of the literature and correspondence with TRW, High-Voltage Engineering, and General Electric indicate that the following are areas in which further development efforts are needed.

a. Fabrication techniques

Because the machines must be operated near their structural and electrical limit, the fabrication problems are quite complex. These problems include:

1. Extremely close mechanical tolerance on plate separation is required. However, the electrostatic forces, which change direction, submit each of the carriers to a force alternately going forward or backward in the direction of rotation, so that in the design of the machine, and in the choice of rotation speed, particular attention has to be given to vibrations.
2. Because of the thin plates and high rotation speeds which are necessary for sufficient weight reduction, stress is high and limitations on diameter rpm exist.

3. All charge carrying parts must have extremely smooth surfaces in order to mitigate the electrical breakdown problems. In vacuum, electrical breakdown is caused in part by the field emission effect, and hence sharp or rough surfaces, even in miniature, are to be avoided.

b. Materials study

In addition to the obvious mechanical properties of materials such as density, ability to withstand the various stresses, etc., investigations into the electrical breakdown resistance of materials under high stress, and dynamic conditions is required.

The vacuum breakdown resistance is generally higher for higher metal work functions, and it is thus possible that a coating technique will improve the breakdown resistance. Also, it has been found that a metal "creep" phenomena associated with microscopically rough surfaces adversely affects the breakdown resistance. Heat treating the surface to reduce irregularities improves the breakdown performance. Other techniques as well as improvements on this one might be investigated.

It has been found that for short cycles of the applied voltage, the breakdown voltage is less than that for long cycles. This is due at least partly to "creep" and is thus a function of the metal. It is apparent that the breakdown voltages will be favorably altered by this effect in a rotating parts environment. On the other hand, microscopic dust particles from

the generator bearings or other friction surfaces and contamination from lubricants can contribute measurably to the breakdown phenomena.

c. Current collection

The current collection system must be designed so as not to aggravate the voltage breakdown problem.

d. Shaft oscillation damping

This is a problem for obvious structural reasons and also because of the adverse effect any vibration has on the breakdown resistance.

e. Fluid leakage problems

To prevent leakage of shaft lubricant, an extremely good seal must be employed. Also, provision must be made to prevent leakage of the turbine working fluid through the shaft coupling. A possible solution of the second problem is a magnetic coupling, although these have proved inefficient.

f. High temperature

The entire electrostatic generating system will have to operate at high temperatures. This increases the need for the development of non organic insulating materials, and investigations into the effects of high temperature on vacuum breakdown, stress limits, etc.

REFERENCE LIST

III-D- 1. A. John Gale: Electrostatic Generators, Advanced Propulsion Systems, pp 161, Pergamon Press, 1959.

III-D- 2. O. P. Breaux, Electrostatic Power Generation for Space Propulsion, AIEE, paper No. CP 59-914, May 1, 1959.

III-D- 3. C. G. Martin, R. J. Denington and V. P. Kovacik: Dynamic Heat Engines, seminar on Advanced Energy Sources and Conversion Techniques, Nov. 1958, Vol. 1, p. 109.

III-D- 4. U. Neubert: Physical Principles Underlying the New High Power Electrostatic Machines, Z. Angerv Phys. 10, No. 2, pp. 100-7, Feb. 1958.

III-D- 5. Emile Labin: Electrostatic Generators, Electromechanical Design 2, No. 9, p. 24, Nov. 1958.

III-D- 6. N. J. Felici: Ten Years of Research on Electrostatics at the University of Grenoble, Brit. Journal of Applied Physics, Supplement No. 2, p. 562, 1953.

III-D- 7. J. G. Trump and R. J. Van de Graaff: The Insulation of High Voltages in Vacuum, J.A.P., pp. 327, 18, 1947.

III-D- 8. R. J. Van de Graaff: Electrostatic Generators for the Acceleration of Charged Particles, Reports on Progress in Physics, Vol. XI, p. 1.

III-D- 9. J. G. Trump: Vacuum Electrostatic Engineering, Thesis for DS degree at Mass. Inst. of Tech.

III-D-10. A. F. Joffe and B. M. Hochbert: Electrostatic Generator, J. of Phys. 2, p. 243, 1940.

III-D-11. W. Herchenbach: Air Resistance of Rotating Circular Disks, Zeitung fur Naturforschung, Vol. 10a, pp. 471-4, 1955.

III-D-12. D. I. Blockinzer, et al: Breakdown in Compressed Gasses at High Pressures and Small Distances, Journal of Physics 2, p. 216, 1940.

III-D-13. S. Ranch and L. Johnson: High Frequency Alternators, Electrical Engineering 73, p. 735, 1954.

III-D-14. R. J. Van de Graaf and J. G. Trump: Method and Apparatus for Electrostatically Generating Direct Current Power, U. S. patent No. 2, pp. 194, 839.

III-D-15. A. S. Denholm: The Electrical Breakdown of Small Gaps in Vacuum, Canadian J. of Physics 36, 476, 1958.

III-D-16. D. Gignoux: Electrostatic Generators for Space Application, Cosmic Inc., August 23, 1960.